A Comparison of ICA versus Genetic Algorithm Optimized ICA for use in non-invasive muscle tissue EMG

Shaun R. Mulligan

Supervised by R. Verrinder and L. John

June 2014

Dissertation submitted to the University of Cape Town in full fufilment

of the requirements for the degree of Masters of Science

in Electrical Engineering

I, Shaun R. Mulligan, hereby declare that this Dissertation is my own, unaided work. I know the meaning of plagiarism and declare that all the work in this document, save for that which is properly acknowledged, is my own. It is being submitted for the degree of Master of Science in Electrical Engineering in the University of Cape Town. It has not been submitted before for any degree or examination in any other University.

I empower the university to reproduce for the purpose of research either the whole or any portion of the contents in any manner whatsoever.

Signed: Signed by candidate

Date:

Abstract

The patent developed by Dr. L. John [1] allows for the the detection of deep muscle activation through the combination of specially positioned monopolar surface Electromyography (sEMG) electrodes and a Blind Source Separation algorithm. This concept was then proved by Morowasi and John [2] in a 12 electrode prototype system around the bicep. This proof of concept showed that it was possible to extract the deep tissue activity of the brachialis muscle in the upper arm, however, the effect of surface electrode positioning and effectual number of electrodes on signal quality is still unclear. The hope of this research is to extend this work.

In this research, a genetic algorithm (GA) is implemented on top of the Fast Independent Component Analysis (FastICA) algorithm to reduce the number of electrodes needed to isolate the activity from all muscles in the upper arm, including deep tissue. The GA selects electrodes based on the amount of significant information they contribute to the ICA solution and by doing so, a reduced electrode set is generated and alternative electrode positions are identified. This allows a near optimal electrode configuration to be produced for each user. The benefits of this approach are: 1. The generalized electrode array and this algorithm can select the near optimal electrode arrangement with very minimal understanding of the underlying anatomy. 2. It can correct for small anatomical differences between test subjects and act as a calibration phase for individuals. As with any design there are also disadvantages, such as each user needs to have the electrode placement specifically customised for him or her and this process needs to be conducted using a higher number of electrodes to begin with.

The study was conducted on 20 healthy, male subjects. A band of 30 evenly spaced electrodes was applied to the subject's upper arm to record EMG signals and each participant was subjected to a defined movement protocol to isolate upper arm muscle activity. The GA based ICA was run on the resulting data and the muscle group signal contribution was extracted. This approach indicated that the number of electrodes needed to reproduce the signal can be reduced by at least two-thirds across all subjects with negligible loss in total signal integrity. Additionally, a generalized electrode pattern could not be generated for the upper arm due to the variation in the participants' musculature and skin impedance. This procedure should therefore be run as a calibration technique to produce a unique electrode pattern for each participant, to improve overall signal integrity.

Acknowledgments

The financial assistance of the National Research Foundation (NRF) towards this research is hereby acknowledged. Opinions expressed and conclusions arrived at, are those of the author and are not necessarily to be attributed to the NRF.

I would also like to acknowledge and thank my supervisor Robyn Verrinder for her continual guidance and constant stream of help and support. Thank you to my co-supervisor Dr. Lester John for his support and help on all things biomedical and for use of the data and ideas from the preliminary study on muscle tissue non-invasive EMG.

Thank you to UCT and the Electrical engineering department for many years of teaching and support, my time here has been an amazing and constructive experience. It will never be forgotten.

A big thank you to my parents, family and friends for the constant encouragement and support, this masters dissertation would never have seen the light of day if not for all of you.

Thank you!

Contents

List of Tables

List of Figures

Nomenclature

Amplifier Gain	In electronics, gain is a measure of the ability of a circuit (often an amplifier) to increase the power or amplitude of a signal from the input to the output, by adding energy to the signal converted from some power supply.
ANN	Artificial Neural Network
Antagonist	A classification used to describe a muscle that causes specific movement or possibly several movements to occur through the process of its own contraction.
ASIC	An application-specific integrated circuit is an integrated circuit (IC) customized for a particular use, rather than intended for general-purpose use.
Besselworth	A hybrid low pass filter made up of a Bessel and Butterworth filter.
Bluetooth	Bluetooth is a wireless technology standard for exchanging data over short distances from fixed and mobile devices, creating personal area networks (PANs) with high levels of security.
BSS	Blind Source Separation
CEO	Chief Executive Officer
Chromosome	An organized structure of DNA, protein, and RNA found in cells.
DNA	Deoxyribonucleic acid, a self-replicating material present in nearly all living organisms as the main constituent of chromosomes.
DRL	Driven Right Leg
HOS	Higher Order Statistics

IC	Independent Component
Kurtosis	is any measure of the peakedness of the probability distribution of a real-valued random variable.
MUAP	Motor Unit Action Potential
Myoelectric	Electrical signals created during the contraction of a muscle.
PC	Personal Computer
PCB	Printed Circuit Board
RMSE	Root Mean Squared Error
SPI	Serial Peripheral Interface
Statistical Independence	Two events are independent if the occurrence of one does not affect the probability of the other.
Synergist	A muscle that performs, or helps perform, the same set of joint motion as the agonists.
Transradial Amputee	Amputation anywhere below the elbow.
ICA	Independent Component Analysis is a blind source separation algorithm capable of separating source signals from a linear mixture of the signals without any prior knowledge of the signal mixing.
MVC	Maximum Voluntary Contraction: this is the maximum force a subject can exert during an isometric contraction.

1 Introduction

This chapter gives a brief background to the study and the problem to be investigated. It also outlines the structure of the document and briefly describes each of the subsequent chapters.

1.1 Background to Study

The human hand is a marvel of the biological world, it is the tool that humans use to interact and interface with the world around them. Without this dexterous and multipurpose tool, menial everyday tasks become incredibly difficult to accomplish. This is the plight of many upper limb amputees.

In many cases the patients suffering from these afflictions still have full or partial use of the muscle groups in the forearm and upper arm. It is often still possible to access the activity of these muscles using a form of bio-signal acquisition called Electromyography.

Electromyography (EMG) is typically a differential measurement scheme aimed at picking up small electrical changes in muscle activity. It is most often used in evaluating and recording skeletal muscles [4]. However, it is possible to use EMG as a control signal for robotic prostheses that could emulate all or at least most of the functionality of the human hand. Ideally this form of prosthesis or orthotic would be as non-invasive as possible and allow for personalized adaption to individual wearers.

Unfortunately current commercial prosthetic and orthotic devices in use are mostly unintelligent and under-actuated, giving the user limited control and functionality. However, this is all changing, as research into so called "active prostheses" is on the rise [5, 6]. Unfortunately in terms of developing a fully functioning hand and arm, capable of complex gripping and maneuvering, current technology is stunted by control and power issues. One of the main hurdles in development is accessing all the information sent to the forearm via the nervous system and discerning the correct control action. Until recently it has been difficult to attain deep tissue muscle activity, which was usually obtained using fine wire intramuscular electrodes [7].

Ideally it would be advantageous to develop a non-invasive acquisition and control system capable of inferring all muscular activity in the targeted muscle group. This would allow for a natural and intuitive robotic prosthesis.

1.2 Problem to be Investigated

The current state of the art research in EMG controlled prosthetic and robotic orthotics rely on surface EMG electrodes carefully placed above muscle bellies to reduce cross-talk from neighbouring muscles and acquire reliable signals. However, this approach has the downside of being unable to access deep tissue muscle activity. Deep tissue muscle activity has traditionally been acquired with the use of fine wire electrodes [7, 8].

Recent research at the University of Cape Town (UCT) Bio-Medical Engineering Department has now made it possible to detect deep tissue muscle activity by a novel sEMG configuration and Independent Component Analysis (ICA) procedure. The system was proposed by Dr L. John [2, 1] and will be discussed later in section 3.3. In the preliminary study, a 12 electrode configuration was used. This configuration had two sets of electrodes placed over the bicep and tricep according to best practices from seniam.org [9] and then the remaining electrodes were spread evenly around the upper arm.

This study will start by replicating the results of [2] and as such will focus only on ICA as an algorithm for source separation and sEMG as a method of muscle activation capture. The study will look to further expand the knowledge on electrode placement and quantity in this ICA sEMG based system.

To complement the study and improve the portability of the testing equipment, a custom frontend electronic design will be produced. The frontend analog system will interface with a microcontroller unit and allow for seamless real-time logging of the EMG data to a central laptop or PC.

In this study, the effect of electrode quantity and placement on signal reception will be investigated. These data could then be used to determine optimal electrode placement regions and electrode quantities. Ideally an optimal solution would be one that produces quality signals with the use of the least number of electrodes possible. Fewer electrodes would reduce the computational load on the system and require less data.

1.3 Purpose of Investigation

In previous research performed in the Bio-Medical Engineering (BME) division at UCT, they proposed that one could extract meaningful muscle activity from deep muscle bellies using a combination of two bands of expertly placed monopolar EMG electrodes and a statistical Blind Source Separation (BSS) algorithm called Fast Independent Component Analysis (FastICA) [10]. However, this research was a proof of the deep muscle EMG extraction concept, and further investigation is necessary to see how electrode placement and number could affect performance.

In this study it is proposed that an optimal electrode number and placement can be determined using FastICA and Genetic Algorithms to potentially reduce the number of electrodes necessary in a prosthetic system.

1. Aim 1: Determine if a Genetic Algorithm can effectively optimize electrode positioning and produce a system that uses fewer electrodes but achieves similar performance. Ideally the investigation will lead to a minimally optimal electrode system for non-invasive recording of deep brachialis muscle activity. See subsection 6.1.2.
2. Aim 2: Determine whether it is possible to propose a general electrode configuration for a particular muscle group across multiple subjects. Ideally, such a solution would be based on similarities in muscle structure and location across all the subjects. See subsection 6.1.3.
3. Aim 3: Design and build a self contained EMG acquisition system

1.4 Assumptions

To attain valid results some assumptions need to be made:

- EMG data acquired meets the requirements listed in the ICA section of literature review.
- The test subjects will be assumed to have no history of neurological or muscular disease or impairment.

1.5 Plan of Development

This dissertation presents the design and validation of a system for detection of deep-tissue EMG activity using only noninvasive electrodes. Further more it presents a method to optimize electrode placement and number of electrodes using a simple genetic algorithm.

The document begins with a brief introduction to and motivation for the study. It then segues into the technical background chapter where the technology and terminology used in this research is discussed. This serves to better acquaint the reader with the subject material. Then a literature review chapter is presented, in which similar works and commercial systems are discussed and focus is drawn on why this research was carried out.

The experimental arrangement and the methods used to gather data from the group of subjects are then presented and discussed in Chapter 4. After which the design and implementation of the hardware system used for data acquisition is reasoned about and discussed in Chapter 5.

Finally in Chapter 6 a discussion on the analysis of the gathered data and the results obtained from these data are presented. The research is rounded off in chapters 6 and 7 with a discussion on conclusions drawn from the results and then recommendations are made on how further extensions to this research could be carried out.

2 Background

In this chapter the background knowledge and ideas that are key to understanding this research are discussed. The field of Electromyography is briefly introduced followed by an introduction to the structure and anatomy of the upper arm. Fnally a discussion and explanation of the two algorithms used in this research, namely Independent Component Analysis and Genetic Algorithms is carried out.

2.1 Electromyography

Electromyography is a bio-signal recording technique used for evaluating electrical activity produced by skeletal muscles. This electrical activity is produced by physiological changes in muscle fiber membrane during a muscle contraction.

A muscle contraction is a combination of many motor unit activations. These motor units are defined as one motor neuron and all the muscle fibers it innervates. When a muscle contraction occurs and a motor unit fires, an impulse called an action potential transmits down the motor neuron to the motor unit end plate [11]. The entire process of electrical activity within a motor unit is known as a motor unit action potential or MUAP. Usually a single EMG signal is comprised of several different MUAPs, this process is graphically represented in Figure 2.1.

The characteristic surface EMG produced by a MUAP lasts about 3 - 15 ms and has a voltage range of between 20 - 2000 μV [12]. Several of these MUAPs are activated to create a useful muscle contraction. Continuous activation of the MUAPs is known as a Motor Unit Action Potential Train or MUAPT, and forms the continuous EMG signal which is seen at sEMG electrode sites.

Characteristic EMG signals have a peak-to-peak amplitude of $0 \rightarrow 10\ mV$, with most of the usable signal energy contained in the $0 \rightarrow 500\ Hz.$ In that bandwidth, the dominant signal energy is contained in the range from $50 \rightarrow 150\ Hz$ [13].

Currently EMG acquisition is done in one of two ways, surface EMG or fine wire EMG. The first method is the use of surface electrodes to pick up tiny changes in electrical activity on the skin surface above the muscle during contraction. For this process to be effective the skin surface first needs to be cleaned and a conductive solution is applied between the electrode and the skin [11].

These surface electrodes present a convenient solution to EMG acquisition as they are non-invasive and do not require a physician to place the electrode. The negative

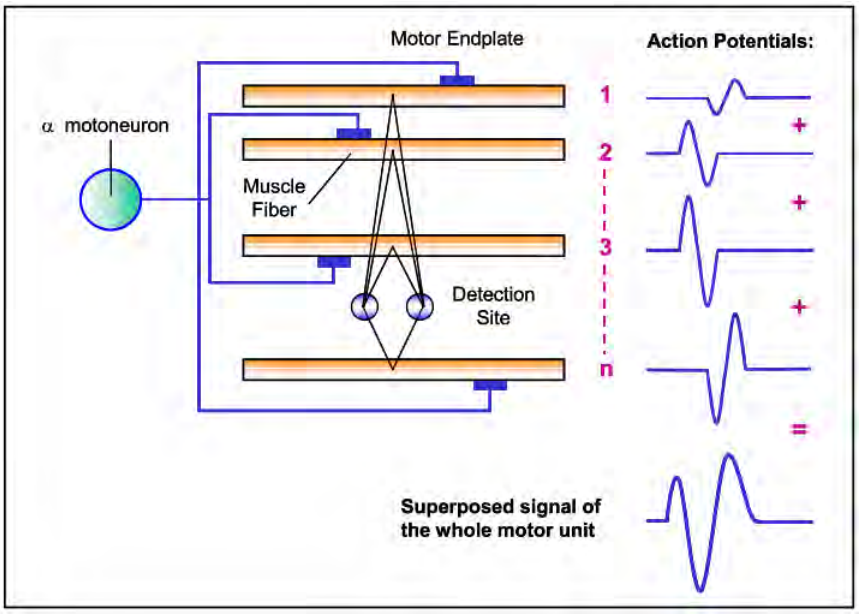

Figure 2.1: Graphical description of the composition of several Motor Unit Action Potentials (MUAP) to make up a EMG signal. Adapted from [11].

aspects of this method is that the signals are subject to cross talk between muscles sources as well as signal degradation due to the underlying tissue variability and thickness [11]. This is further explained in Figure 2.2.

For surface electrodes there are two configurations, namely monopolar or bipolar. In the bipolar configuration, there are 2 electrodes per instrumentation amplifier (IN-amp) [14]. One electrode connected to the negative input of the IN-amp and the other connected to the positive input. Each of these are then, by design, referenced to the Driven Right Leg (DRL) or virtual/body ground. This configuration allows you to reduce the common mode signals between these two electrodes [15, 13].

Monopolar electrode configurations differ in that all the negative inputs of the IN-amp channels are connected together to form one common electrode. This electrode is then placed on an bio-electrically inactive area, similarly to that of the DRL or ground electrode. What this means is that none of the common mode signals are removed by the differential inputs of the IN-amp [14]. This allows much more crosstalk to be introduced into the system.

Cross talk is the additive affect or interference of myoelectric activity from neighbouring muscles, this is especially relevant for sources that are tightly grouped. Typically for most muscle groups the cross-talk effect will only additively inject less than 15% of the overall signal content [11]. In large muscle groups, cross talk can be significantly reduced by well placed electrodes. An additional drawback to surface electrodes is that they are not able to reliably detect deep tissue muscle activity.

The second method commonly used is intra-muscular electrodes. In this method

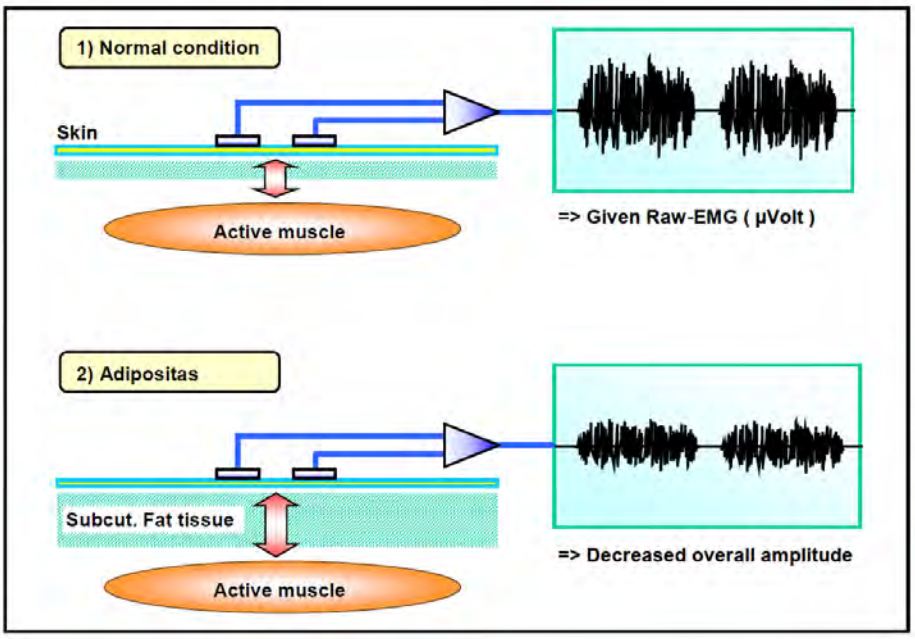

Figure 2.2: The influence of varying tissue thickness on EMG signal quality. Given the same amount of signal activity, condition 1 produces greater EMG magnitudes because the signals have to travel through less subcutaneous fat tissue. Image adapted from [11].

the needle or fine wires are surgically inserted into the muscle being studied, this allows one to position the electrode directly at the source, in the deep tissue, see Figure 2.3. This reduces the influence of cross talk in the measurements [14].

Fine-wire EMG only records the activity of a few motor units at the needle site as opposed to surface EMG which measures compound activity of many motor units [16].

Another disadvantage of fine-wire EMG is its repeatability, as the needle is difficult to position. Often a trained clinician is needed to position the electrodes. Additionally this method is uncomfortable to the user as the needle or fine wire can cause tightness or spasticity in the muscle [16]. It is for these reasons that this method is traditionally used when the analysis of specific motor units is required.

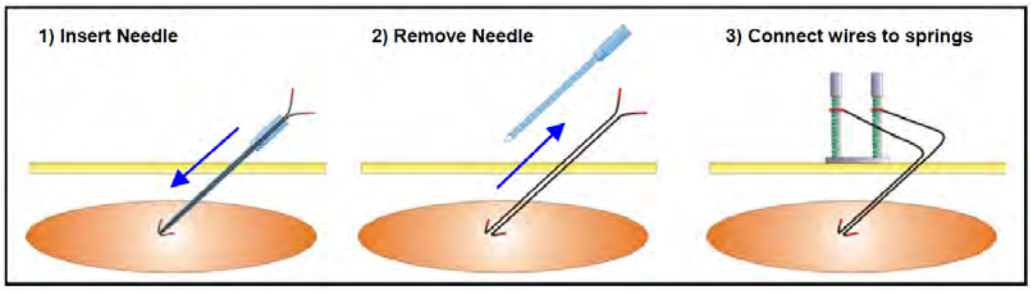

Figure 2.3: Insertion of fine wire electrodes for intra-muscular electrodes. After removing the needle, the distal endings of the wires are connected to steel spring adapters, which are then connected to the regular EMG pre-amplifier. Image adapted from [11].

2.2 Upper Arm Anatomy

For the purpose of this study experiments were conducted on the muscle group contained in the upper arm. This was based on the muscle selection by Moroaswi and John [2] as it allowed for relative isolation of the deep versus superficial muscle activity. It also represents a group of muscles that are in relatively close proximity, so it proves a good testing ground for the efficacy of the algorithm and allows the ability to investigate electrode placement fairly easily without many cofounding factors.

This muscle group consists primarily of 4 independent muscles, namely bicep brachii, coracobrachialis and brachialis occupying the anterior compartment of the Brachium or arm, and the triceps brachii occupying the posterior compartment [18].

The coracobrachialis is small muscle that extends from the tip of the Coracoid process of the scapula to the medial side of the mid shaft of the humerus. It flexes the arm about the shoulder joint [19]. Since the electrode band will be positioned midway between the elbow and the shoulder joints, the affect of the coracobrachialis are considered minimal as the electrodes are positioned roughly over the insertion of this muscle's tendon into the humerus. Additionally, the movement protocol used during the experiementation, has been designed so that no shoulder movement occurs, so the coracobrachialis should have very limited activation potential.

The bicep brachii comprises of two heads. The short head of the muscle starts from the Coracoid process in conjunction with the Coracobrachialis and the long head originates as a tendon from the supraglenoid tubercle of the scapula. Both of these attachments can be seen in Figure 2.4. These two heads then converge into a single tendon that connects to the radial tuberosity [19].

The bicep brachii is a strong flexor of the distal portion of the arm. It is largely responsible for flexion of the forearm at the elbow joint. Additionally it is the most powerful supinator of the forearm when the elbow joint is flexed [19].

The largest muscle in the upper arm group is the triceps brachii. The triceps consists

Table 2.1: Table of Upper arm muscles, their insertions, Origins and actions. Table adapted from [17].

Anterior Compartment						
Muscle	Origin	Insertion	Artery	Nerve	Action	Antagonist
Coracobrachialis	coracoid process of scapula	medial humerus	brachial artery	musculocutaneous nerve	flexes humerus	-
Biceps Brachii	Short head: coracoid process of the scapula. Long head: supraglenoid tubercle	radial tuberosity	brachial artery	Musculocutaneous nerve	flexes elbow and supernates forearm	Triceps Brachii muscle
Brachialis	Anterior surface of the humerus, particularly the distal half of this bone.	coronoid process and the tuberosity of the ulna.	radial recurrent artery	musculocutaneous nerve	flexion at elbow joint	-
Posterior compartment						
Muscle	Origin	Insertion	Artery	Nerve	Action	Antagonist
Triceps Brachii	Long head: Infraglenoid tubercle of the scapula. Lateral head: posterior humerus. Medial head: posterior humerus	olecranon process of ulna	Profunda brachii	radial nerve	extends forearm, caput longum and adducts shoulder	Biceps brachii muscle
Anconeus	Lateral epicondyle of the humerus	lateral surface of the olecranon process and the superior part of the posterior ulna	Profunda brachii, recurrent interosseous artery	radial nerve	Partly blended in with the triceps, which it assists in extension of the forearm. Stabilises the elbow and abducts the ulna during pronation.	-

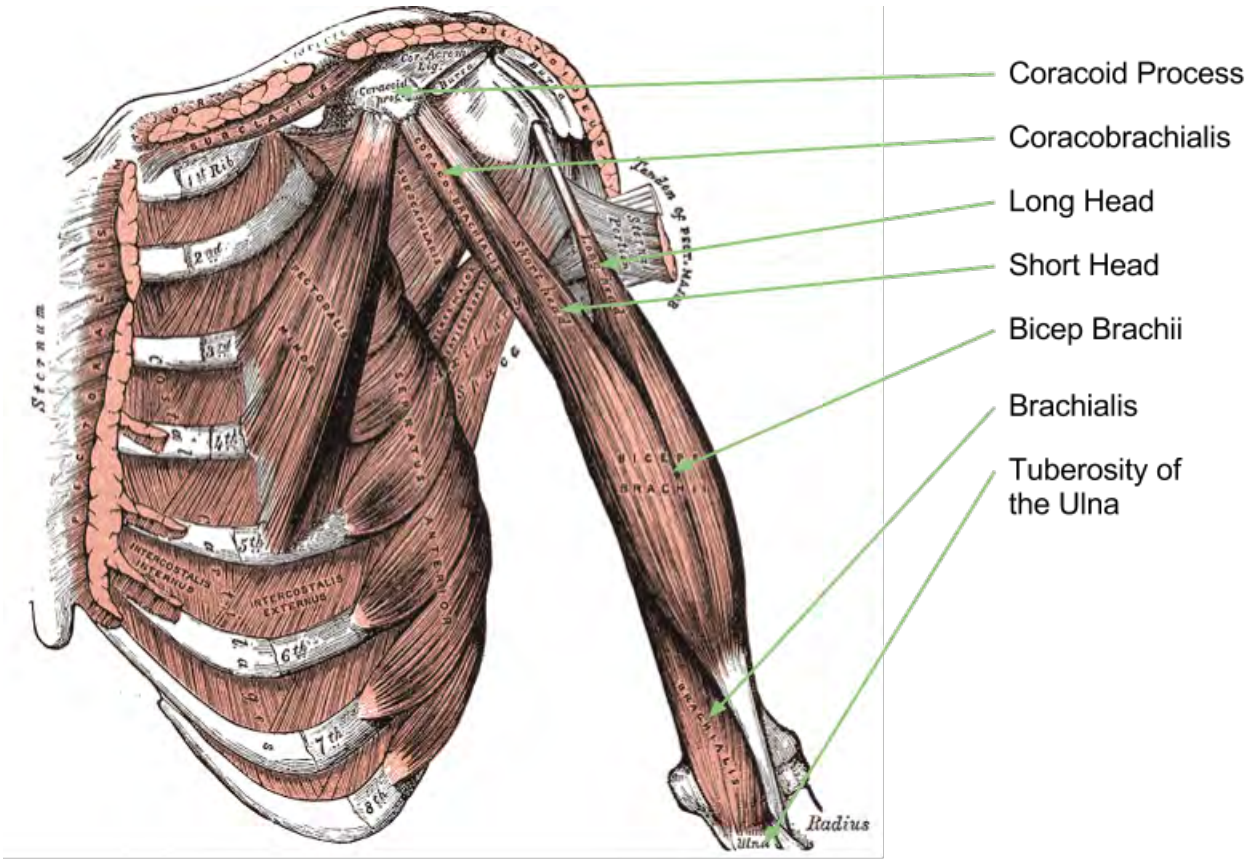

Figure 2.4: View of muscles in the anterior compartment of the right arm. Image adapted from [20].

of three heads (long head, medial head and lateral head) and is the only muscle in the anterior compartment of the arm. The triceps is an antagonist to the biceps brachii and is responsible for the extension of the forearm about the elbow joint [21].

In the case of the bricep brachii and tricep brachii, it is assumed that the individual heads of the muscle are activated together and are dependent. So together they form only two independent sources, namely bicep and tricep, not five sources.

Finally, the brachialis originates from the lower half of the anterior side of the humerus, near the insertion of the deltoid muscle and converges into a tendon that inserts into the tuberosity of the ulna and the coronoid process. The brachialis is a synergist that lies deeper in the posterior compartment behind the bicep brachii, see Figure 2.4. It assists the bicep brachii in the flexion of the forearm about the elbow joint [20]. It seems the brachialis becomes more readily activated during isometric elbow flexion whereas during dynamic flexion, the bicep becomes more activated than the brachialis [22].

In Figure 2.5 it can be seen how the brachialis muscle belly is positioned behind the biceps brachii in the deep tissue. Additionally it can be seen that these relatively

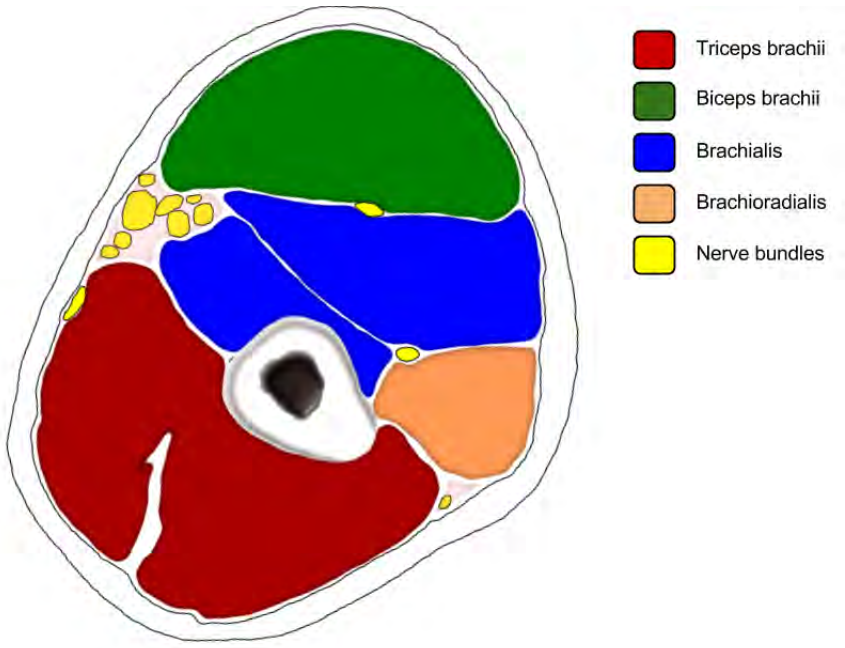

Figure 2.5: Cross sectional view of the upper arm. Image adapted from[23].

large muscles are tightly packed, causing the impact of crosstalk to be high. The crosstalk and signal integrity is worsened by excessive subcutaneous fat layers [24, 25], as was mentioned in section 2.1, making this an excellent candidate muscle group to analyze with the ICA separation algorithm.

In Figure 2.5 an additional muscle, the brachioradialis, can be seen. This was not mentioned above because this muscle is largely associated with the forearm muscle group, but its head originates from the lower half of the humerus. The image used for this cross section is cut at the lower third of the upper extremity, so one can see the head of the brachioradialis present, however, in the experiments conducted in this research, the band is situated higher up the arm than this cross section.

2.3 Independent Component Analysis

In recent years much research has gone into the development of Blind Source Separation algorithms. BSS algorithms perform unmixing filter estimation despite having no knowledge about the true mixing filter [26]. This allows one to separate multiple mixed signals into their original signals without knowing the nature of the original signals. One of the most popular BSS algorithms receiving attention in the bio-medical field is Independent Component Analysis (ICA). ICA is a statistical separation algorithm that uses higher-order statistics (HOS) of the data to minimize the dependence of components on the system output [24]. The basic idea behind

ICA is that given some linear mixing model:

$$x = As \tag{2.1}$$

where A is an $N \times M$ scalar matrix representing the unknown mixing of the source signal, x is the vector of N observed sensor signals and s is a vector of M unknown source signals. The ICA algorithm tries to find a linear transformation W that accurately inverts the mixing process so that one can estimate the source signals from the sensor signals x, as shown:

$$\hat{s} = Wx \tag{2.2}$$

where $\hat{s}$ is a vector of the estimated source signals. The sources are exactly recovered when W is the inverse of A up to a permutation and scale change [24]. In the algorithm, W values can often be seen to be minimized to near zero, in this case, one can interpret that the x signals associated with these weights are inconsequential to the reconstruction of the source signals. A systems block diagram of the mixing and unmixing can be seen in Figure 2.6.

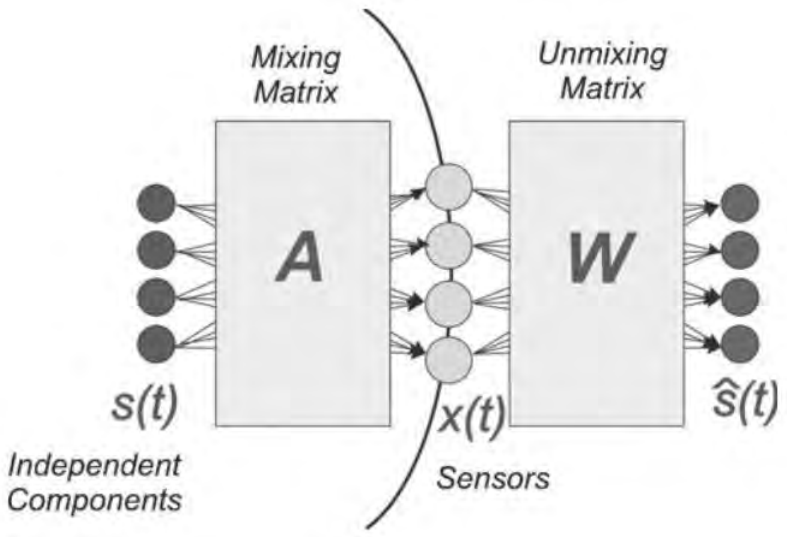

Figure 2.6: The general ICA process block diagram. Here *s(t)* is the independent source components, *x(t)* is the sensor measurements assumed to be a linear mixture of the independent sources. Matrix A is the linear mixing matrix. Matrix W is the estimated inverse matrix of A responsible for reproducing the source signal estimates $\hat{s}$. Diagram adapted from [27].

To make the ICA algorithm more tractable a few basic assumptions are made. Some of the more important assumptions are listed below:

- *Linear Mixing:* For the above equations to hold, the assumption of linear mixing is used. In a bio-signals context, this linear mixing assumes instantaneous

mixing of the sources using a simple superposition of the attenuated sources at the sensor [27], which is reasonable for signals traveling as quickly as EMG.

- *Noiseless Mixing:* Another simplifying assumption is that the signals have no additive sensor noise. While this may seem unrealistic in a practical implementation, it is a valid assumption because it allows ICA to separate the sources of interest even if the separated sources themselves remain contaminated by measurement noise [27].
- *Square Mixing:* In most classical ICA problems, the mixing matrix is assumed to be square meaning that there are an equal number of sources and sensor channels. This assumption makes the computation more tractable and is a valid assumption in EMG provided it is possible to increase the number of sensor channels in the system to match the number of muscle sources.
- *Stationary Mixing:* Another common assumption is that statistically the mixing matrix A does not vary with time. For example the sensors do not move spatially relative to each other, so the mixing remains constant with time.
- *Statistical Independence:* Finally one of the most important assumptions made in ICA is that the sources are statistically independent. Two signals/sources are independent if the occurrence of one signal does not make it more or less probable that the other signal occurs. More correctly this means that the two random variables (sources) are uncorrelated and have no higher order correlations [27].

Along with these assumptions, ICA also has some drawbacks or limitations but these are not insurmountable and can easily be remedied with help of *a priori* knowledge of the system. Some of the limitations imposed by the ICA are (a) it is not possible to determine energies nor signs of the source signals and, (b) it is unclear as to the ordering of the sources at the output [27].

One of the most referenced ICA algorithms in the literature is the FastICA developed by A. Hyvärinen at the Helsinki University of Technology [28]. This is an efficient algorithm based on a fixed-point iteration scheme which estimates the unmixing matrix by maximizing the non-Gaussianity, using kurtosis as a measure of statistical independence [28]. The core of the FastICA algorithm is a one unit process which estimates the weighting of one vector in the unmixing matrix, thereby giving one of the Independent Components (IC).

This iterative algorithm finds the "direction" of a weight vector i.e. a unit vector $\boldsymbol{w}$ such that the projection $\boldsymbol{w}^{\mathbf{T}}\boldsymbol{x}$ maximizes non-Gaussianity [29]. The basic form of the FastICA algorithm is as follows:

1. Choose an initial (e.g. random) weight vector $\boldsymbol{w}$
2. Let $w^{+} = E\left\{xg(w^{T}x)\right\} - E\left\{g'(w^{T}x)\right\}w$
3. Let $w = \frac{w^{+}}{\|w^{+}\|}$

4. If not converged, go back to 2.

Here, $g(u) = \tanh(a_1 u)$ and $g'(u) = u \exp(\frac{-u^2}{2})$, where $1 \leq a_1 \leq 2$ but more often than not a_1 =1. $g(u)$ is known as a contrast function.

Note convergence is achieved when the old and new values of $\boldsymbol{w}$ point in the same direction, i.e. their dot-product is nearly equal to 1 [29].

Therefore several of these one unit processes can be used to estimate the entire unmixing matrix, provided each of the ICs are decorrelated with one another so that the possibility of finding the same component again is eliminated [10]. Decorrelation can be achieved simply using a deflation scheme based on a Gramn-Schmidt-like decorrelation [30]. Further details of the FastICA algorithm implementation and parameters is given in subsection 5.4.2.

2.4 Genetic Algorithms

Evolutionary Computations or Algorithms are a set of computer programs which mimic biological process to perform some kind of computation. A subset of these algorithms are the Genetic Algorithms (GA). Genetic Algorithms are an approximate way of solving optimization problems, using a mechanism very similar to biological evolution. Much of the theory of Genetic algorithms is based on the work and theories of Charles Darwin, as published in his well-known work *"The Origin of Species By Means of Natural Selection or the Preservation of Favoured Races in the Struggle for Life"* [31].

In its simplest form a genetic algorithm consists of a population with a binary mask, a selection technique, a crossover operator and a mutation operator [32]. This is often referred to as the canonical Genetic Algorithm or Simple Genetic Algorithm (SGA). There are multiple variations and improvements to the canonical version of the algorithm including island model/parallel, hybrid and messy GAs, but these are far beyond the scope of this research and as such will not be discussed here.

The Simple Genetic Algorithm is an iterative procedure which traditionally operates on a population of constant size. Initially the population of solutions (or Genome) is created randomly [31]. Each row of this population is a solution and is represented by a binary string of a set length. The 1's and 0's and their interaction in the bit string are analogous to strings of DNA in a chromosome. Each one of these bits represents a characteristic/feature of the solution.

During each iterative step, known as a generation, this population of bit string solutions is evaluated. A flow chart of a SGA is shown in Figure 2.7, the inner loop depicts one full iteration or generation. Each solution is evaluated by a fitness function (also known as a cost function). This fitness function assigns a fitness to each individual, the fitness of an individual solution then determines the probability of that particular solution to breed with another solution. Therefore the fitness of

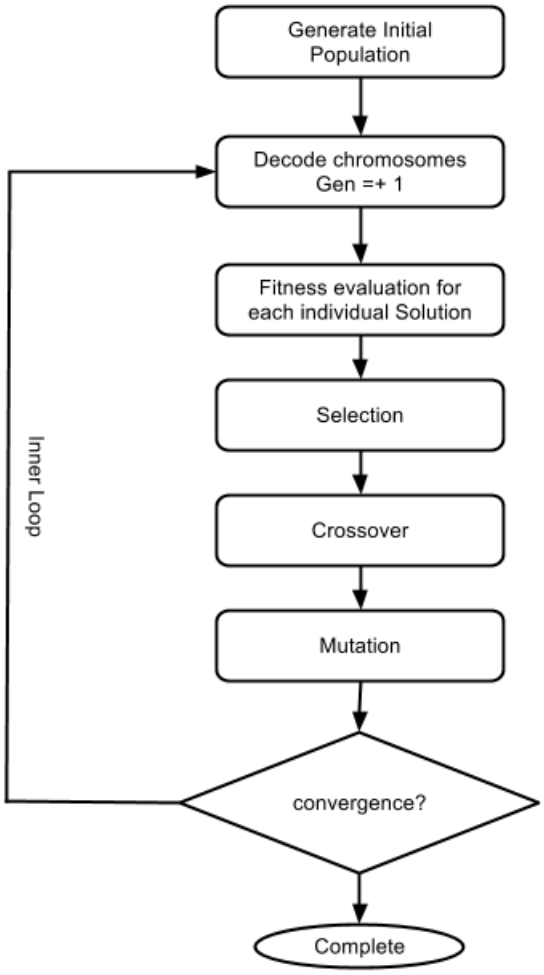

Figure 2.7: Flow diagram of Canonical Genetic Algorithm. Adapted from [32].

a particular solution determines the solutions ability to pass its genetic information or features on to the subsequent population.

In the canonical form, the main algorithmic process happens in the inner loop in the processes called *selection, crossover and mutation.*

Selection is the process of selecting how often and with whom each solution will breed. There are multiple different strategies for selection.

The selection method commonly associated with SGA is Proportional Selection (also known as Roulette wheel selection). In this strategy the expected number of descendants for an individual solution i is given as $p_i = \frac{f_i}{\overline{f}}$ with $f : S \to \mathbb{R}^+$ denoting the fitness function and $\overline{f}$ representing the average fitness of all individuals in the population [31].

This selection thus allows an individual to produce a number of children in the next generation which is proportional to it's fitness relative to the population average fitness. It is analogous to spinning a roulette wheel, where sections of the wheel are represented by solutions and the size of these sections are proportional to the solutions fitness. A random spin of the wheel will select one individual to be used in the reproduction.

Therefore, fitter individuals with larger portions of the wheel will have more opportunity to create children in the subsequent population.

However, roulette wheel methods have been known to have poor performance when a particular individual has a very large fitness in comparison to the average. Resulting in a loss of diversity in the population as this super-individual overwhelms the population. This lack of diversity in the solutions population is often called stagnation, or premature convergence, and results in a plateau in solution fitness. This is often a cause of a poorly performing GA as it results in the algorithm returning a shallow local minima, far from the global minima the algorithm is searching for.

Other popular selection methods are rank selection and Tournament selection. In rank selection, each solution is ranked or sorted according to its fitness relative to the entire population [33]. In this method the most fit individual will have a rank of N, the second most fit, N-1 and so on. The worst solution having a rank of 1. In this way rank based methods can lessen the influence of super-individuals and maintain a constant selection pressure [33].

In tournament selection, a group of n solutions or individuals are selected at random and made to compete with each other on fitness [31]. This is most often done with *n=2* (binary tournament*)* and the more fit individual is selected to join the new population [33]. Tournament gives all individuals a chance to be selected and in this way preserves diversity, sometimes at the loss of covergence speed [33].

Another fitness proportionate selection (FPS) method is stochastic universal sampling (SUS) algorithm, which is actually just a variation of the roulette wheel selection. SUS works by only spinning the roulette wheel once, but having multiple sample points which are evenly spaced. This has been illustrated in Figure 2.8. The advantage of SUS is that it is an optimal algorithm as it has zero bias and minimal

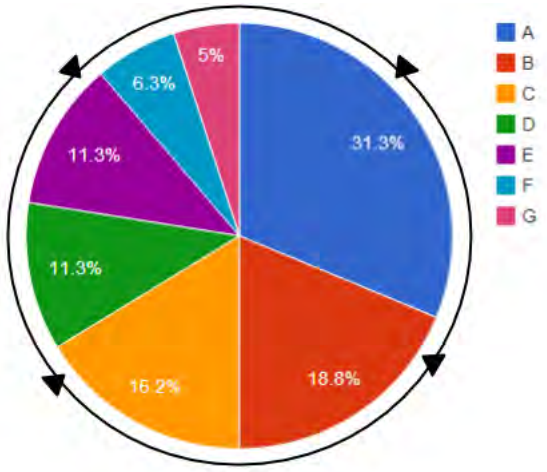

Figure 2.8: Illustration of Stochastic Universal Sampling (SUS) Algorithm. Here the black arrow heads represent the 4 selection points resulting in individuals A,B,C and E being selected to reproduce.

spread [34]. These properties allow SUS to make selections without losing diversity and allowing one individual to dominate.

After selection has taken place, the selected chromosomes/individuals have to breed a new population. The creation of the new population is done via two genetic operators, crossover and mutation.

The primary genetic operator for creating new unique children is called crossover or recombination. In the binary version of SGA this is done simply with either 1-point or 2-point crossover. Both of these techniques involve selecting a sub-string of bits from the one parent using randomly selected indices along the chromosome and placing that sub-string in the same position in the second parent. This has been demonstrated graphically in Figure 2.9.

Both of these crossover techniques allow for the preservation of smaller sub-strings or "features" of the parents which when combined will hopefully produce a child that is a fitter solution than it's parents.

The second genetic operator is mutation, which acts on the newly formed child chromosome. This operator is essentially a randomized modification of the chromosome. In the case of binary chromosomes mutation is normally just an arbitrary flipping of bits in the string with a certain probability called the mutation rate [31].

Mutation allows undirected and random jumps in the solution space, introducing new "traits", not in the original population, into the newly created population. This "jumping" around the solution space sporadically helps prevent the algorithm from converging too fast and hindering sampling/exploring most regions of the solution space [32].

The last piece of the SGA puzzle is the convergence check. Convergence depends

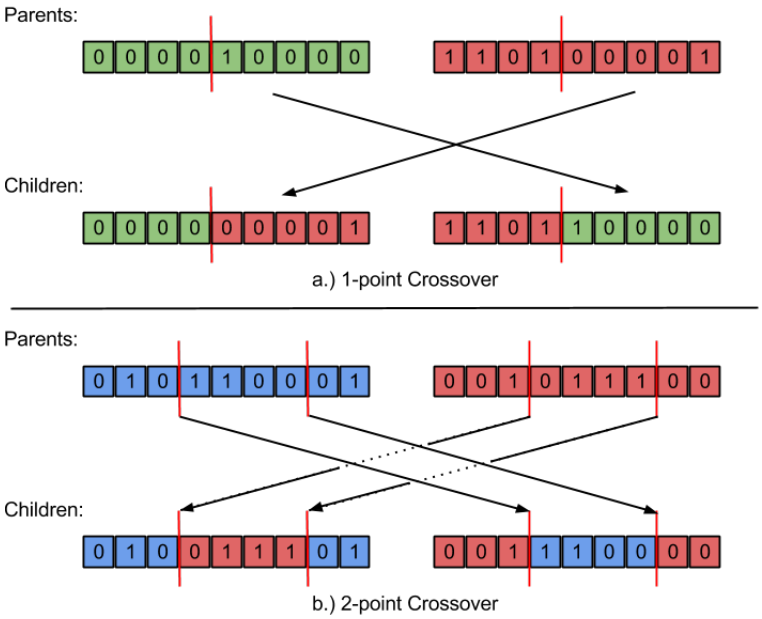

Figure 2.9: Crossover techniques used in Simple Binary Genetic Algorithm. (a) is a 1-point crossover producing two new children to be entered into the next population. (b) Shows a 2-point crossover method.

on whether an acceptable solution is reached or a set number of iterations is exceeded [32]. A "reasonable" solution is reached when there is no significant change in solution performance (usually populations average fitness) from generation to generation.

What this means is that all of the solutions are in a similar valley or area in the solutions space, and only mutation would be able to create new solutions outside of this valley and possibly improve performance. Unfortunately mutation is a subtle genetic operator, normally only affecting 1%-5% of all bits in all solutions. So one would have to wait very long for this operator alone to produce a fitter solution. So at this point it is often best to stop and return the fittest solution as the global solution.

3 Literature Review

In this chapter recent advances in assistive robotics and electronics are considered and investigated. The first two sections look into developments in EMG driven exoskeletons and protheses, while the third section expands on research in the area of EMG signal separation and classification. Finally, the state-of-the-art consumer solutions are discussed and evaluated.

Assistive robotics mainly comprise of two classes, namely orthotics/exoskeletons and prostheses. Prostheses being electro-mechanical parts which replace a human body part and its function, while orthotics or exoskeletons augment the body part by attaching to the body part externally and assisting it to perform function, these are often referred to as exoskeletons [6]. In the following two sections each of these classes are explored.

3.1 EMG driven Exoskeletons or Orthotics

Many exoskeleton systems have been developed in recent years with varying control schemes. Some of these systems include Infrared Cameras for sensing joint angles [35], inertial measurement units (IMU) allowing for kinematic assistive exoskeletons [36]. Other systems use a combination of pressure and IMUs to detect the users volition and the exoskeleton assists that motion [37, 38]. However, by far the most widely used control input for upper extremity exoskeletons is EMG.

Largely the research dedicated to EMG controlled exoskeletons is focused on rehabilitative or assistive systems which focus on assisting hand and wrist movement in stroke patients and patients that have partially lost ability to properly control their musculature [40]. Much of this research is focused on the design and safety of the actual mechanical orthotic and often a basic EMG control scheme is used.

Often these systems focus on 1 or 2 constrained degrees of freedom (DoF) [41, 42, 40] and thus only need to use a few well placed electrodes. This allows them to avoid the problem of muscle crosstalk, provided the select muscles with large, easily locatable muscle bellies.

At the Technical University of Berlin, Wege and Zimmermann, created a 4-DoF, full hand orthotic exoskeleton, see Figure 3.1, which used 10 EMG electrodes to detect 5 of the superficial muscles in the forearm associated with hand movement [39]. Their

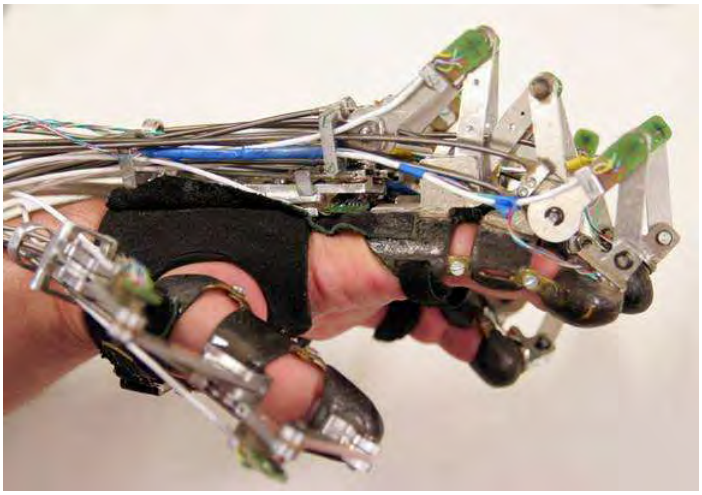

Figure 3.1: Full hand rehabilitative exoskeleton developed at the Technical University of Berlin, German, by Wege and Zimmermann, 2012 [39].

system additionally uses force and angle sensors to assist with correct movement of the hand.

Wege and Zimmermann also noted that it was not possible to access all the muscles responsible for hand motion as many of them lay under several layers of tissue. Additionally they ran into the problem of high density of muscles in a small space which leads to signal mixing at the surface electrodes [39]. They overcame the mixed signal problem partially by using a blind source separation method called EASI [43]. One of the noted limitations in Wege and Zimmermann's system was that electrode placement was critical and a very time consuming procedure.

3.2 EMG driven Prostheses

The design and control of robotic or "active" prostheses is very closely aligned with that of the above mentioned exoskeletons, however, much more development has gone into control with and classification of EMG signals.

There are various implementations which use either Support Vector Machines (SVM) [45, 44, 46] or Artificial Neural Networks (ANN) [47, 48], with varying levels of success in controlled environments often using only isometric muscle contractions.

Additionally many of these prosthetic control systems focus on On/Off types of control and do not allow one to finely control digits or joint angles. However, there are systems that are starting to overcome these problems such as the Anthropomorphic controlled hand prosthesis system (pictured in Figure 3.2) developed at Harbin Engineering University, China. This system aims to allow near natural control of the prosthesis using a system of hierarchical controllers, a low level controller to reflexively adjust grip and a high level controller using SVM algorithm to process EMG

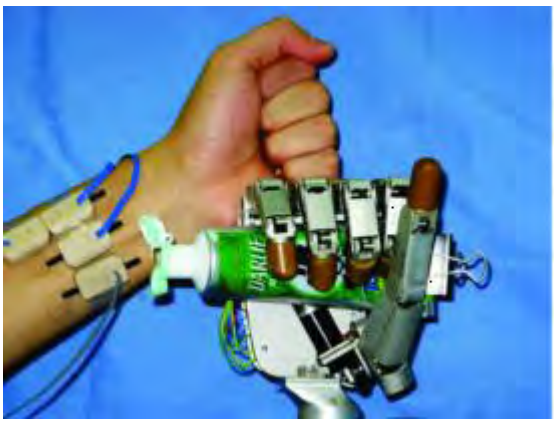

Figure 3.2: Robotic prosthetic hand developed at Harbin Engineering University, China, by Huang *et al.* [44].

movement intentions from three forearm muscles to provide the subject–prosthesis interface control with electro-cutaneous sensory feedback (ESF) [44].

This allows the system to achieve 10 different gripping and pinching postures, however, the training time for this SVM seemed to be extremely time consuming and would need to be improved before it could be used out of the lab environment.

Research conducted by C. Cipriani *et al.* involved creating a control system that allowed the trans-radial amputee to effectively and intuitively/naturally control the robotic hands digits. This was achieved using a *lazy Learner* [49] controller that was trained using a data glove on the opposite (healthy) hand of the user.

The user then repeated 7 different gestures with both hands, and the output of joint angles from the data glove was used to train the SVM system to respond to EMG signals in the correspondingly correct way. This system used EMG data from 8 electrodes carefully placed above the relevant forearm muscles and was tested on 5 amputees and 5 able-bodied subjects. The system was able to classify individual finger movements with an average of 89% accuracy in the able bodied subjects and with a lower accuracy of 79% for amputees.

3.3 Developments in EMG Separation and Classification

Although EMG controlled prostheses and orthotics have been the subject of research for many years, they are still limited in functionality and often confined to a controlled lab environment. Most of the commercial prosthetic hand control systems are not much better, usually only capable of performing closing and opening of a hand and not much fine control is possible.

3.3.1 ICA applied to EMG signals

In Taylor's [50] research he proves that ICA can effectively reduce crosstalk between the forearm muscles and even detect muscle activity from deeper tissue muscles, namely flexor digitorum superficialis. He then used the output of this ICA to feed an Artificial Neural Network (ANN) for the classification of 4 different gestures. Again this had limited functionality as not enough muscles were isolated for use in the complex gesture classification.

Research done by G.R. Naik [51] has indicated that ICA is a viable method of EMG crosstalk reduction, in this research they investigate the benefits of having a fixed unmixing matrix for an individual. This fixed unmixing matrix circumvents the problem of source order determination discussed in section 2.3. In this research ICA was considered viable because sEMG satisfies a number of assumptions for ICA to function correctly. However, in this research they do not compare ICA to another form of crosstalk reduction. Rather they do a comparison of the output of their neural network, given raw sEMG and ICA processed sEMG. The neural net is taught to classify four different hand gestures, this learning process was aided by a data glove, equipped with joint angle sensors. This glove was worn by healthy patients and the performance of the classification was compared to the position of the fingers determined from the data glove. This study validates that sEMG crosstalk can be reduced by ICA, but is limited in its exploration of how much better or worse this method is relative to existing crosstalk reduction methods.

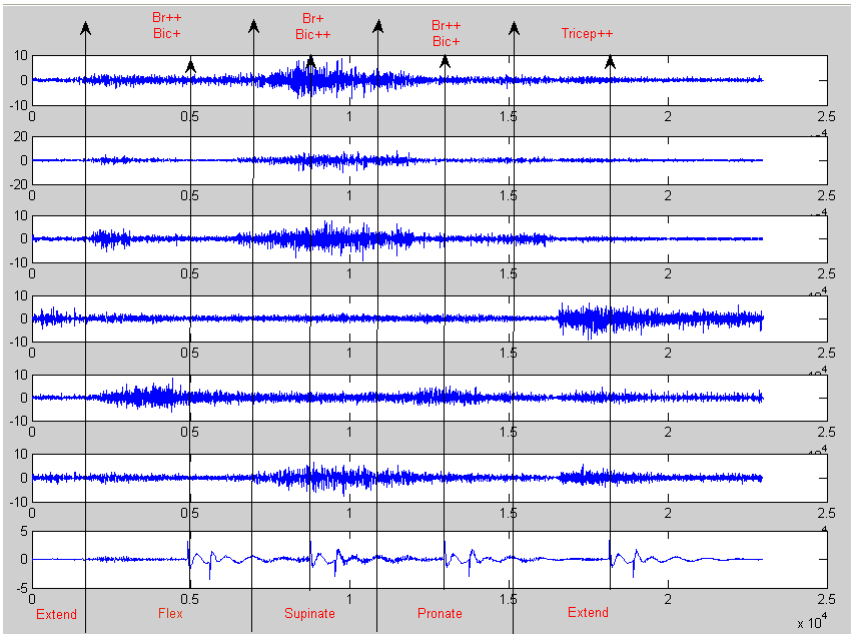

Figure 3.3: Separated EMG signals as output by ICA algorithm for the duration of all 5 actions performed by the test subject in Dr. L. Johns study at the University of Cape Town. Image adapted from [2].

Another interesting implementation of FastICA on myoelectric signals was carried out at the Taizhou University, China, by [52]. In this research they implemented a FastICA that fed a fuzzy logic controller which controlled a basic robotic prosthesis. Here they showed that the FastICA was capable of dealing with the EMG measurement noise and managed to isolate specific muscles in the forearm very easily despite crosstalk.

In the recent past, research has been carried out by S.P. Moroaswi and L.R. John [2, 1] at the University of Cape Town, in the field of non-invasive deep tissue EMG signal acquisition. In this research it is proposed that using two rings of sEMG electrodes encircling a muscle group, one can use FastICA to produce a inverse mixing matrix capable of pulling out all the EMG source activity in the targeted muscle group. This is possible provided that the number of sEMG electrodes is greater than the number of muscles in the group.

A preliminary study was carried out on the upper arm to see if it was possible to isolate the EMG activation activity of the deep muscle brachialis. This muscle is responsible for flexion of the elbow when the forearm is pronated. The testing procedure consisted of placing the two rings of six electrodes on the bicep and the patient then performed five actions. Then raw EMG recordings were processed by FastICA and the independent muscle activities were extracted. Intuitively, based on the way ICA works, it would seem one would only need roughly 4 electrodes to extract the 3 muscle signals, however, Moroaswi and John [2] found that they were not able to extract the deep-tissue brachialis source signal with less than 12 electrodes. More over, they found that it was necessary to split the electrodes into two bands o 6 electrodes about *2 cm* apart. A diagram of the twin ring EMG system arrangement can be seen in Appendix B.

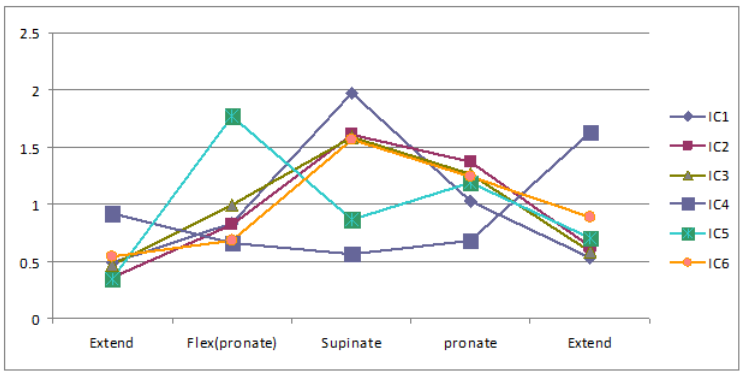

Figure 3.4: Magnitude activation of each IC through out the 5 action process performed by the test subject. Image adapted from [2]

In Figure 3.3 and Figure 3.4 one can clearly see that IC5 has the most activation energy during a pronated flex and from *a priori* knowledge of anatomy one can deduce that this IC must be the brachialis muscle. Therefore these results seem to imply

that deep tissue muscle activity can be obtained non-invasively using a combination of sEMG electrodes in a ring formulation and the ICA separation algorithm.

3.4 State-of-the-Art consumer products

3.4.1 iLimb and ProControl

The iLimb [53], developed by Touch Bionics Inc., is the premier active prosthetic in production today, it offers a multi-articulated hand with various different adaptive gripping strategies. According to the marketing website, *"The iLimb ultra offers more dexterity and moves more like a natural hand than any other powered prosthetic hand. Each finger bends at the natural joints so that it can accurately adapt to fit around the shape of the object you want to grasp."*. However, it only has the ability to receive two myoelectric signals from the residual limb.

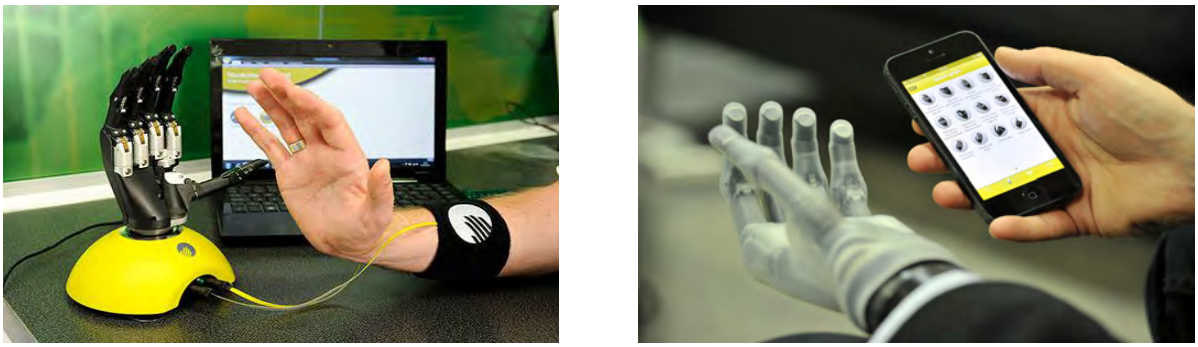

Figure 3.5: iLimb control armband with a set of bi-polar electrodes (left) and the iLimb ultra hand and quick grip selection app.

This allows the user to open and close a specific grip. No documentation or mention is made of signal pre-processing or whether the system is proportionally controlled or just a digital on and off. The different grips and pinches are selected on a mobile app, which connects to the arm via a bluetooth link.

Another commercially available control system option is the ProControl developed by Motion Control Inc. [54], for use in conjunction with their active prosthesis, the Utah Arm. The ProControl system also consists of a two site electrode configuration, which allows open and close control of the prosthetic hand. It appears from the documentation that this is indeed a digital on/off signal as the user can preset a threshold comparison value for the amount of EMG activation at each electrode site.

3.4.2 Myo HCI System Developed by Thalmic Labs

More recently a start-up company from Ontario, Canada, developed a myoelectical control system for computer and mobile interactions. This system comprises of a

ring of electrodes on a stretchable band which fits comfortably around the users forearm, just below the elbow.

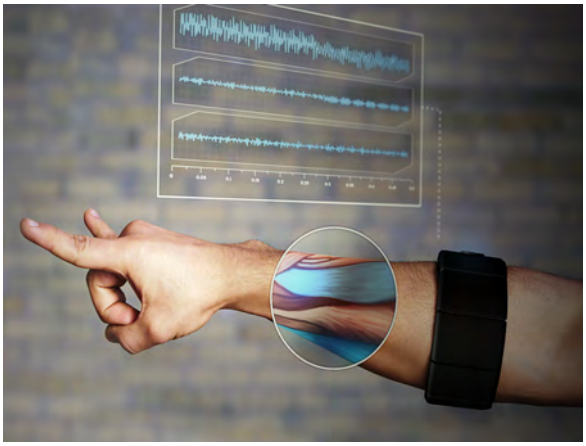

Figure 3.6: Myo Armband developed by Thalmic Labs, Ontario, Canada. Image adapted from the Myo's 2013 press kit [55].

The product developed and set to launch at the end of 2013 can be seen in Figure 3.6. The technology is proprietary and currently very little is known of the inner working regarding algorithms, electrodes, etc. According to the manufactures website, www.thalmic.com, the system runs a low-power, low-speed 150 *MHz* ARM processor connected to an array of 16 bar type EMG electrodes that encircle the arm.

It appears that that these electrodes are used in a bipolar configuration, as Stephan Lake, Thalmic CEO, is quoted as saying "There's only eight channels of data coming in, It's not like vision processing where you have millions of pixels, and so we can run pretty sophisticated algorithms on those eight channels and not use a ton of CPU power." However, it is unclear how the system achieves a stable Driven Right Leg (discussed in subsection 5.2.1) connection. The electrodes appear to be dry electrodes and according to the designers, arm hair, fat content and arm size do not affect the systems performance.

The system features a Bluetooth 4.0 Low Energy chip, which facilitates communication with the computer or mobile device as well as a 9-axis inertial measurement unit [56].

No mention is made of any algorithms used, however in an interview at fastcolabs.com [56], alludes to several details of the Thalmic teams implementation. CEO of Thalmic Labs, Stephan Lake, said "We basically bring in volunteers and bribe them with free food. We have a camera sitting there and a guy says okay, we'll do this one a bunch of times, and we'll take that data over a bunch of people and then our machine learning guys run a bunch of analysis on it. They have all these fancy 3-D plots they use to figure out the characteristics. There's different, subtle ways to look at it. Part of it is which muscles are activated, but part of it is also characteristic of the signal or the frequency content or power spectrum of it."

From this statement it seems that the Thalmic team has used an extremely large data set to infer the most common and easily attainable muscle activations in the forearm. These data fused with that of the inertial measurement system data allows the myo algorithms to find a set of easily classifiable "on/off" gestures and actions to use in their product, without the need for calibration to individual users.

According to the website the system currently boast six simple gestures combined with motion, which allows for a multitude of combinations as input to the system. From the promotional video, it seems as though the supported gestures are all based on superficial muscle activation in the forearm.

The system seems locked to this small set of input gestures and would not allow for intuitive control of a a prosthetic or exoskeleton, as it seems to only access about four of the forearm muscles.

4 Experimental Methods

In this chapter the reasoning and choice of a movement protocol is discussed. Then the experimental procedure is unpacked and explained. It then goes on to discuss some sample size considerations in order to attain significant results. This is then followed by a look at some of the experimental inclusion criteria, ethical considerations and participant risk. Finally, the chapter is wrapped up with a discussion on experimental verification.

4.1 Selecting a Movement Protocol

It was necessary to use a reasonably simple muscle group to correctly validate that the physical position and number of electrodes has a marked affect on ICA electromyography systems. An important factor in considering muscle group selection is the independent control of each of the muscles with in the group. It is critical that a movement protocol can be developed that is capable of activating singular muscles independently.

At the outset of this research, the muscle group in the forearm was selected as it had multiple deep tissue muscles and is a natural candidate for prosthetic and exoskeleton control as it contains the majority of musculature to control the human hand. However, the hand musculature, and hence the forearm group, is extremely complex and the muscles are tightly bunched. It also it difficult to train subjects to effectively activate individual muscles in their forearms during test protocols.

For these reasons the forearm as a candidate muscle group was abandoned and the distal upper arm was selected as the primary muscle group under investigation. The distal upper arm consisting of the two bicep muscle bellies, the three tricep bellies and the brachialis muscles forms a sufficiently simple muscle group to confirm the experimental results without experiencing any additional confounding factors such as unexpected co-contraction of muscles. In the unpublished work of Moroaswi *et al.* carried out at the University of Cape Town (UCT) Biomedical Engineering Department (2011), the ICA algorithm was successfully used to separate the source signals of three muscles in the distal upper arm. This was achieved using a movement protocol validated by anatomists.

In this research the above mentioned movement protocol was adopted because of its proven efficacy at isolating the source signals activation. This protocol is described in section 4.2.

4.2 Experimental Protocol

- **Skin Preparation:** The skin surrounding the upper arm muscle group is lightly abraded with sandpaper and cleaned with a 70% alcohol solution. This is to ensure good electrical conduction and reduce skin impedance, thereby improving signal quality and reducing electrical mains interference.
- **Band Placement:** The two band electrode design is positioned midway between the shoulder and the elbow of the upper right arm. The bands consist of 30 silver electrodes coated in electrolyte gel. The distance between the two rings of electrodes is 2 *cm*.
- **Standard Configuration:** The standard configuration as it is referred to in later sections is a 30 electrode band that is based on the 12 electrode setup proposed by Moroaswi *et al. [2]*. This setup is used as a base comparison for testing whether the GA systems have equal performance or not.

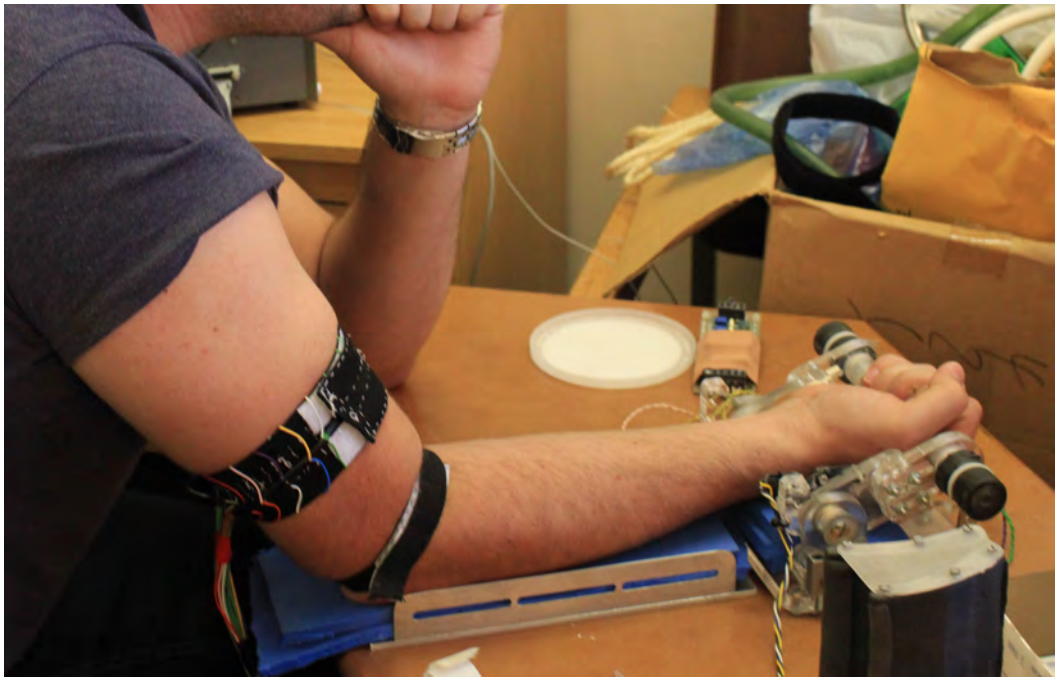

Figure 4.1: A subject participating in the second test protocol. Here the static pull bar can be clearly seen. This mechanical static rig was designed and developed at the UCT BME department by N.V. Divekar, S. Stoeckigt and L.R. John [3]

- **Movement Protocol:** Following successful application of the electrode array, the subject will be required to complete three test protocols while the acquisition system records the resulting EMG signals. The first test is to determine the Maximum Voluntary Contraction (MVC) of the subject. Here the subject is asked to pull or push on a rigid bar for a few seconds and repeat this procedure three times. The static pull bar apparatus can be seen in Figure 4.1 The

second test is the Isometric contraction test. In this test the subject performed the following set of actions, resisting against the rigid bar.

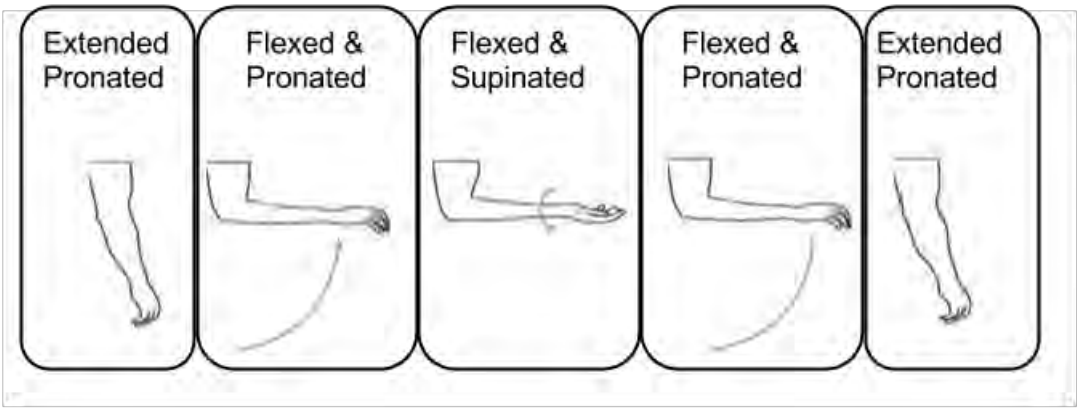

Figure 4.2: Dynamic movement protocol. Image adapted from [1]

- Isometric Contraction, Static Pull Test:
  1. Push down on the fixed bar for 3 seconds, this is called pronated resistance.
  2. Rest for 4 seconds.
  3. Repeat 3 times
  4. Pull up on the fixed bar for 3 seconds, this is called supinated resistance.
  5. Rest for 4 seconds.
  6. Repeat 3 times.

  The third test is a dynamic movement test, here the subject is required to perform different arm movements while holding a *1 kg* dumbbell weight. The *1 kg* dumbbell equates to 5%-15% MVC for all subjects partaking in the study. A sketch of the protocol can be seen in Figure 4.2. The movements are as follows.
- Dynamic Contraction:
  1. Hold weight at side with arm relaxed and hand pronated. (i.e. palm facing backwards.)
  2. Pull the weight up with palm facing down, until the forearm is 90° to the upper arm. (called Pronated flexion)
  3. Rotate the arm so that the palm face up, towards the ceiling, hold for 1 second. This is called supination of the forearm.
  4. Rotate the forearm back to the position in instruction 2, palm facing down. This is called pronation

5. Now with the hand supinated extend the arm back down to into the relaxed position.
6. Repeat the procedure 3 times.

- **Benefit:** During the testing there is no direct benefit to the subjects, however the results of the research will be used to add to the understanding and application of non-invasive deep tissue EMG.
- **Repetition:** Each participant will be required to repeat each of the three tests twice to reduce the error and test the repeatability of the measurements. A rest time of a few minutes between repetitions of the protocol will be observed to allow the muscles to recover and to ensure muscle fatigue does not affect the results.

4.3 Sample Size Selection

The sample group size selected is based on a single sided t-test formulation to ensure statistical significance. Usually a statistical power (1-β) probability of 0.8 or greater is required for statistical significance. The significance of a hypothesis test is based on the small chance of rejecting a true null hypothesis, this is know as α, the significance value is usually attributed to a *type I* error.

It is also dependent on β, the statistical probability of accepting a false null hypothesis, this is know as a *type II* error. To avoid this error the sample group must be made sufficiently large so as to ensure that random sampling error does not skew the results and is rather representative of the population [57].

Typically α is either 0.01, 0.03 or 0.05 and β is 0.2. The formulation to calculate approximate sample group size is:

$$N = \frac{2SD^2(z_\alpha - z_\beta)^2}{\Delta^2} \tag{4.1}$$

Here N is the sample size, SD is one standard deviation, $(z_\alpha - z_\beta)^2$is the power index, this depends on α and β, and is selected from a table. Δ is the minimum distance between populations that is detected as significant. From [57] an α of 0.05 and β of 0.2 gives a power index of 6.2 and the Δ can be take as one standard deviation, therefore the above equation reduces to:

$$N \approx 2 \times (6.2) = 12.4 \tag{4.2}$$

This tells us that the minimum sample size for statistical significance of the study is 13 individuals. Since this is an estimate, it is customary to over compensate, so a sample size of 20 individuals was selected.

4.4 Experimental Inclusion Criteria

Volunteers with the following criteria were selected to participate in the study:

- Healthy, right handed male.
- 18 years of age and above.
- No evident abnormal motion restriction.
- No history of neurological or neuromuscular impairment or disorders, as well as no history of myopathy.

4.5 Ethical Consideration

Ethics approval was received from the University of Cape Town's Engineering and Built Environments Ethics committee prior to beginning these experiments.

- Individuals participating will only be subjected to the testing procedure once they have read, understood and signed the consent form. The consent form can be seen in Appendix D.
- All private information submitted by the participants as well as the data collected will be kept confidential.
- All data and artefacts produced during the study will be the sole property of the University of Cape Town. The University of Cape Town has the right to reuse or distribute the data and findings as they see fit.
- Prior to the testing procedure, the full experimental process and details of the study will be carefully explained to the participant.
- The testing procedures will be conducted in accordance with the Declaration of Helsinki (2008), ICH Good Clinical Practice (GCP) and the law of South Africa.
- At anytime during the testing, the participant can withdraw from the test with out reason or prejudice. If deemed necessary the researcher may also withdraw participants at any time from the study.
- The researchers, working under the mandate of the University of Cape Town, will be responsible for treating any adverse or untoward events arising from the participation in this study.
- Participants of this study will be covered by the UCT no-fault insurance policy.

4.6 Participant Risk

EMG readings are inherently safe and pose very little if any discomfort for the wearer. Surface EMG electrodes consist of small circular metal pads with an adhesive

electrolyte gel. The only substantial risk of discomfort to the participant is in the skin preparation prior to electrode application. In this process, the skin is lightly abraded with fine sandpaper and then the skin is cleaned with a medical alcohol swab. Both of which can irritate the users skin. There is additionally a remote possibility of the user having an adverse allergic reaction to the electrolyte gel used in the electrodes.

The testing procedure will only be performed on the right arm of participants. This, along with the electrical isolation of the participant from the mains power supply, means there is no risk of cardiac arrest or electrical shock due to the testing procedure.

The whole experimental arrangement is run from a laptop unplugged from the power outlet, further reducing the risk of electrical shock.

4.7 Experimental Verification

- Once the data have been captured they will be post processed by the FastICA algorithm. The standard configuration of two bands of 15 electrodes equally spaced, as proposed by Moroaswi *et al. [2],* will be used as the base standard for comparison to other configurations .
- The activation of the Independent Components, i.e. muscle sources, should visually correlate with the movement protocol activations.
- Multiple variations of electrode configurations will be tested and their performance will be compared with the base standard. These configurations will be a result of including or excluding certain electrodes in the ICA input data stream.
- Since ICA does its own type of electrode reduction by minimizing some electrode weights near to zero, it will be necessary to compare the GA systems signal output and electrode reduction, to the standard ICA electrode reduction and its subsequent output. This will determine the effectiveness of a GA guided ICA optimization of electrode selection.

5 Design

In this chapter, an overview of the hardware system is discussed. Then an in-depth look at the electronic system design as well as the electrode arm band design is presented. Finally this chapter concludes with a look at some design and parameter considerations used in both the independent component analysis and the genetic algorithm.

5.1 Hardware System Overview

The system consists of a stretch band that encompasses the subjects upper right arm. This band has two rings of 15 EMG gel electrodes fixed onto the inner wall of the band. These 30 electrodes have shielded leads which connect into the analog electronics board. Intuitively, based on the way ICA works, it would seem we would only need roughly 4 electrodes to extract the 3 muscle signals, however, Moroaswi and John [2] found that they were not able to extract the deep-tissue brachialis source signal with less than 12 electrodes. More over, they found that it was necessary to split the electrodes into two bands about *2 cm* apart. Since this study is an extension of their work, the initial setup was designed in the same way, however, in this design we packed as many electrodes as would possibly fit around an average upper arm. Having more electrodes would allow for more variation in electrode configuration and this is why a 30 electrode configuration was selected.The analog board is responsible for amplifying the micro volt signals and filtering out environmental and system noise. This board has the ability to deliver variable amplifier gain for each channel.

A separate digital potentiometer board is responsible for adjusting the amplifier gain on the analog board. This digital potentiometer board receives gain adjustment control commands from the main microcontroller unit (MCU).

The main MCU interfaces with the analog board through the onboard Analog-to-Digital Converter (ADC), this ADC digitizes the analog signals fed from the analog board and passes them into system memory of the MCU. The MCU pre-processes the data and establishes a network connection with the client PC.

Once the connection is established, packets of data containing the digitized EMG signals are continually transferred to the client PC whenever new data are available. The PC then stores the data to log files as it is receives as well as plots it in real time, to give the user visual feedback of the signals.

5.2 Electronic System Design

The full electronics system comprises of four main units, namely an analog amplifier board, a digital gain control board and a microcontroller unit with an ADC. The MCU then communicates with the fourth unit, a client laptop computer for signal visualization and user input controls. An overview of the system can be seen in Figure 5.1. In this configuration, the laptop is run as a client and listens on a socket for incoming data from the MCU, which acts as a server. Additionally the laptop client can send control requests to the server to adjust channel gain settings and data capture rates.

A custom analog amplifier board was designed to record all 30 different monopolar electromyography signals simultaneously at a sampling rate of 2000 *kHz*.

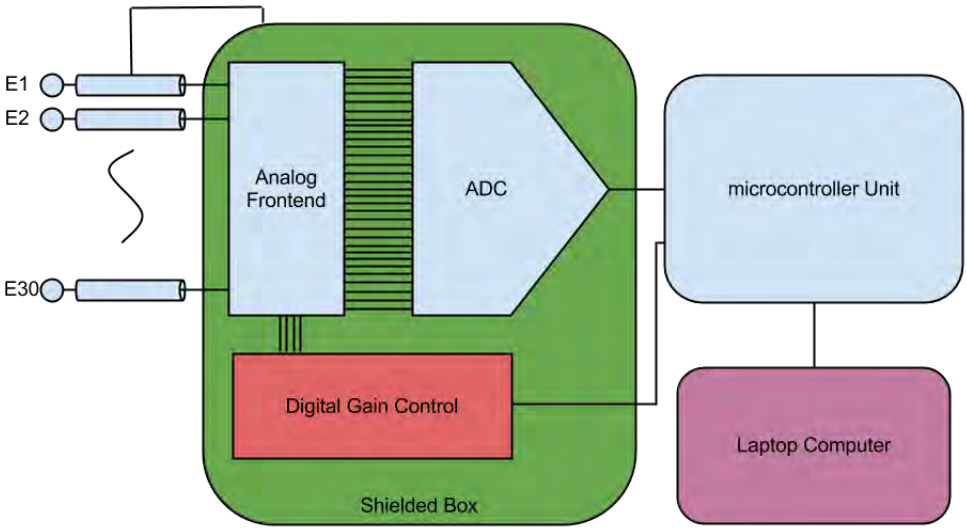

Figure 5.1: Electrical System Overview. The circular discs on the far left represent the 30 electrodes that are embedded in the arm band and have direct contact with the subjects skin. The digital gain control board allows the user to individually adjust the signal gain on each channel, this digital gain board is controlled via an SPI command interface with the microcontroller.

Originally the scope of the project was to develop a FPGA implementation of the FastICA algorithm. It was thought that the inherent parallelism in ICA would lend itself well to a FPGA type architecture. This would then allow the system to process sEMG signals in near real-time. For this reason off the shelf EMG logging units were not considered. However, after much trial and error, the author determined that the memory requirements of batch processing ICA were to severe for the FPGA. As a result the project aim was shifted and the hardware was simply repurposed.

5.2.1 Analog Board

As mentioned in section 2.1, surface EMG signal voltages range between 20 - 2000 μV [12]. This means that to attain useful signals from the skin surface these microvolt fluctuations need to be amplified several thousand times. These tiny signals coupled with a huge amount of electrical interference in most modern buildings calls for design of a specialized, high-gain, high common-mode rejection amplifier.

As discussed previously, at the beginning of the project the aim was to build a compact FPGA based system. In order to do this, the FPGA needed to be able to read raw analog signals. Most of the commercial and ready made EMG solutions were disregarded as they often have their own filtering and signal correction algorithms built in. Additionally these systems make it difficult to get to the raw analog signals and often require some proprietary software and a usb connection to a laptop to log the data. For these reasons, the OpenEEG design was selected. This design allowed more flexibility and a cheaper price point than commercial off-the-shelf EMG systems.

To begin with the design was based on an open source reference design developed by the team at OpenEEG (openeeg.sourceforge.net) and modified for EMG using the guidelines put forward by the Division of Biomedical Engineering (BME) at UCT [58]. This design consists of an initial protection circuit, an instrumentation amplifier stage and two addition amplification and filtering stages. This design was originally created for Electroencephalography (EEG). The full schematic can be seen in Appendix B.

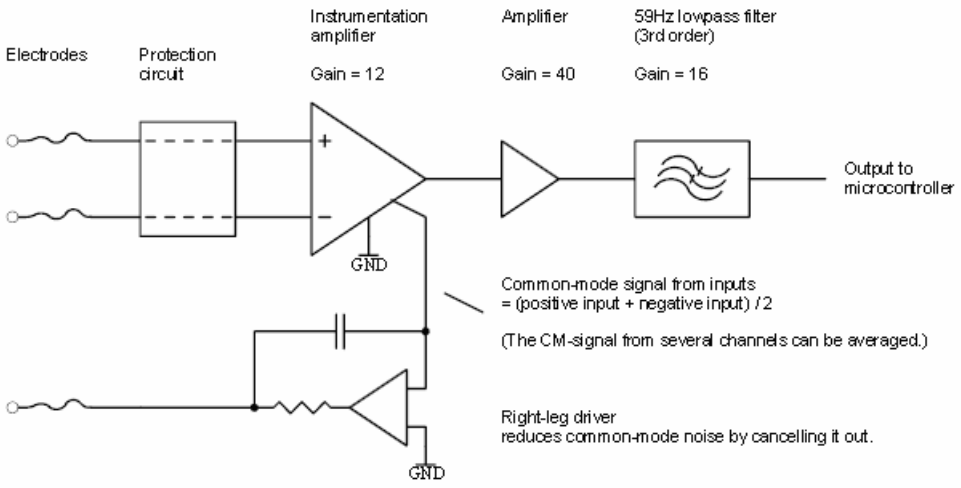

Figure 5.2: Block Diagram of the open source openEEG electroencephalography signal amplifier design. Image taken from the OpenEEG website [59].

In the openEEG design, EEG signals from electrodes are first fed into the protection

circuit. The protection circuit performs two functions. It protects the instrumentation amplifier and other circuitry from electrostatic discharge (ESD) and also protects the user from a failure in the system circuitry, which could otherwise result in electrical shock.

After the protection circuit, an instrumentation amplifier stage is encountered. Typically most bio-signal amplifier systems have a differential amplifier stage at the input. This helps reduce the injection of common-mode signals into the system. A common-mode signal is a signal that appears simultaneously at both inputs of the differential amplifier.

After the first amplifier section a high-pass filter is inserted. The high-pass filter is responsible for reducing the DC-voltage accumulation associated with polarizable electrodes, such as gold or steel. If this filter is excluded, the accumulation of a relatively large DC-voltage will result in a saturation of output after the later amplification stages [59].The high-pass filter has been excluded on the diagrammatic representation in Figure 5.2.

The final section of the OpenEEG design consists of two amplification stages and another high-pass filter in between them. These amplification stages have a variable amplification, which allows for adjustments in system. Cumulatively the entire design has a nominal gain of 7812.5 (min:1171.2; max:19520), allowing the board to amplify a variable range of μV signals into a $-2V \rightarrow +2V$ range.

In addition to the high-pass filters inserted between the gain stages, the OpenEEG design employs a 3rd order "Besselworth" filter which has a cut-off frequency of 59 Hz, to try eliminate interference from 60 Hz mains, the system has been designed taking into consideration the U.S.A. electrical grid. The final component in the OpenEEG design is the Driven Right Leg (DRL). The DRL replaces the ground electrode in older EEG system designs. It greatly reduces common-mode noise signals such as mains hum by inverting the common mode noise signal present in the differential amplifier and feeding it back to the user, thereby reducing the noise present in the body.

The analog board design used in this project was largely based on the OpenEEG design. In this design, like the OpenEEG, the first stage was the protection circuitry, this was unchanged. Much like the OpenEEG, this design employed an instrumentation amplifier first stage followed by two stages of amplification and filtering, however, the frequency response of the filters was adjusted to better suit electromyography, according to the recommended adjustments given in the BME technical note by McNaught and John at the BME division at UCT [58].

For the instrumentation amplifier stage the Texas Instruments INA128U [60] amplifier was chosen as a replacement to the Texas Instruments INA114 present in the OpenEEG design. This was due in part to the form factor of the INA128. The INA128 comes in much smaller packages, which allowed for a much more compact design. The INA128 (CMR = 120 dB) also has slightly better Common-Mode Rejection (CMR) to the INA114 (CMR = 115 dB), and as mentioned earlier, common-

mode rejection is highly desirable in bio-signal acquisition systems. This initial amplification stage was set to a gain of 12.36. This amplification gain was selected at the first stage, as it amplified the signal by an order of magnitude, but kept it small enough so that the effects of electrode polarization did not cause the output to be saturated. This allowed the polarization offset voltage to be removed after the first stage, with out loss in amplification.

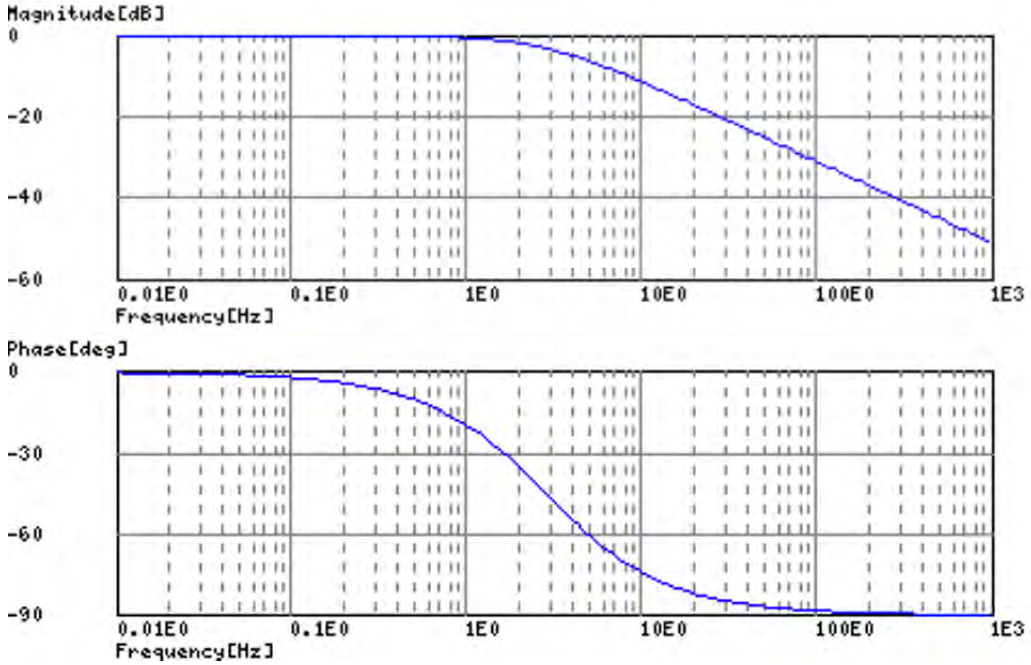

Figure 5.3: Frequency Response of Low Pass Filter used to reduce polarization voltage effects.

The passive low pass filters used to reduce the affects of polarization voltages (see Figure 5.6) were designed to have a cut-off frequency of 2.84 *Hz,* this removes DC polarization voltage without compromising the overall EMG signal. The filter frequency response can be seen in Figure 5.3. These LPF filters additionally remove slow movement artifacts introduced when the subjects move during experimentation.

Stages 2 and 3 were designed using the Texas Instruments quad amplifier, TLC2274 [61]. This chip was chosen because of package size and number of amplifiers per chip which greatly reduced the physical size of the board design. The TLC2274 also has excellent noise immunity (typically 9 $n\mathrm{V}/\sqrt{Hz}$) and full rail-to-rail output voltage swing, which helps avoid clipping of the output signals. For the design of these two phases a standard non-inverting amplifier design was used. A variable resistor included in Stage 2 of the amplifier which could be used to adjust the gain in this stage between 10 and 101. Additionally each of these gain stages have a built in high pass filter (HPF) with a cut-off frequency of 1591.54 *Hz.* This cut-off frequency was selected because it well encompasses the bandwidth of EMG ($0 \rightarrow 500Hz$) and

cuts out any high frequency noise from the environment. The frequency response of these HPFs can be seen in Figure 5.4.

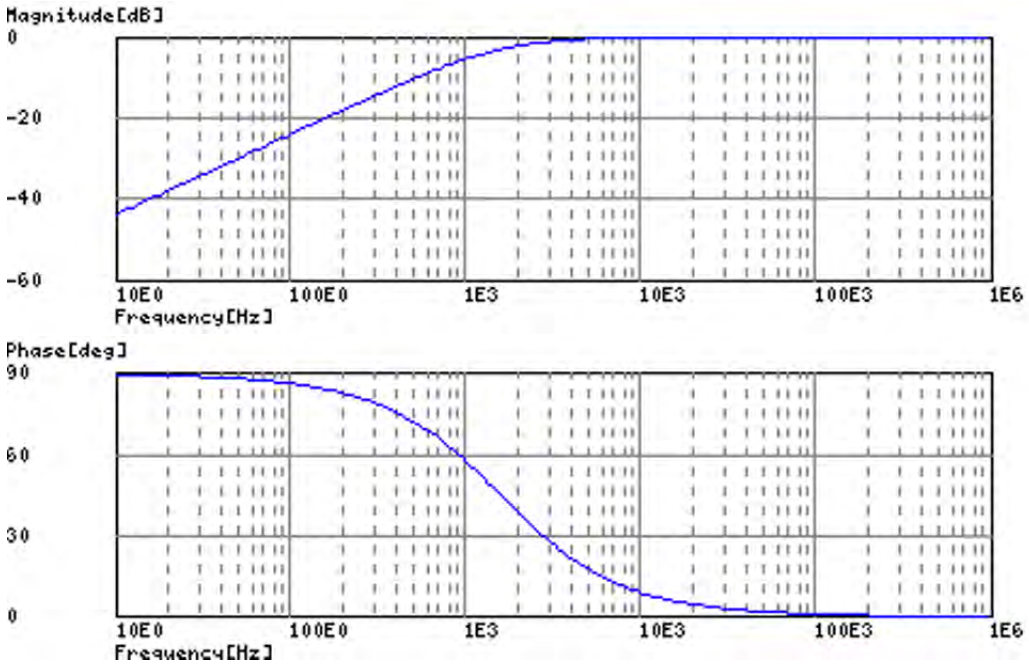

Figure 5.4: Bode plot of High Pass Filter.

This board design, shown in Figure 5.5, allowed for the use of either digital or analog potentiometers and the facility to include an external DRL circuit. The 90° molex™ connectors allowed multiple boards to be stacked on top of each other, enabling a high density of electrodes to connect to a relatively small package. approximately 30 electrodes were used in this case.

To adjust the gain quickly and accurately for a large number of channels digital potentiometers were used, this design was based on previous work done at UCT BME by Stoeckigt, Divekar and John [3]. This is discussed in subsection 5.2.2 below.

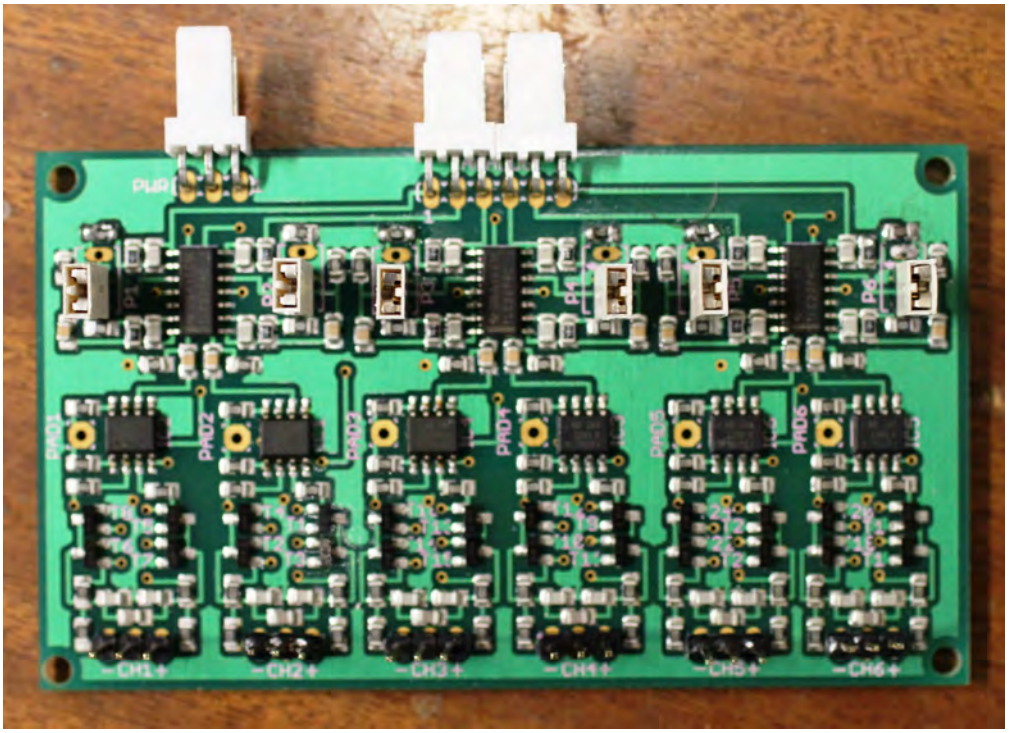

Figure 5.5: Final EMG analog board design. Here the 6 bipolar channel connections can be seen near the bottom edge of the board. At the top edge connectors for power and analog output are seen.

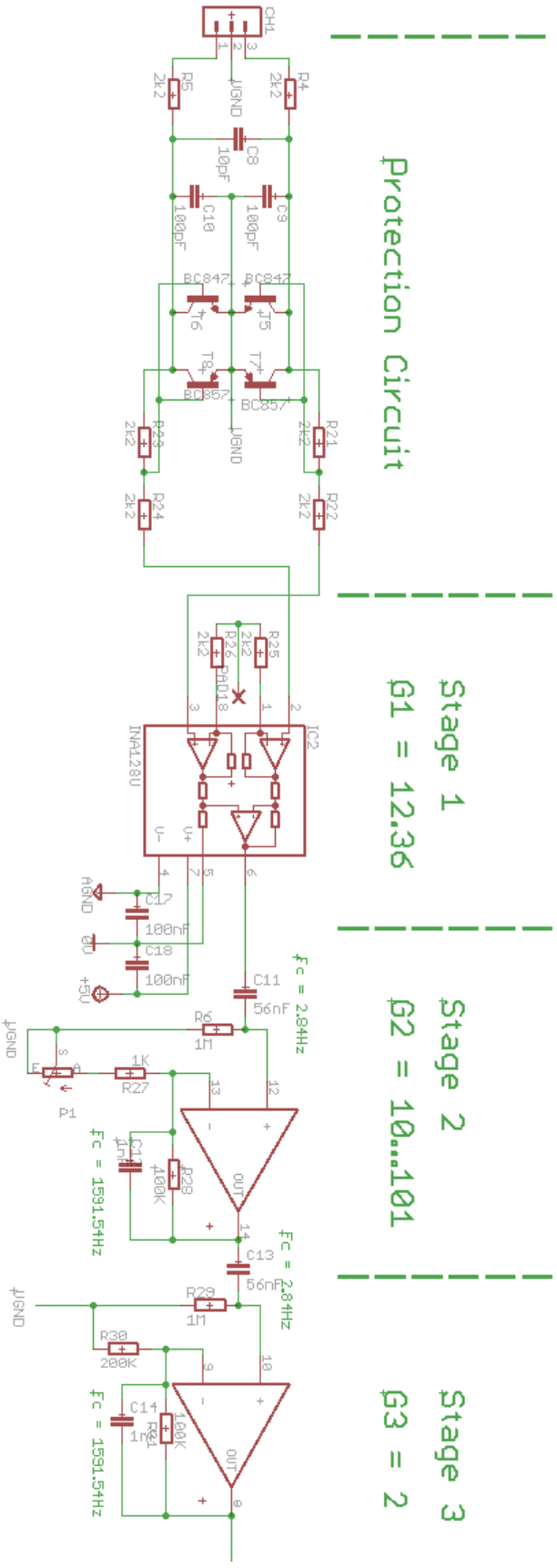

Figure 5.6: Single channel EMG analog circuit. Design adapted from OpenEEG [59] and modifications note suggested by the BME division at UCT [58].

5.2.2 Digital Gain Controller

To effectively manipulate the gain of all 30 channels on the analog board, it was necessary to design a digital interface. A digital interface would allow the gain to be adjusted in software, eliminating the need to manually adjust 30 potentiometers as well as providing the ability to automate the procedure of adjusting all the channels to the same gain level, the design of this system was based on previous work by Stoekigt, Divekar and John at UCT [3].

To achieve this digital gain control, a extension board was designed around Analog Devices AD5206 chip [62]. This chip has six digital potentiometers, each with 256 set-points. Each potentiometer is addressable through a SPI interface and can be independently controlled. For the total 30 channel system, five AD5206 chips were assembled and daisy chained on to the microcontroller boards serial peripheral interface (SPI) interface. The AD5206 were chosen as the 10 $k\Omega$ variant as this would allow for the secondary gain stage to have a variable gain between 10 and 101.

5.2.3 Microcontroller Board

The microcontroller board selected for the project is the National Instruments Single Board RIO 9612. This board is a co-processor single board computer, which is a 400 *MHz* processor running VXworks with an integrated two million gate reconfigurable I/O (RIO) FPGA for custom timing, inline processing, and control.

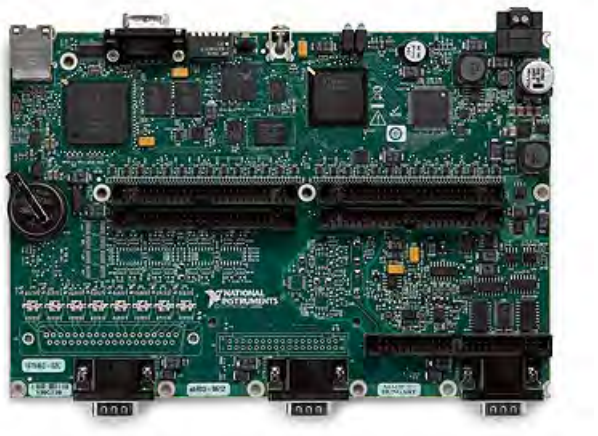

Figure 5.7: National Instruments Single Board Reconfigurable I/O board. Image taken from http://sine.ni.com/ [63].

The board additionally has a 32 channel, 16-bit resolution Analog-to-digital converter (ADC), capable of 250 *kS/s* and a maximum voltage range of -10 V to +10 V. This ADC coupled with the real-time (RT) abilities of the co-processor allows the system to continuously capture, record and display all 30 channels of EMG data

simultaneously and reliably at 2 *kHz,* which is well above the Nyquist sampling criterion for EMG signals, avoiding signal aliasing.

The board also included 10/100 Ethernet network connection, which allowed the VXworks processor to communicate with the client-side laptop. The network connection allowed raw data to stream from the MCU to the laptop for visualization as well as allowing the client-side to send control requests to the MCU.

At the outset of this project, this board was selected because of the sizable FPGA, thought to be power enough to process batch mode ICA in realtime. Unfortunately as the project progressed, the near real-time processing of ICA on a FPGA proved infeasible. The author then made the decision to continue developing on this hardware, as it was more than capable of performing the functions necessary for the adjusted project aim.

Figure 5.8: Final system design, with MCU unit at the back connected to the analog boards and digital potentiometer boards in front (grey box) accompanied by 30 electrode armband and elbow band for the common electrode.

5.2.4 Power Supply Board

The power supply for the system required several different supply voltages as well as isolation from mains supply for safety reasons. The MCU was powered from an isolated 20 *Vdc* workbench power supply. The board itself handled the supply conditioning, allowing the digital gain control board to "piggy-back" on the MCU power supply by running off one of it's 5 *Vdc* outputs.

The analog board however required a separate supply and was run from a 9 *Vdc* battery. The 9 *V* supply is then regulated down to 5 *V* and isolated using the TMV0505S [64] chip which is 5 *V* DC-to-DC converter, this design, was based on the OpenEEG design [59] and the work by Stoeckigt, Divekar and John [3]. The isolation helps reduce the injection of mains noise into the amplifier as well as protects the user from direct connection to mains. In order to run the dual-supply INA128 and TLC2274 chips used in the design, it was necessary to create a dual voltage power supply, in the previous designs they used a combination of a zener diode and a programmable shunt regulator (TL431CLP [65]) to create a virtual ground reference at 2.5 *Vdc*. However, in this design a Texas Instruments TLE2426 precision virtual ground chip was used as it simplified the design and gave a stable and precise virtual ground [66]. All the analog boards were then powered off this -2.5 *V* to +2.5 *V* supply allowing them to output a filtered and amplified signal of between -2.4 *V* and +2.4 *V* which is a feasible range for the ADC on the MCU.

5.3 Mechanical Interface Design

For the mechanical design of this system an arm band was designed to secure the electrodes to the users arm. Additionally simple re-usable silver electrodes were designed and fabricated by by Jeremy Pitman as attributed in Appendix B, Electrode Design section. Additionally some mechanical hardware was needed for the testing procedure, but these were designed in a previous project by S. Stoekigt and N.V. Divekar [3] and adapted for this system.

5.3.1 Electrode Design

Re-usable electrodes were developed to test multiple users and gather enough data to make reasonable assumptions. These electrodes also needed to be small and light, so that roughly 30 or more could be fitted around the average persons upper arm. Additionally, as discussed in subsection 5.2.1, it is necessary to develop electrodes that reduce polarization voltage build up as much as possible.

To achieve these specifications, pure silver electrodes where used along with an adhesive, low impedance gel. Both can be seen in Figure 5.9. The electrodes have a shallow cup design with a small hole in the center. The hole allows excess gel to push

Figure 5.9: Re-usable silver cup electrodes and Elefix^{TM} adhesive gel.

through and allow the gel and cup to make a even connection with the users skin. The gel helps reduce electrode dead-zone, the dead-zone is the area of non-contact between the skin and electrode, this in turn decreases impedance [67]. The electrodes have a diameter of 10 *mm* and are 23 *mm* long including the wire mounting tab. The electrodes were punched out of 2 *mm* thick pure silver plates using a custom made electrode press. The electrode press and electrode dimensioning was designed by Jeremy Pitman, a fellow student at the Department of Biomedical Engineering at the University of Cape Town. A Computer Aided Drawing (CAD) of Jeremy's design can be seen in the Appendix A.

5.3.2 Arm Band Design

The arm band was designed to hold 30 electrode tightly against the users skin to decrease electrode dead-zones. The center of each electrode is spaced approximately 2 *cm* from its adjacent electrode, this is because 2 *cm* is the recommended standard inter-electrode distance [11, 9]. To get quality and relatively low noise signals, it is important to have Common and Ground electrodes which are positioned above a relatively electrically inert point. For this system, the elbow area was selected and a second band with the two reference electrodes was used. Both bands can be seen in Figure 5.10.

The arm band also needed to be adjustable to be used on subjects with differing upper-arm sizes. This adaptability was achieved by including a Velcro® strip on the band. Additionally the adjustable nature insured that all the electrodes had good electrical contact. The electrodes where numbered in a zig-zag fashion. A design concept diagram can be seen in Figure 5.11 and depicts the channels associated with each electrode. Note, only half of the 30 electrodes are shown in this diagram.

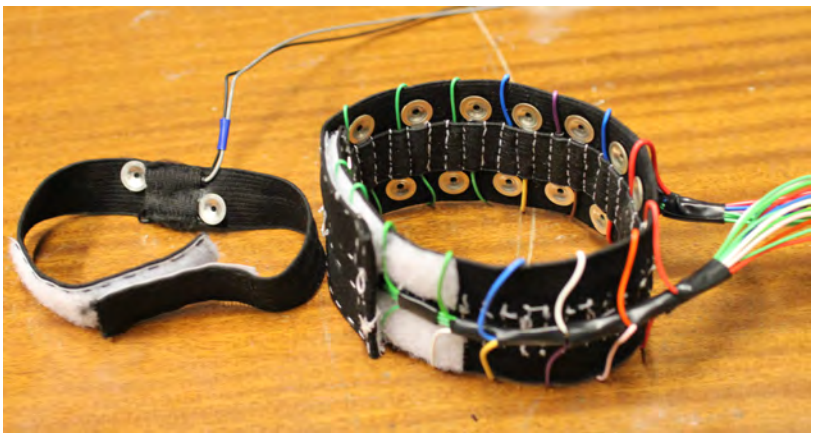

Figure 5.10: Elastic arm band used to secure electrodes to users arms during testing pictured right. Virtual ground and Common electrode references pictured left.

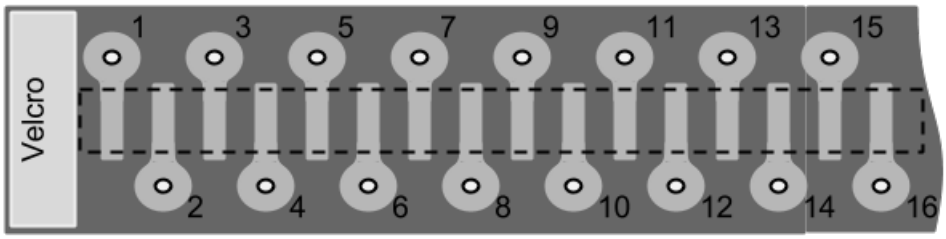

Figure 5.11: Arm band design and electrode numbering scheme. The electrodes are numbered in a zig-zag fashion as shown. Each number is the channel number that the accompanying electrode is attached to.

5.4 Software and Algorithm Design

5.4.1 Software Interface and Controller

The acquisition system for the collection of EMG signals is a combination of software running on an embedded processor and on a client computer. The embedded system firmware is built on a FPGA and co-processor system. This system uses a real time data acquisition structure and non-blocking communication protocol, allowing uninterrupted recording of the subjects signals during testing.

Data are read into each of the 30 channels of the Analog-to-Digital Converter (ADC) at 2000 *Hz* on the FPGA system. Additionally the FPGA handles the low-level SPI communication protocol to the digital potentiometers (AD5206) responsible for adjusting the channel gain for the system. The digitized EMG signals are then passed from the FPGA to the co-processor via a buffered Direct Memory Access (DMA) channel. The DMA allows the MCU to accomplish other tasks like communicating

with the Host PC while data are being transferred from the FPGA and then the DMA will interrupt the MCU when it has completed the transfer.

The DMA is constantly being filled by the FPGA and emptied by the MCU as it transfers the data to the host PC. The MCU transfers the data to the Host PC using a TCP/IP software stack. This stack allows the MCU to transfer the data over ethernet to a networked Host PC on a predefined socket. In this system, the MCU and embedded system acts as a data server and servers the data to clients that are listening on the correct socket.

The client in this case is the client PC or laptop, the client console along with an explanation can be seen in Figure 5.12. This PC initiates communication with the acquisition system by listening on the appropriate socket. When a communication channel is established, the client starts to read EMG data being pushed through the socket and graphically displays 6 out of 30 channels of data in real-time. The channels that are currently being viewed can be changed on the fly.

When a test is started on a subject, the user can set the system to start logging. The data of all 30 channels will then be logged to the specified log file. When the experiment is complete the user can stop logging and all the data can be visualized and inspected in the second tab on the client called *"Logged Data"*.

All of the experimental data are then written to a file and stored for later analysis with the ICA and GA. A flow diagram showing the interaction of these two algorithms in the analysis methodology during a test on one subject can be seen in Figure 5.13.

5.4.2 ICA Algorithm

For the Independent Component Analysis implementation on the device, an algorithm with reasonable accuracy and a fast execution time was needed. Speed of the algorithm was critical as the system would be dealing with large data sets and in future implementations users would like the system to customize to their musculature as quickly as possible.

To achieve this one of the most popular ICA algorithms was selected, the kurtosis-based FastICA method [68].

Originally at the outset of this research, the goal was to build a high speed ICA system on a FPGA to quickly and decisively determine deep tissue activity. It was thought that due to the parallel nature of the ICA algorithm an FPGA system would be the ideal architecture. However, this became increasingly complex as the "batch" nature of the ICA algorithm needed for EMG processing resulted in the system running out of system memory while only processing 6 channels of EMG data.

However, this exploration into the design of FastICA on a FPGA gave the author a good understanding of the inner workings of the algorithm, and after careful

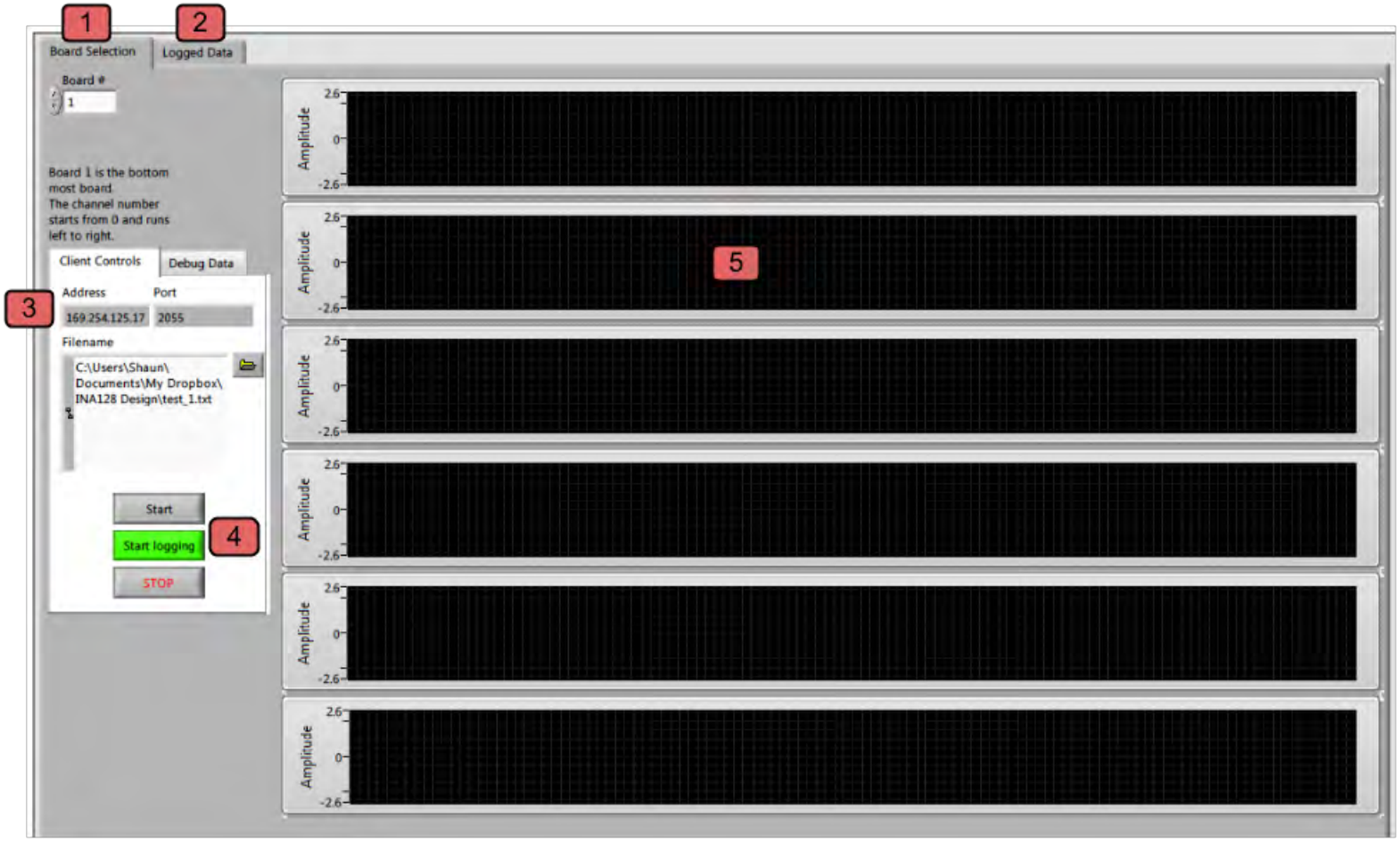

Figure 5.12: Client side control console on the Host PC. (1) This is the primary control tab, where the user can create a connection to the EMG system, visualize incoming data and start and stop logging the data during the testing procedure. (2) This is a visualization tab that allows the user to see all the recorded signals after the logging of data has been stopped. (3) These two inputs allow the user to adjust the connection settings to the appropriate EMG data server. (4) These controls allow the user to start a connection to the host and start logging data to file. When stop is clicked, the log files are saved and the connection is broken. (5) EMG data being sent over the network is visualized here. One can select 6 out of 30 channels of data to be visualized in real time.

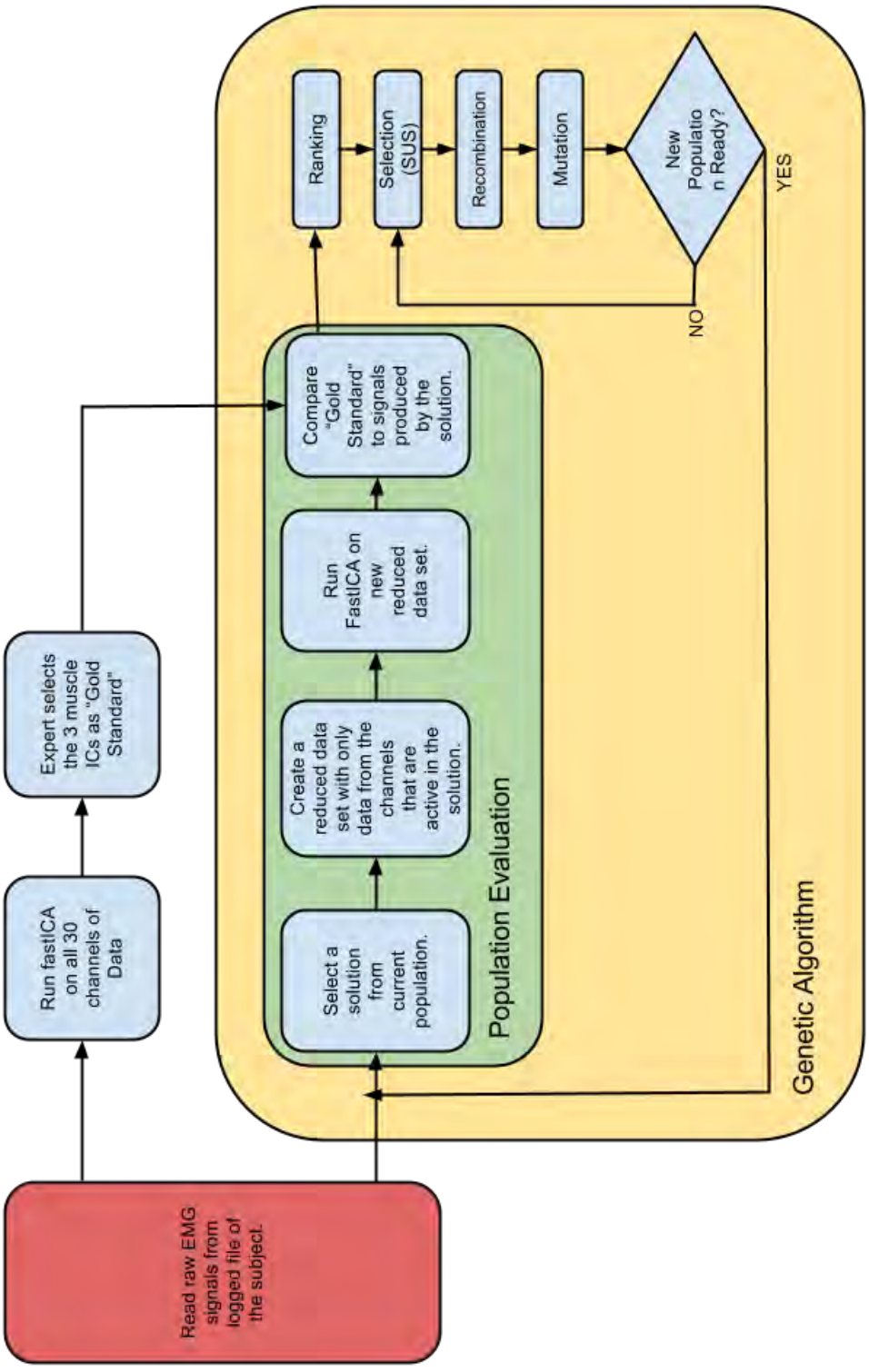

Figure 5.13: A flow diagram of how the two algorithms interact and the key stages in the analysis methodology . Here it is evident that the FastICA is used in the development of both the gold standard signal and the evaluation of each of the solutions in the genetic algorithm.

consideration it was decided that it would be easiest and most efficient to use the already built FastICA MATLAB® package [69] developed by Hyvarinen and his research group at the Department of Information and Computer Science, Aalto University, Finland [28].

This package would more than likely be far more efficient and higher performance than the authors implementation as it is built on top of the Intel BLAS (Basic Linear Algebra Subprograms) library for high throughput Linear Algebra operations.

In terms of parameters, $f(u) = \frac{1}{a_1} \log \cdot \cosh(u)$ was used as the non-quadratic non-linearity, with its derivative $g(u) = \tanh(a_1 u)$ and $a_1 = 1$ was used as recommended. This contrast function was chosen due to its robustness and its applicability to many problems [28].

The stopping criterion for the algorithm was set to 0.0001 and a maximum of 1000 iterations was set. If either of these conditions was met, the algorithm would exit and return the current solution matrix.

The algorithm was constrained to only estimate 15 Independent Components as it was found during testing that most of the important information was found in the first 15 ICs and the trailing 15 were mostly noise. Reducing the number of output ICs greatly reduces the execution time of the algorithm.

The initial $\mathbf{W}$ matrix was set randomly each time the ICA was called and the decorrelation method used was the deflation approach as it was simple and allows the algorithm to find stronger or more "privileged" ICs first [28], unlike other decorrelation methods such as Symmetrical Decorrelation, which all ICs are estimated simultaneously [70].

5.4.3 Genetic Algorithm

The Genetic Algorithm was built on top of the MATLAB Genetic Algorithm Toolbox [71], created by the Department of Automatic Control and Systems Engineering at the University of Sheffield. The GA was developed using this package and implemented on a 2.3 *GHz* Intel Core i5 with 4 GB of RAM.

As discussed in section 2.4 the genetic algorithm was based on the canonical GA implementation. A binary string of length 30-bits was used to represent a solution in the population. Each bit represented an electrode, and 1's indicated that the electrode was active in the solution, while 0's indicated the converse.

For the selection method, the author deviated partially from the standard GA by using a Stochastic Universal Sampling method to select individuals for breeding. This was done so that relative diversity from generation to generation was preserved and no one individual was allowed to overwhelm the population.

For crossover and mutation the standard binary 2 point crossover and bit flip mutation was used as described in section 2.4.

Fitness evaluation was performed using the FastICA algorithm to produce 3 signals which represented the bicep, brachialis and tricep. These signals where then compared to their "gold standard" counterparts which were produced when the FastICA was run with all 30 channels of data active. The fitness of an individual is then measured as a weighted sum of differences in the 3 output signals and their gold standard counterparts as well as an inverse measure of how many electrodes are active in the solution. Detailed formulaic descriptions of the fitness function can be seen in subsection 6.1.2.

The run of the GA on each test subject's data was allowed to run for 25 generations with an initial population size of 50 individuals. These parameters where chosen to try reduce execution time as much as possible without reducing the GAs performance. A cursory test demonstrated that performance did not significantly increase with an increase in population size relative to the time increase. Additionally any number of generations above 40 resulted in an unreasonable execution time, and after inspection of the fitness vs. generation traces produced during the tests, the trend was that fitness plateaued between 20 and 25 generations.

An issue that greatly affected the running time of the GA was that of population initialization. Each individual in the population is created randomly, however, the way in which these individuals are randomly created is very important. Originally the population was created just using the built in psuedo-random number [0,1] generator, selecting the bit "high" or "low" depending on whether the random number generated was greater or less than 0.5. This however produces a large number of individuals with 15 or more electrodes activated in its solution. This is not ideal, since we are trying to optimize for as few electrodes as possible. So it would make algorithmic sense to rather have a set of solutions with a very small number of electrodes initially and allow the GA to slowly build up solutions by combining these smaller groups of electrodes. To create this sparsely activated population, all that is necessary is to adjust the threshold value of 0.5 to something higher like 0.8 or 0.9.

In Figure 5.14 the result of two GA executions with different population initializations is presented. Execution 1 has been initialized with the sparse electrode activation population, while execution 2 has been initialized with the standard random population. It is clear to see from here that both initializations yield similar solution accuracy or fitness after 25 generations, however, execution 1 takes about 2.5 times less processing time than execution 2 to get the same accuracy. This is because the solutions with less activated electrodes require less data to be fed into the ICA algorithm, and in the GA, the ICA algorithm is a bottleneck when evaluating solution fitness.

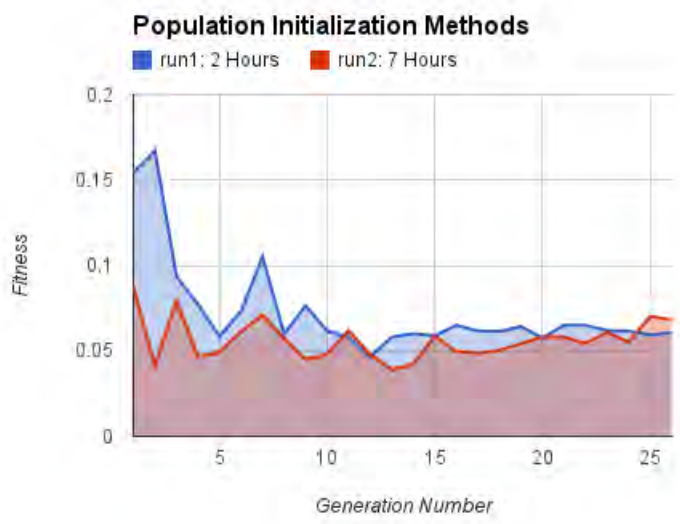

Figure 5.14: Here trend data for 2 different executions of the same GA is presented. However, in run 1 the population is initialized with a sparse population and run 2 is initialized with a standard randomized population. These tests were run on a 2.3 *GHz* Intel Core i5 with 4 GB of RAM.

5.4.4 Comparison Mechanism

To compare effective electrode reduction of the ICA and GA solution with the stand alone ICA solution, it was necessary to develop a procedure that would zero out mixing matrix weights if they are below some small threshold in the stand alone ICA solution. As the ICA algorithm effectively reduces weighting of electrodes that do not contribute to the overall signal reconstruction. So by setting these minimized weights to zero, it can be determined how many electrodes have been disregarded. A block diagram representation of each of the procedures can be seen in Figure 5.15.

The zeroing of the weights in the mixing matrix were set to zero according to their comparison to a preset threshold value. This preset threshold value was a small percentage of the overall range of the data. The experiment was run with 5 different threshold values set at 0.2%, 2%, 5%, 10% and 15%. This was done to get a fair overview of the effect of the threshold size on electrode reduction and signal output quality. The results of which can be seen in the subsequent section.

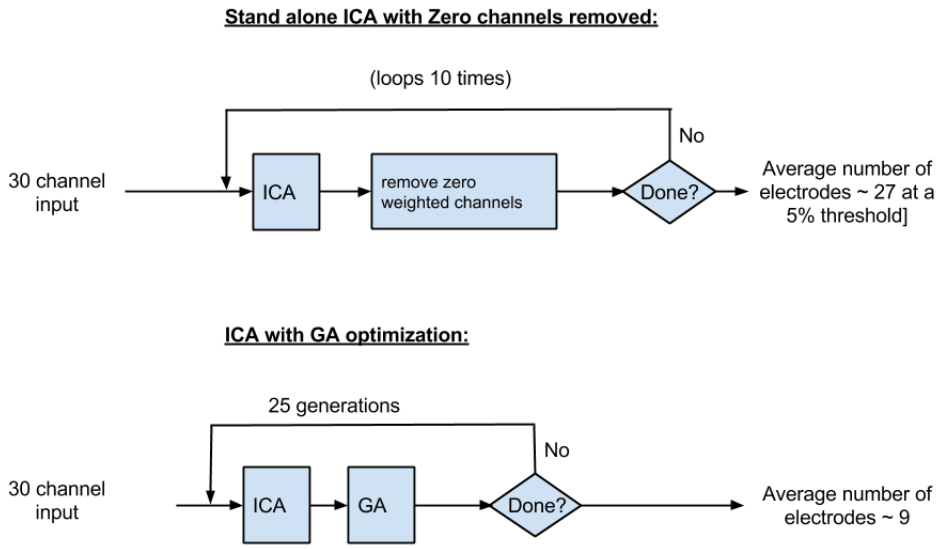

Figure 5.15: Simplified flow diagrams of the two algorithms used for comparison. In both case the feeback loop in the top just checks and increments a count variable to ensure the algorithm only runs the specified amount of times.

6 Results and Analysis

In this chapter, the results of the experiments described in chapter 4 are presented. These data, as well as the analysis performed using the Genetic Algorithm are then discussed.

6.1 Dynamic Movement Test

The Dynamic movement test was performed using the protocol discussed in section 4.2 and was performed on 20 healthy male subjects [2].

In the following section the results of particular subjects in the test will be discussed and some of the successes and short comings of the experiment will be highlighted. The focus is on the ICA performance, examining a 30 electrode configuration, and is followed up by an investigation into electrode reduction using genetic algorithm optimization.

6.1.1 Golden Standard

Each test subject was tested twice in the session, using the movement protocol and the 30 electrode configuration as described in Appendix B Figure B.1. It was decided that the best separated set out of the two tests would represent the "Golden Standard" of source separation for each individual. It is assumed that since the ICA algorithm had access to all the data from each electrode it could make the most informed source separations and hence produce the "best" signal set.

For this experiment, the ICA used was a deflation decorrelation approach with a hyperbolic tangent non-linearity [30]. This produced a 30×30 de-mixing matrix and 30 independent components or source signals.

The first 10 channels of raw data from one of the subjects can be seen in Figure 6.1. This subset of signals illustrates how similar each of the monopolar EMG signals can be. It is difficult for one to determine visually which of the 30 signals will add useful information to the source separation algorithm. The signal variations are too subtle for the human eye. However, the hypothesis is that an evolutionary search approach could uncover at least most, if not all, of the significant electrodes used in the formation of the independent components.

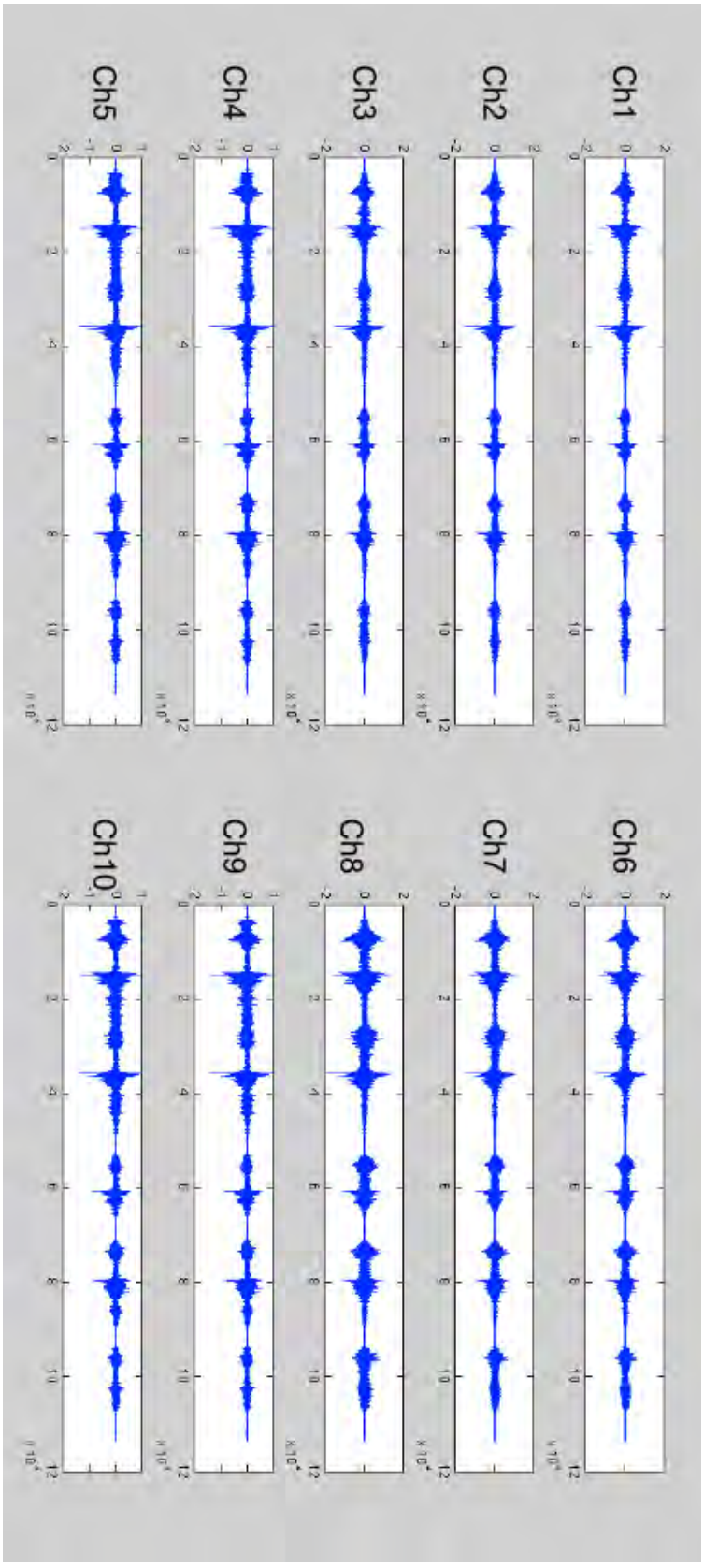

Figure 6.1: Illustration of the similarity in raw electrode signals from test subject 1, highlighting the difficult task of extracting individual muscle activity and electrode significance.

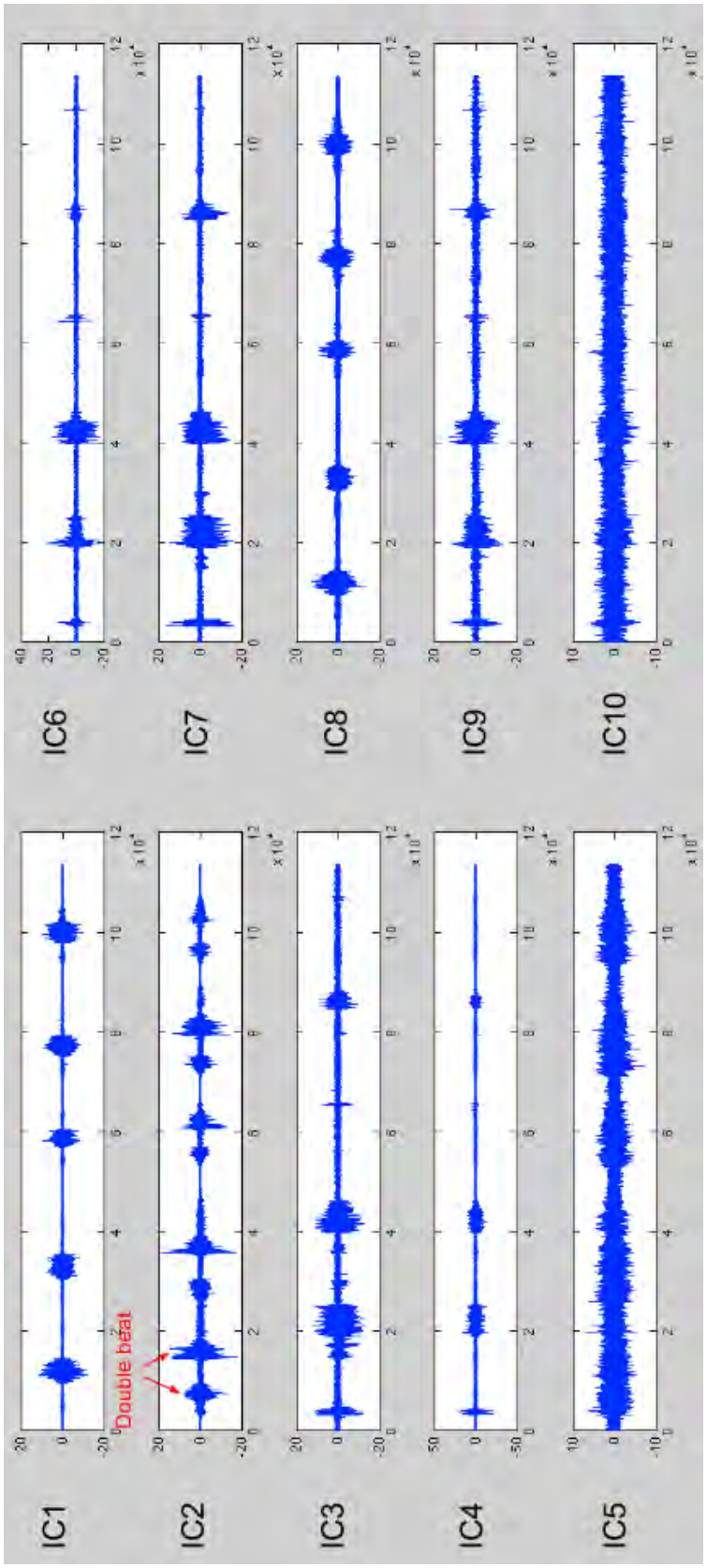

Figure 6.2: 10 independent components produced by the ICA algorithm when run on the data captured from subject 1 (the same data presented in Figure 6.1). Illustrated on this figure are the twin "beat peaks" of the brachialis, which indicate supination and pronation of the hand when the task of sustaining the elbow at 90º is transferred from the brachialis to the bicep and back to the brachialis.

After the ICA algorithm has run, it is possible to see the different source signals present in the subject's arm, shown in Figure 6.2. It is also possible to see that there are copies or similar signals, as in the case of signals IC1 and IC8. This is due to the abundance of electrodes relative to source signals. Since the algorithm produces a 30×30 matrix, some of the matrix coefficients are not valid independent sources, but rather mixtures or replicas of the actual independent sources [72].

Figure 6.3 is a closer inspection of the first three independent components, shown in Figure 6.2, which were produced by the ICA algorithm. These signals will be referred to as the "gold standard" set in the subsequent sections. The gold standard for each test subject was classified by a person with *a priori* knowledge of the movement protocol and upper arm anatomy.

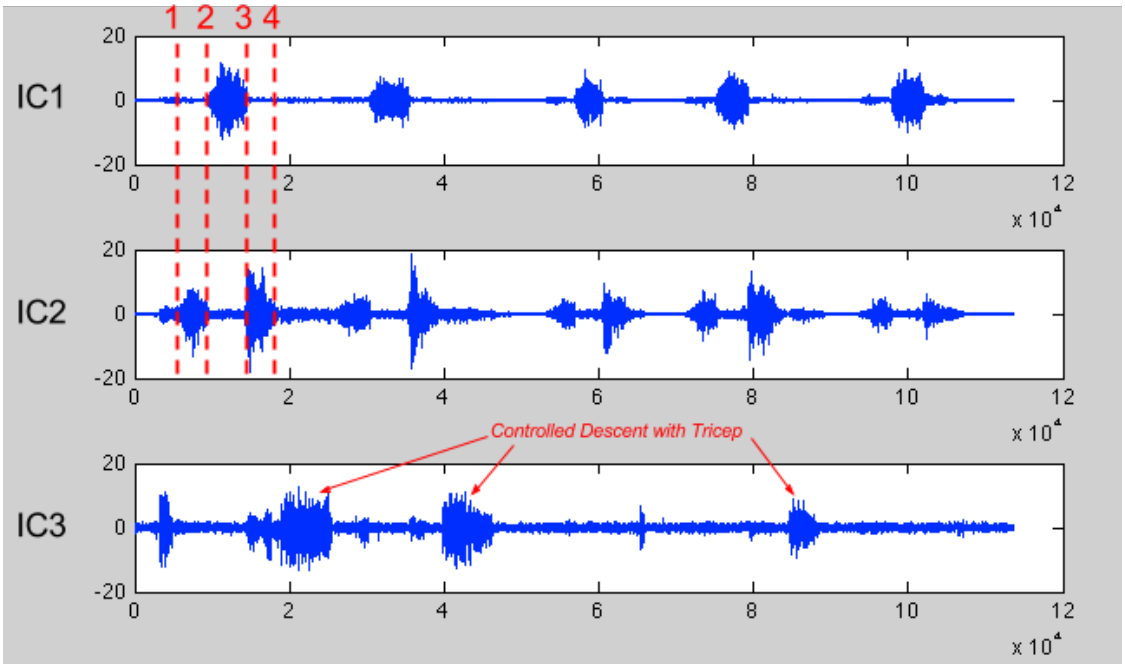

Figure 6.3: Bicep, brachialis and tricep independent component signals of subject 1. Here the switch between brachialis and bicep activity can be seen. (1) Shows when the brachialis activates, during pronated flexion of the elbow. (2) Shows the switch over from brachialis to bicep during the supernation of the hand, so that the palm is facing upward. (3) Shows the switch back to the brachialis and (4) shows the brachialis is relaxed. Also indicated is the controlled descent activity of the tricep. As mentioned before, this does not happen in all subjects or in every iteration of the movement protocol.

From Figure 6.3 one can conjecture, based on the replication of both the method and results of S.P. Moroaswi and L.R. John [2] and an *a priori* knowledge of the upper arm, that these are the 3 muscle source signals. It can be seen that IC1 is the bicep signal and IC2 is the brachialis signal, since one can see that each one of the

5 fluctuations on IC1 is a result of *step 3* in the movement protocol. When the arm is supinated so that the palm is facing towards the ceiling, the bicep muscle takes over the task of maintaining the elbow at a *90°* lock, and the brachialis muscle will relax. This is indicated by the second dotted red line in Figure 6.3. The opposite will happen when the arm pronates back, indicated by the 3rd red dotted line. That is why it is possible to see the double muscle *"beat"* in the signal shown in IC2.

The two strongest sources (IC1 and IC2) which were isolated first, were the two signals produced by the brachialis and bicep respectively. The tricep signal is more difficult to isolate as many test subjects do not consistently use the tricep to control the descent of the arm during the experiments. Therefore the signal for the tricep is either minute or non-existent. However in the case shown in Figure 6.2, the subject used their tricep to control the descent on three occasions and it is reasonable to assume that IC3 is the tricep signal. This can be seen in Figure 6.3. One can see that there are muscle fluctuations after the brachialis has relaxed, indicating that the tricep is taking over control of the descent of the arm back to the relaxed position alongside the subjects body, these activations have been indicated in the Figure 6.3.

The data in this subsection further validates the findings of Moroaswi and John [2] and helps support the hypothesis that it is possible to extract the deep-tissue brachialis muscle using only monopolar surface electrodes in the configuration mentioned in Appendix B, Figure B.1. The setup worked across all 20 of the test subjects, a random selection of subject's output signals can be seen in the Appendix A.

However, a 30 electrode configuration to isolate only 3 signals is inefficient both spatially and temporally. Through further investigation of the weighting matrix output by the ICA algorithm, it is possible to identify how many of the electrodes are actually contributing to the output signals. Electrodes that have relatively low or zero weighting can be seen as inactive in the source signal construction. After applying this inspection method to the 20 subject weighting matrices, it was found that the average number of active electrodes in the 30 electrode solution was 23.25 $\pm$5.665 with a median value of 25 electrodes, still a significant number of electrodes for so few source signals. The active electrode count in the 30 electrode configuration can be seen side-by-side the results of the genetic algorithm tests in Table 6.1.

Table 6.1: Active electrode count for Test1, Test2 and the Standard 30 electrode configuration.

Active Electrode Count			
Test	Median	average	STD
30 electrode test	25	23.25	5.665
GA Test 1	7	7.45	1.7614
GA Test 2	8	9.05	2.7237

Therefore based on the ICA functionality, it was proposed that the number of elec-

trodes could be reduced to some optimal number and positioning, with minimal loss in signal integrity. This optimization could reduce the data needs of the system and improve the speed of the ICA algorithm. In the following section a discussion on how a genetic algorithm was used to optimize the number of electrodes and their placement is presented.

6.1.2 GA optimized Individual

To reduce the number of electrodes, it is necessary to determine which electrodes are most significant to the final output signals. There are $30! = (2.6525286e^{32})$ possible combinations of electrode activations and positions. In this instance an activation means that the signal captured from the electrode will be included in the ICA algorithm input. Conversely, a non-activated electrode will not have any effect on the ICA algorithm output as it will this electrodes signal will not be fed in. In essence this is simulating the act of physically adding or removing electrodes in different positions and combinations.

The inherently large search space and relatively slow speed of ICA, makes it virtually impossible or at least unreasonable to traverse the solution space using standard search techniques or brute force approaches. For this reason an evolutionary approach such a Genetic Algorithm (GA) is necessary. The GA has an advantage in this large search space because it can make large stochastic jumps around the solution space.

Two variants of the GA, called Test 1 and Test 2, were created. The main difference in these two implementations is in the way the fitness of a solution is evaluated.

Test 1's GA is set up with a fitness function based on the similarity of the 3 signals to their respective gold standard set and the number of electrodes in the solution. It is set to have a emphasis on electrode number. The fitness function for Test 1 is shown here:

$$fitness = 1 - (w_1 \times sim(S1) + w_2 \times sim(S2) + w_3 \times sim(S3) + w_4 \times (1 - \frac{\#Electrodes}{30})) \quad (6.1)$$

where w_i is a scalar weight, $sim(x)$ is a function that returns the similarity [0,1] of signal x relative to its gold standard. This similarity is based on the Pearson Correlation[1]. *S1, S2* and *S3* are the signals selected as bicep, brachialis and tricep. These signals are selected automatically out of all the output signals using the best correlated matches to the gold standard. Finally *#Electrodes* is the number of electrodes that are activate in the solution.

[1]Pearson product-moment correlation coefficient is a measure of the linear correlation (dependence) between two variables X and Y, giving a value between +1 and −1 inclusive.

Test 2 is developed with an root mean squared error (RMSE) based fitness function. The focus of this fitness function is on accuracy of output signals relative to the gold standard and less emphasis is placed on electrode number. The Test 2 GA fitness is shown here:

$$fitness = w_1 \times RMSE(S1) + w_2 \times RMSE(S2) + w_3 \times RMSE(S3) + w_4(\frac{\#Electrodes}{30}) \quad (6.2)$$

Again, here *S1, S2* and *S3* are the output signals corresponding to brachialis, bicep and tricep. *#Electrodes* represents the number of active electrodes in the solution and w_i is a scalar weighting. In effect the weighting adjusts the importance of the variable in the optimization. The function *RMSE(X)* is a function that returns the root mean squared error of the input signal relative to its golden standard.

As the evaluation of the fitness of a solution is dependent on first obtaining the three output signals from the ICA, the evaluation of the fitness function is time consuming. This affected the way in which parameters such a population size and number of generations were selected. Ultimately a population size of 50 randomized individual solutions was chosen and it was allowed to run for 25 generations.

Each run of the GA, *i.e. 25 generations* of *50* individuals, takes 2 hours per subject to complete on a 2.3 GHz Intel Core i5 with 4 GB of RAM.

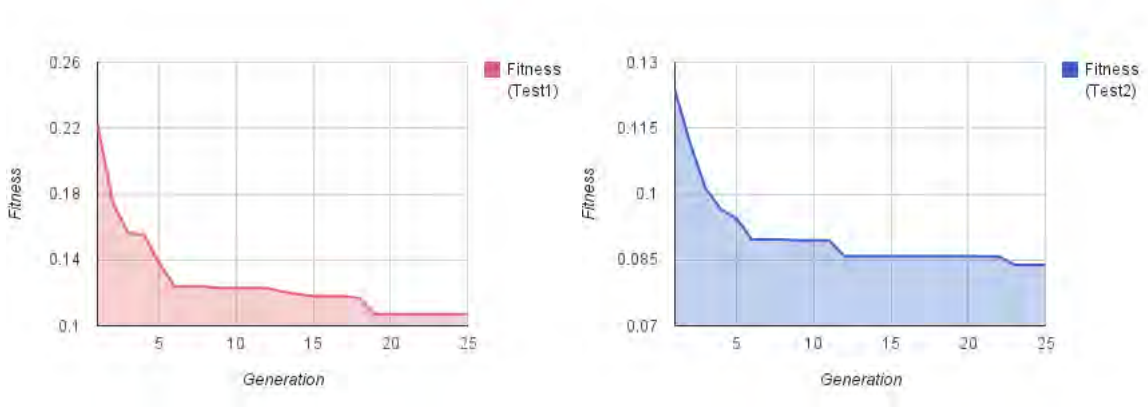

Figure 6.4: Trend lines for one run of fitness of optimized solution as a function of generation for Test 1 and Test 2 on subject 1. Here each successive generation will produce one or more individuals that will solve the problem more accurately than all the individuals in the population of the generation before.

In each successive generation of a GA there will be one or more individuals that out perform or are equal to that of the best performance in the previous generation. These individuals are then given the best opportunity to populate the next generation with their "children". In Figure 6.4 one can see the trend lines for the fittest individuals over the 25 generations for Test 1 and Test 2. As stated, the trend is to

decrease or stay the same with each new population. In this instance a lower fitness is a more optimal solution.

In the beginning, the fitness trend dives rapidly down as new combinations with large stochastic jumps create better and better solutions. However, towards the 20th generation the population tends to stagnate and the fitness plateaus. There are more advanced methods of GA implementation, which try to reduce population stagnation and maintain solution diversity. However, these methods are beyond the scope of this dissertation, and the general GA presented will produce sufficient enough solutions for a proof of concept. After running for 25 generations on each subject, the Test1 GA converged with an average fitness of 0.085 and the Test2 GA average fitness after convergence was 0.0628. The reader will notice the discrepancy between the fitness and the RMSE error reported for Test1 in Table 6.3. This is due to the fact that RMSE was used as the defining measure of comparisons between the output signals and the gold standard signals. Test1 is not optimized to minimize this type of error.

Table 6.2 shows the normalized RMSE values of the output solutions for each subject in Test 1. It can be seen that the number of electrodes for each subject is variable. However, each solution only require at most 11 electrodes. Test 2 and the 30 electrode configuration RMSE results can be seen in Table A.1 and Table A.2 respectively in Appendix A.

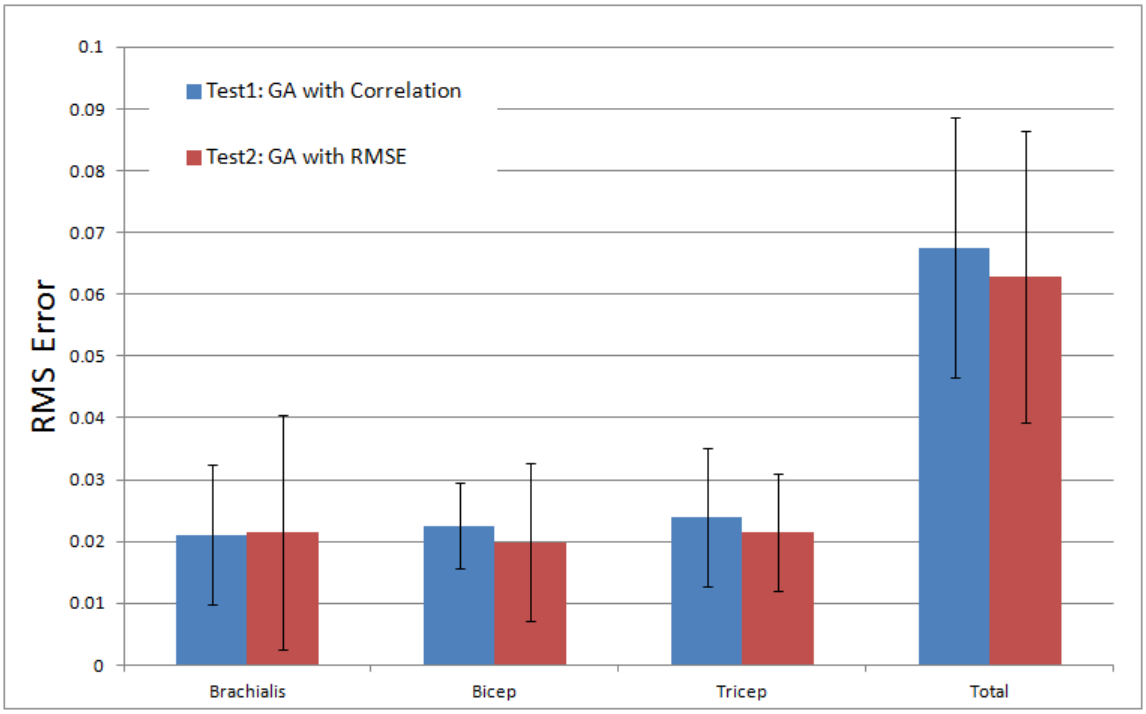

Figure 6.5: Comparison of normalized RMSE average for Test 1, Test 2 and their respective deviation from subject to subject.

Table 6.2: RMSE results for each muscle of all 20 subjects for Test 1.

RMS error for all 20 subjects during Test 1					
	Brachialis	Bicep	Tricep	Total	# of Electrodes
1	0.009820765686088	0.021300316070699	0.023556094441733	0.05467717619852	7
2	0.005478521454055	0.028783335683532	0.026705952712094	0.060967809849681	6
3	0.019664464269729	0.017659799541282	0.033469432408441	0.070793696219452	5
4	0.025504234909619	0.012517731477625	0.032775256368422	0.070797222755666	6
5	0.023830534058134	0.019877729862563	0.024118002577308	0.067826266498005	6
6	0.019002005342901	0.028427898850217	0.021856087481341	0.069285991674459	9
7	0.031455159290133	0.01539803911022	0.016728736023389	0.063581934423742	8
8	0.04765389724026	0.033603882512986	0.056359747973711	0.137617527726957	9
9	0.016892179034559	0.008309034686942	0.021746798794584	0.046948012516085	8
10	0.016048107676976	0.03069987430655	0.024645458276912	0.071393440260438	6
11	0.008291564824256	0.021455873733161	0.008291564824256	0.038039003381673	6
12	0.037461339825907	0.027031528357719	0.025075809375737	0.089568677559363	5
13	0.019628247501952	0.020004577049475	0.007185168147946	0.046817992699373	11
14	0.018662905907468	0.026920512339813	0.020874835300934	0.066458253548215	7
15	0.007574222991547	0.016211271360816	0.020174139528998	0.043959633881361	8
16	0.014200910425223	0.02513720404263	0.041902379849443	0.081240494317296	9
17	0.03804487407617	0.017730568885581	0.022878765665679	0.07865420862743	10
18	0.009441754828638	0.033085694320907	0.020601288548505	0.06312873769805	6
19	0.027049127797114	0.028909486290828	0.01784396122876	0.073802575316702	7
20	0.026413419638054	0.018735348770118	0.011036979735079	0.056185748143251	10
average	0.021105911838939	0.022589985362683	0.023891322963164	0.067587220164786	7.45
STD	0.011279230155965	0.007004348576538	0.01118829682593	0.021075474756037	1.7614288458372

Table 6.3: Normalized RMSE average of all subjects for Test 1, Test 2.

RMS error and Standard Deviation Averages for all subjects				
Test	Brachialis	Bicep	Tricep	Total
GA Test1	0.0211±0.0113	0.0226±0.007	0.0239±0.0112	0.0676±0.0211
GA Test2	0.0215±0.019	0.0199±0.0128	0.0215±0.0096	0.0628±0.0236

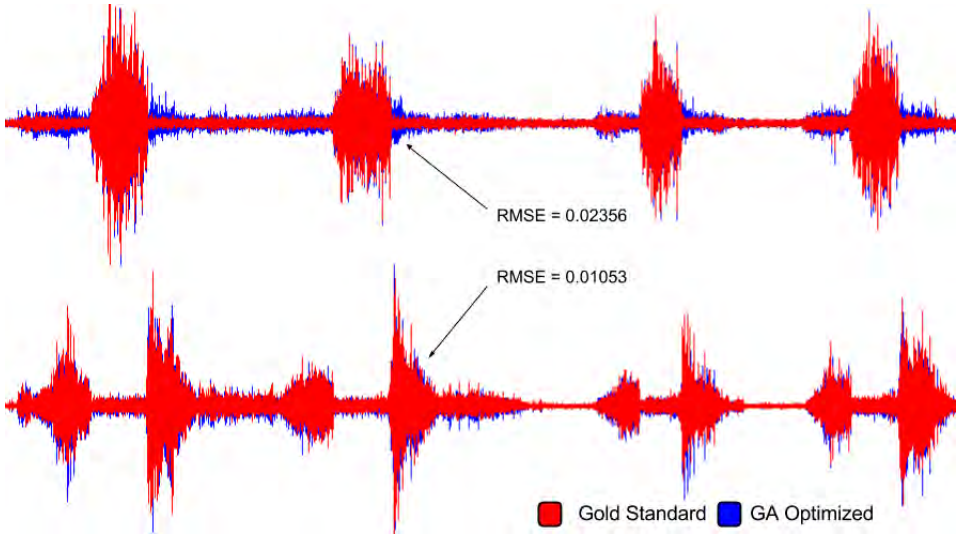

Figure 6.6: Here the bicep and brachialis muscle signals of the GA optimized solution from Test 1, subject 1 are presented. The signals in blue are the solution outputs for bicep and brachialis, with the "gold standard" signal overlaid on top of them in red. This serves to highlight the error between the optimization and its "gold standard". Here one can see that the optimized bicep signal carries more error than that of the optimized brachialis signal. This is affirmed by our RMSE reading for each signal.

A comparison of the RMS errors of Test 1 and Test 2 can be seen in Figure 6.5. Here the RMS error is measured relative to the 30 electrode gold standard. What Figure 6.5 shows us, is that both GA 1 and GA 2 perform equally well, however, GA 1 on average uses less electrodes per user and has less error on the brachialis muscle output. Additionally, it appears that GA 1, with a fitness function based on Correlation, has less deviation from subject to subject.

In Figure 6.6 a portion of the output source signals of subject 1 from Test 1 is visualized. Here the GA optimized output signals have been overlaid with the corresponding gold standard, so that the error between the two signals can be emphasized. The error can be seen as the blue fringe surrounding the red signal. The red signal is the gold standard, so if there existed a GA optimized solution that had zero RMSE, one would only see the red signal and no blue fringe.

In the example displayed in Figure 6.6 only the bicep signal (at the top) and the

brachialis signal (below) are shown. From this one can see that the optimization has performed sufficiently for the brachialis muscle as very little blue is visible, RMSE = 0.00982. Whereas, the bicep signal has marginal error before and after the peak "beat" sections in the signal, RMSE = 0.02130.

However bicep inaccuracy is viewed as much less of a problem since it is possible to extract very usable bicep signals by using only one set of bipolar EMG electrodes on the surface above the muscle. So a concentration on brachialis accuracy is of higher importance. The solution for subject 1 only uses 7 of the 30 available electrodes, which represents a 76% reduction in data bandwidth needed. However, this only proves that the GA solution is better in one case, the case of subject 1.

Table 6.4: Mann-Whitney U Test. Test parameters: N_a and N_b= 20, Sample A = active electrode count for 30 electrode configuration , Sample B = active electrode count for GA tests, Mean Rank (versus Test 1) = 30.1, Mean Rank (versus Test2) = 29.8 .

Mann-Whitney Test		
	Test1	Test2
Ua	7.5	13.5
Ub	392.5	386.5
Mean Rank	10.9	11.2
z	5.19	5.03
p	< 0.01	< 0.01

To determine if the GA solutions reduction of active electrodes is significant in general, it is necessary to preform some statistical analysis. The standard method to compare two samples is to use the students t-test. However, according to Fay and Proschan [73], it is said that t-tests perform rather poorly on flat or skewed data distributions such as the one shown in Figure A.17 of Appendix A for the 30 electrode configuration. For this reason an alternative test was used, namely the Mann-Whitney U test.

In this test the null hypothesis is that the two sets of samples, namely the active electrode counts from the standard test and the GA test, have the same distribution of active electrodes. The alternative hypothesis is that the active electrode counts in the 30 electrode configuration is significantly larger than those in the GA's solutions. The results of the Mann-Whitney test for both GAs are shown in Table 6.4. The critical z-score for the 99% confidence interval is 2.34 [74]. In both test cases it can be seen that the z-scores are greater than the critical z-score and therefore it is possible to reject the null hypothesis.

The fact that the number of active electrodes in the data of the 30 electrode configuration is greater than those in the GAs solutions, as hypothesized, tends to support the alternative hypothesis that the GA solutions distribution is significantly less than those of the standard configuration.

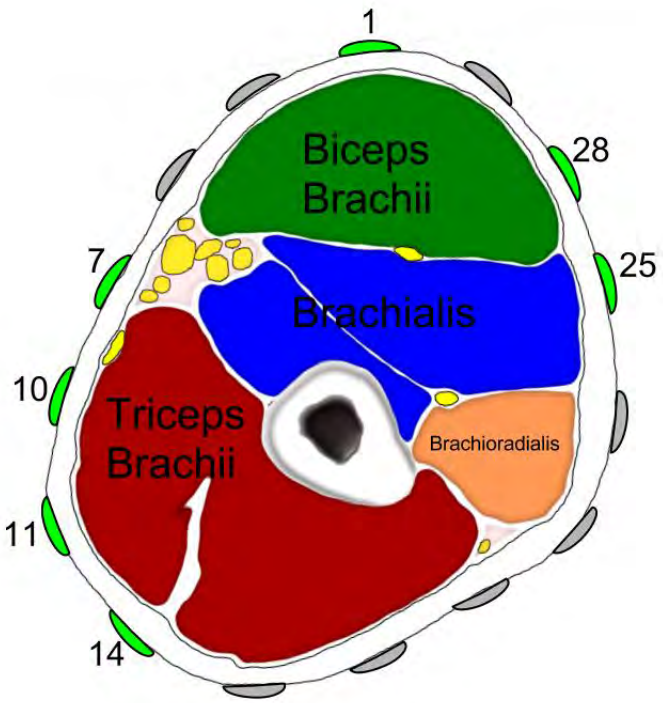

Figure 6.7: Cross-section through upper arm, depicting electrode positions of GA optimized solution for subject 1. The figure shows clustering of electrodes on the inner side of the arm as well as a few electrodes positioned over the Bicep bellies. Image adapted from [23]

Now the GA solutions positioning for subject 1 are explored more to investigate which factors could be influencing the electrode placement in these solutions. If the electrode placement in Figure 6.8 and Figure 6.7 of the GA solution for subject 1 in GA Test 1 is examined one can see that there is a cluster of 3 electrodes, namely 10, 11 and 14. This cluster looks to be positioned on the inner side of the right arm. This is presumably the portion of the arm where the electrodes are closest to the tricep. The concentration of electrodes over the tricep here is most likely because the subject used their tricep to slow the descent of their forearm during the extension of the arm.

From the diagrams one can surmise that a combination of electrodes 7, 25 and 28 interact to produce the brachialis component. It seems that since the muscle belly of the brachialis is deeper, it requires a composition of electrodes on either side of the arm to reconstruct the source. The bicep signal would most likely be constructed by the interaction of electrodes 1 and 28, and possibly with a minor influence added from electrode 25.

One caveat to note in this diagrammatic representation is that the cross sectional image is actually cut at a lower point then the electrode band was positioned. This

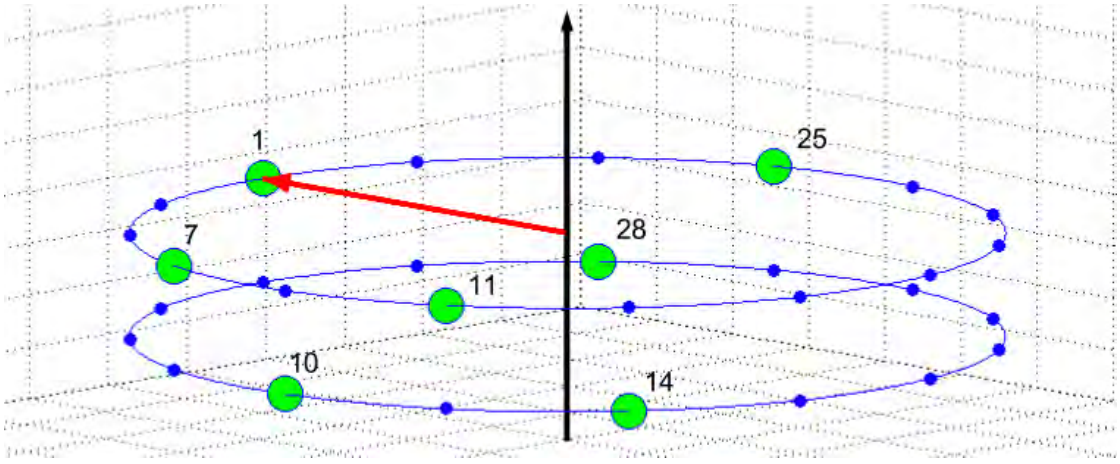

Figure 6.8: A 3D representation of electrode placement from subject 1 after GA optimization. This electrode configuration produced the output signals seen in Figure 6.6. Here the black arrow pointing up represents the position of the *humerus* bone running through the upper arm. The red arrow points towards electrode 1. Electrode 1 is placed directly above the subjects bicep muscle belly.

results in the addition of the head of the brachioradialis, which leads into the forearm. It should be noted that although this muscle is present in the diagram, it was not necessarily as prevalent during the testing because the electrode band was placed roughly above or inline with the insertion of the brachioradialis head into the humerus. Therefore minimal electrical muscle activation could be captured from this muscle as the electrodes were essentially places above the tendon of this muscle.

Table 6.5: Results of Test 1 and Test 2 on subject 1. Here Test2's output configuration contains 10 electrodes versus the 7 in Test1 and produces a more accurate result. This seems to indicate that an increased electrode count improves accuracy, so there is room for a tradeoff between electrodes needed and accuracy of the signal.

G.A.	Brachialis	Bicep	Tricep	Total	# Electrodes
Test 1	0.009820765	0.021300316	0.023556094	0.054677176	7
Test 2	0.006842108	0.011429447	0.019382168	0.037653725	10

Now that we have determined that the reduction of electrodes is significant and since it has been stated that the electrodes are effectively ignored by the ICA when their weights are reduced to near zero. It is prudent to compare the GA based algorithm to a standard ICA electrode reduction. This will give an indication of whether the GA solution is as good or better at reducing the active electrodes while maintaining accurate output source signals.

To do this, the experimental procedure highlighted in section 4.7 and further expanded on in subsection 5.4.4 was followed. This involved running the standard

ICA for each subject ten times. Each time all the weighting values for the electrodes were compared to a threshold value. If the values were lower than the threshold, that weight was set to zero and the electrode was effectively discarded from use in reconstructing the muscle source signals. As mentioned earlier the threshold was determined as a percentage of the full range of the weighting matrix data values and five different threshold values were used. From this it was possible to count the number of active electrodes present in the standard ICA reconstruction.

In Figure 6.10 the effect of removing the near-zero weights before source signal reconstruction can be seen on subject 5. When the threshold is set low, as in the first diagram, where the threshold is 0.2%, one sees that all of the electrodes are activated, so all 30 channels of data are used in the reconstruction. This produces a signal very near the gold standard, which is indicated in red. As the threshold increases, effectively "removing" or zeroing more weight values in the W matrix, it can be seen that the signals start to degrade. At a 5% threshold, the active electrode count is 28 and it becomes difficult to discern the brachialis signal features. At 15% the electrode count has been reduced to only 12 electrodes, but the output has become unusable for brachialis extraction.

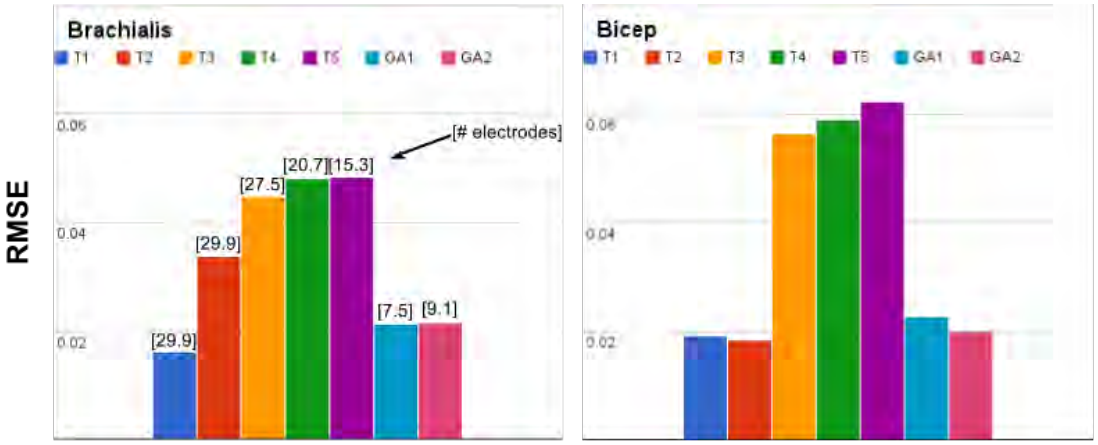

Figure 6.9: Effect of different threshold values on the RMSE average value across all 20 subjects. The RMSE average for both genetic algorithms is included in the chart for comparison. It can be seen that thresholds T1 = 0.2% and T2 = 1% both perform similarly in comparison with the RMSE of the GA solutions. The values atop each column indicated the number of electrodes active in signal reconstruction for that solution. These values are not indicated on the bicep chart to the right because they are the same as for the brachialis chart.

If one looks at the averages across all 20 subjects in the experiment as seen in Figure 6.9, it is possible to see that threshold T1 [= 0.2%] and T2 [= 1%] perform similarly to the GA solutions in terms of RMS error. However, at this threshold value the majority of subjects still used 30 electrodes in the signal reconstruction. It is also possible to see the increase in RMS error as the threshold is increased. For

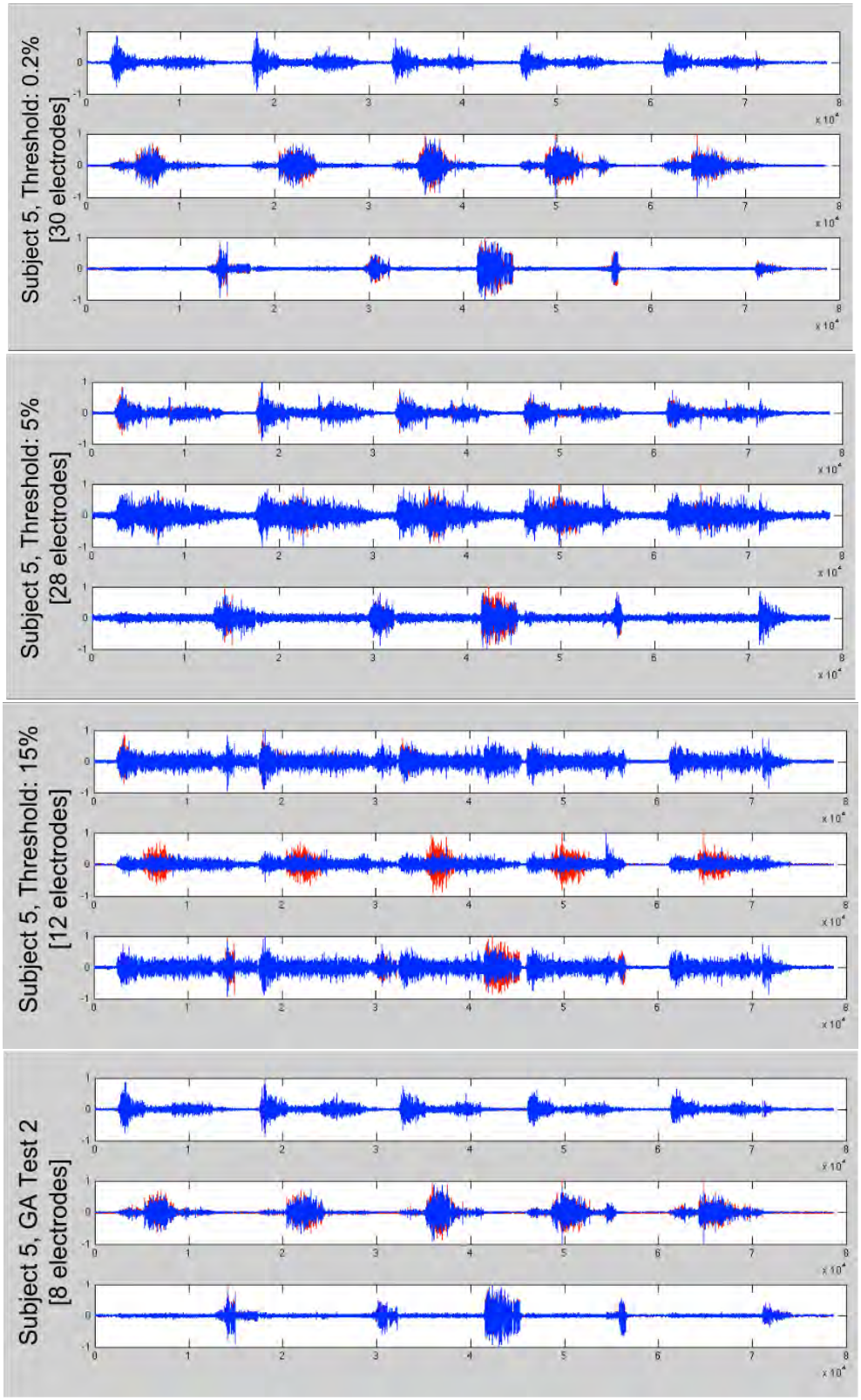

Figure 6.10: Effect of zero weighting electrode reduction of ICA on subject 5. The experiment was run with 5 different thresholds [0.2%, 1%, 5%, 10%, 15%], however, for brevity only the outputs for 0.2%, 5% and 15% are shown. For comparison the final figure shows the GA derived solution, which manages to extract usable signals with 8 active electrodes.

a more comprehensive look at the data, refer to Table A.4 and subsequent tables in the Additional Data section.

6.1.3 A Generalized Solution?

To find a "one size fits all" generalized solution, the global similarities in the solutions data needed to be found. However, the electrode band positioning as a whole is very fallible. This coupled with different arm circumferences and underlying musculature of the subjects, makes the likelihood of finding a good general solution comparable to the individualized GA solutions very low.

Each of the 20 subjects were tested with the same two optimizing GAs. The idea was to see if some pattern or similarity would emerge in the solutions to indicate which electrodes or general regions of electrodes were of importance to the ICA algorithm during the separating process.

If one considers the electrode placements for Test 1 in Table 6.6 one can observe that the spread of electrodes is very noisy or random. There does not seem to be any underlying pattern or schema inherent across all solutions. This can also be seen in the Test 2 GA data supplied in the Appendix A.

Table 6.6: Electrode activations for all 20 subjects after optimization with Test 1 GA. Each row in the table represents the 30 electrodes in the arm band, starting from electrode 1 on the left. The cells indicated with a 1 and highlighted in green are the electrode which are actively contributing to the solution.

Subject #	Electrodes which are active in the solution (green)																														Electrode #
1	1	0	0	0	0	0	1	0	0	1	1	0	0	1	0	0	0	0	0	0	0	0	0	1	0	0	1	0	0		7
2	1	0	0	0	0	0	0	0	0	0	1	0	0	1	0	0	0	1	0	0	0	0	0	0	0	0	1	0	0	1	6
3	1	1	0	0	0	0	0	0	0	0	1	0	0	0	0	0	0	0	0	1	0	0	0	0	0	0	0	1	0	0	5
4	0	0	0	0	0	0	0	0	0	1	0	0	0	0	1	0	0	0	1	1	0	0	0	0	0	0	1	1	0	0	6
5	0	0	0	0	1	1	0	0	0	0	0	0	0	0	0	0	0	0	0	0	0	0	0	1	1	1	0	0	1	0	0	6
6	0	1	1	1	0	0	0	0	0	0	0	0	0	1	0	0	0	0	0	1	1	0	0	0	0	0	1	1	0	1	9
7	0	0	0	0	0	0	0	0	1	1	1	0	1	1	0	0	1	0	0	0	1	0	0	0	0	0	0	0	0	1	8
8	1	0	0	0	0	0	0	0	0	1	1	0	0	1	1	0	0	0	0	0	0	0	0	1	0	1	1	0	1	0	0	9
9	0	0	0	0	1	0	0	0	1	1	1	0	0	0	1	0	0	0	0	0	1	0	0	0	1	0	1	0	0	0	8
10	0	0	0	0	0	0	0	0	0	0	0	0	0	0	0	0	0	0	1	1	0	0	1	1	0	0	1	1	0	0	6
11	0	1	0	0	1	0	0	0	0	1	0	0	0	0	0	0	0	0	0	1	0	0	0	0	0	0	1	1	0		6
12	0	0	0	1	1	0	0	0	0	0	0	0	0	1	0	0	0	0	0	0	0	0	0	0	0	0	0	1	1		5
13	0	0	0	0	1	1	0	0	0	1	0	1	0	1	1	0	0	0	1	1	0	1	0	1	0	0	0	0	0	1	11
14	0	1	0	0	1	1	0	1	0	0	0	0	0	0	0	0	0	1	1	1	0	0	0	0	0	0	0	0	0		7
15	0	0	0	1	0	0	0	0	0	1	0	1	0	1	0	1	0	0	1	0	1	0	1	0	0	0	0	0	0	0	8
16	0	0	0	0	0	1	0	0	0	0	1	1	0	1	0	0	0	0	0	0	0	1	0	0	1	0	1	1	0	1	9
17	0	1	1	1	0	0	0	1	0	1	0	0	0	0	0	0	0	0	0	0	0	0	1	1	1	0	0	1	1	0	10
18	0	0	0	0	0	0	0	0	0	0	0	0	1	0	1	0	1	1	0	0	0	0	1	0	0	1	0	0	0		6
19	0	1	1	0	0	0	0	0	0	0	0	0	0	0	0	1	0	0	0	0	0	1	1	1	0	1	0	0	0		7
20	1	1	1	1	0	0	0	1	1	1	0	1	0	0	0	0	0	0	0	0	1	0	0	0	0	0	1	0	0		10

Even though the data are noisy and no pattern is evident, it is hoped that one may be able to gain insight into electrode placement by taking a cumulative total of

electrode activations per position. The electrode locations with the highest number of active electrode contributions would naturally point to the areas of the arm band which need the highest density of electrodes. From this it may be possible to suggest a suitable "pseudo-generalized" electrode placement.

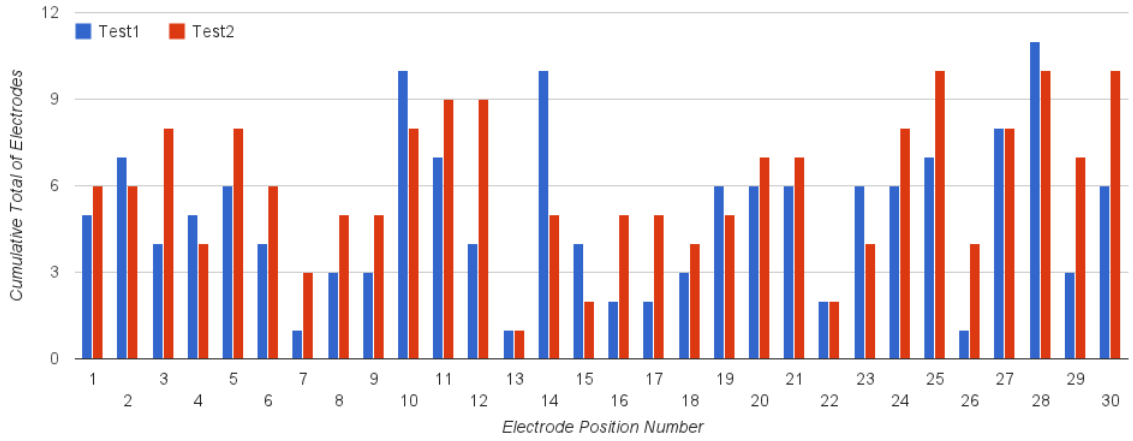

Figure 6.11: Electrode distribution over electrode position. This histogram was used to determine which areas of the arm-band played a significant role in signal production, averaged over the 20 test subjects.

To determine this "pseudo-generalized" solution a histogram representation of electrode tally relative to position for each GA test was created. In Figure 6.11 a combined histogram for both Test 1 and Test 2 can be seen. The histogram gives some idea of which regions of the electrode arm-band contribute the most to signal separation in all of the test subjects. Using a threshold value at each electrode position, the active electrodes were selected based on whether their cumulative total was higher than the threshold value. This allows the creation of a solution with an averaged electrode pattern, with active electrodes at the peaks in the histogram.

The thresholds were selected so that the generalized solutions had close to the average number of electrodes present in the GA optimized placements for Test 1 and Test 2. A second threshold was selected to produce a general solution with a much larger number of electrodes than the averages of Test 1 and Test 2.

Thus in testing, two different threshold values were applied to each set of GA solution tallies. For the Test 1 GA these values were 6 and 5, resulting in solutions with 8 and 16 electrodes respectively. For Test 2 the threshold values were 7.5 and 6, resulting in solutions with 10 and 13 electrodes respectively.

Once again, from Figure 6.12, one can not easily see a pattern in electrode placement, however, there are a few electrodes and regions which are present in all 4 average representations.

If the performance of each of these 4 "average" electrode placement variations in Figure 6.13 is examined, one can see that the best performance is that of Test 1 with

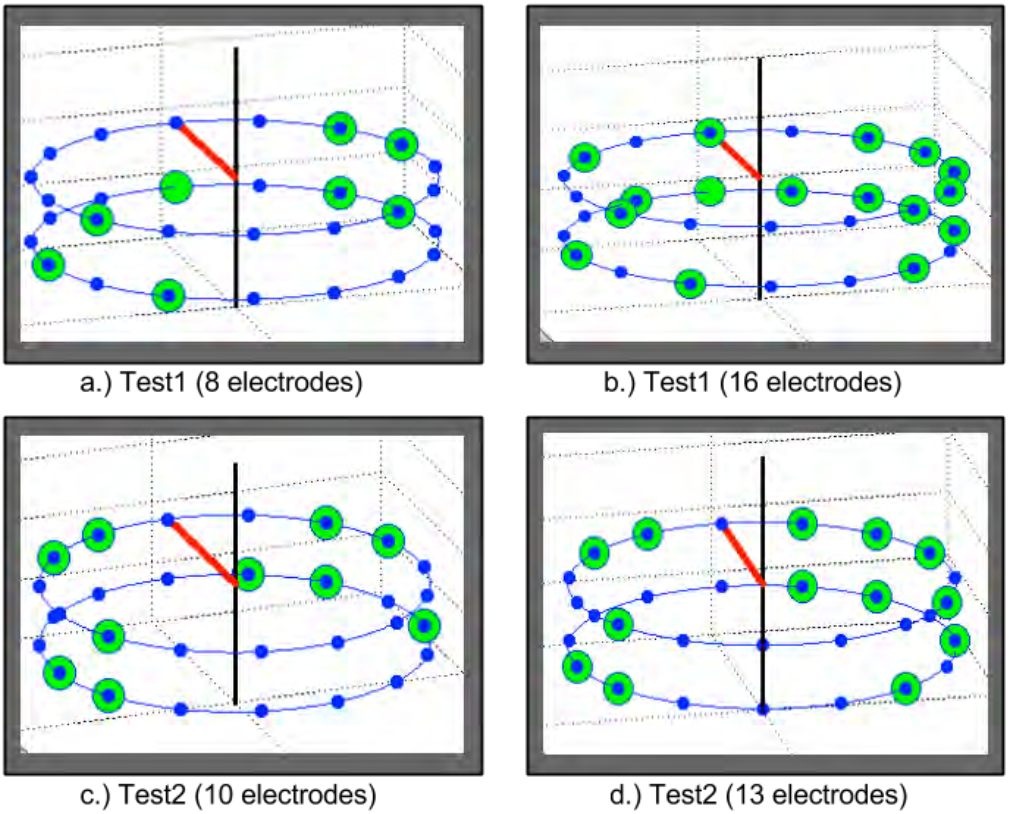

Figure 6.12: 3D representations of electrode placement for the 4 GA guided test solutions.

16 electrodes, represented at image (b) in Figure 6.12. The second best "pseudo-general" solution is Test 2 with 13 electrodes, see image (d). It seems intuitive that these two would perform the best as they have more electrodes contributing greater amounts of information to the ICA algorithm, but would obviously lose out on speed performance, however negligible it may be.

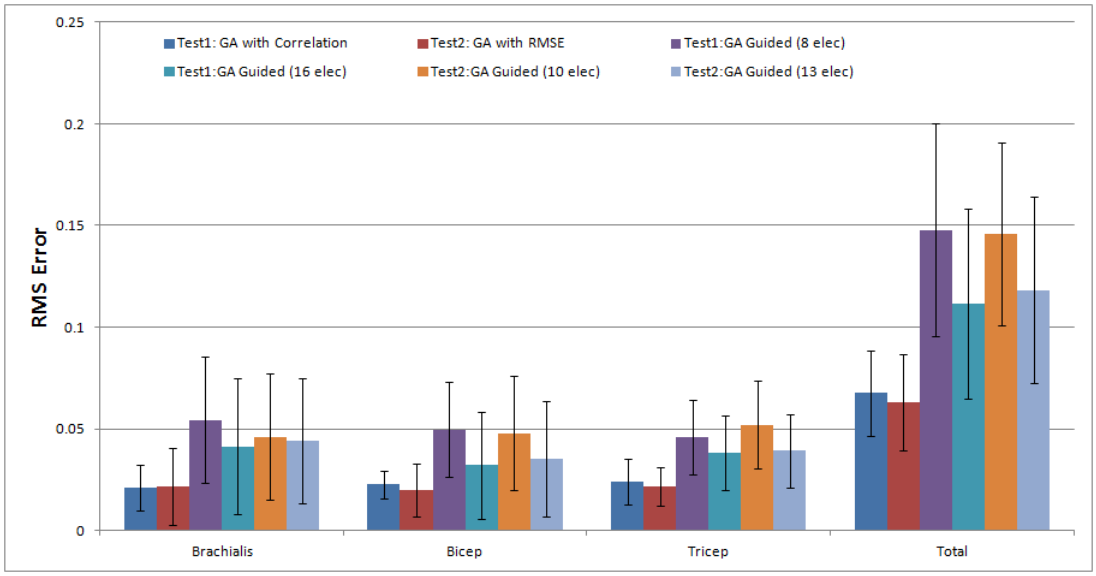

Figure 6.13: Average RMSE values for each variation of electrode positioning solutions. Error bars represent standard deviation.

This general solution, Test 1 with 16 electrodes, produces more error in comparison to the 30-electrode standard configuration, although uses only about half of the available electrodes. However, the pure GA solutions from Test1 and Test2 still have lower error and use even fewer electrodes, albeit at the cost of computational complexity.

6.2 Isometric Contraction Test [3, 2]

To validate the separation of source signals, it was necessary to evaluate the system while the muscles move as little as possible relative to each other, as well as maintain joint angle. This is achieved by performing isometric contraction tests on the right arm.

As mentioned in section 4.2, the test consists of pulling and pushing against a static bar, with the elbow joint fixed at 90°. One should be able to see distinct activations of the bicep muscle during the pulling actions and conversely see activations of the brachialis during the downward pushing. In this testing, the tricep does not play a roll as it is primarily used in extension of the elbow.

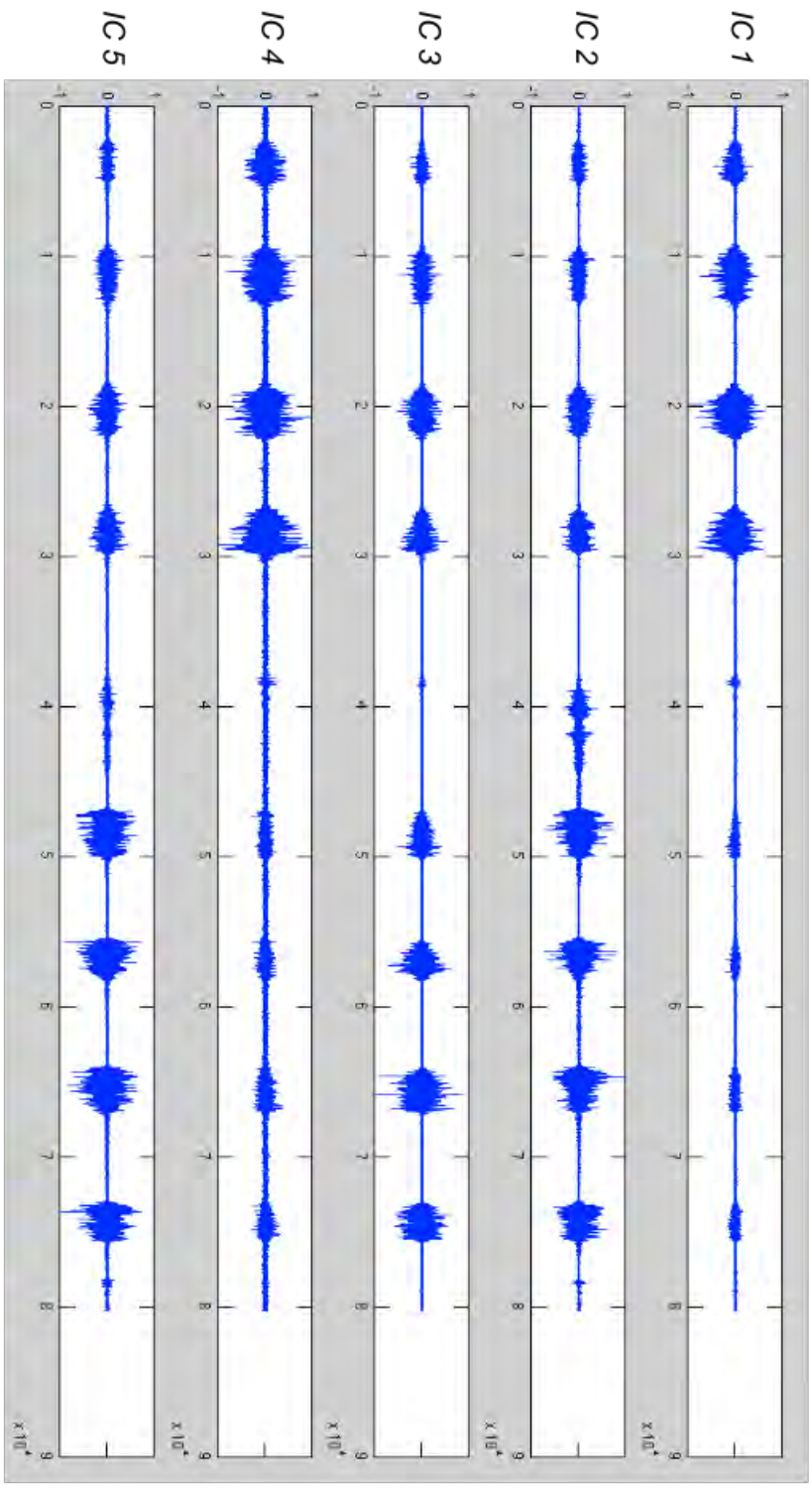

Figure 6.14: Five ICA signals from a subject during the isometric contraction testing.

Figure 6.14 shows some of the ICA signal outputs from the isometric contraction test. It is not clear from here which signals belong to which source as both seem to activate on both the pull and the push portion of the test. This is the case for all the test subjects, a random selection of these results can be seen in the Appendix A. It is suspected that the MVC percentage of 15%, set during the test, was too high and thus caused the subjects to pull too hard, co-contracting the bicep and brachialis during both the pull and push.

However, if one examines the signals in Figure 6.14 closely, one can see that *IC 1* has higher EMG activity for the first four "beats" in the signal, during the pull. Conversely *IC 5* has higher peaks during the push. This would seem to indicate that these are the bicep and brachialis signals respectively, although they do not appear to be independent of each other.

To determine whether this was the case, a reliable bicep signal was needed to compare to the ICA output signal. This can be done by selecting a pair of electrodes directly above the bicep muscle belly and using the two monopolar signals to create a bi-polar bicep signal. This mimics the way one would normally acquire bicep muscle signals with surface EMG electrodes placed as described by the SENIAM project (Surface Electromyography for the Non-Invasive Assessment of Muscles) [9].

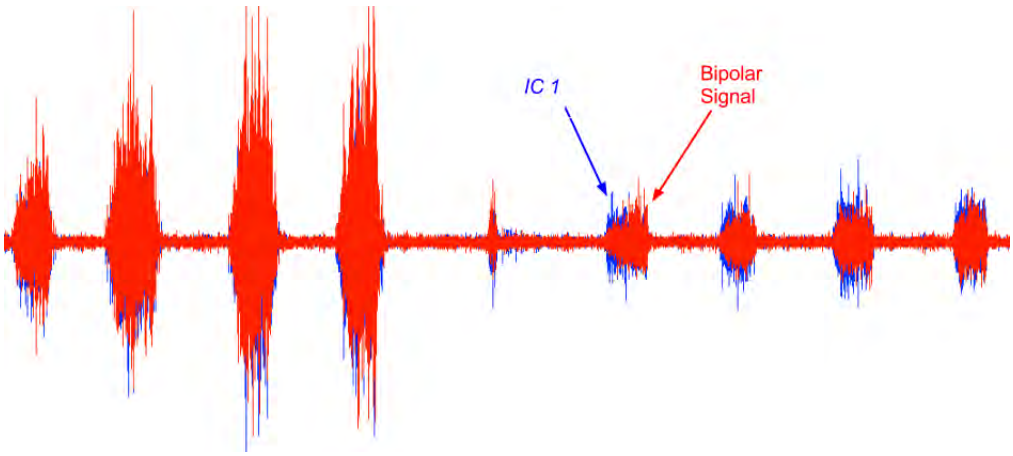

Figure 6.15: Bi-polar bicep signal (red) overlaid with *IC 1* from Figure 6.14. For this particular bipolar bicep signal, electrode 5 and 6 were chosen as the bipolar pair.

The attained bicep signal was then compared to *IC 1* which is believed to be the bicep. The error (RMSE) between *IC 1* and the bipolar signal is then 0.0285, with a correlation of 0.8412 (max = 1.0). This accompanied with the visual evidence in Figure 6.15, seems to suggest at the very least, that the bicep is co-contracting on the push down portion of the isometric test.

This interdependency between the two muscles violates the independence specification in the ICA algorithm, and as such may reduce the efficacy of the separation for this test.

7 Conclusions

In this research a fully fledged hardware system capable of acquiring and logging EMG data in real-time was developed. This system was then used to gather data from 20 able bodied subjects and tested the applicability of the FastICA on EMG data for the extraction of deep-tissue muscle activity using only non-invasive electrodes. A simple genetic algorithm was then developed to optimize the placement and necessary number of the electrodes in the acquisition system.

The hardware development used a ready made solution available from National Instruments as the microcontroller unit (MCU) in conjunction with several fabricated printed circuit boards (PCB). The PCBs created were the analog frontend and the digital potentiometer board. These boards amplified and conditioned the the millivolt signals acquired on the surface of the subjects skin via electrodes.

The electrodes were hand made pure silver electrodes with an electrolyte gel to improve conduction and reduce impedance. The final acquisition system was able to simultaneously log 30 channels of EMG data. Each channel was sampled at a rate of 2000 *S/s*. The system was then able to log all the data during a subject test to a data file for later analysis and manipulation.

Additionally the system was able to give the person conducting the experiment visual feedback on the input signals being acquired. This was achieved by plotting a selected subset of the incoming EMG signals in real-time to a computer console. On top of this the user was able to manipulate individual channel gain as they saw fit during the test using a software control panel also present on the computer console.

All these features resulted in a versatile and adjustable system capable for use in multiple biosignal projects, allowing for the collection and data logging of 30 channels easily and effectively.

Through the implementation of the experimental methods and the designed movement protocol, the author was able to successfully replicate and further validate the results found in the preliminary study performed by Moroaswi and John [2, 1]. The author reconfirmed that FastICA was capable of isolating the deep-tissue muscle signal emanating from the Brachialis muscle in the upper arm during dynamic contractions. This was confirmed across multiple test subjects and indicates that the ICA could be used in future EMG systems to extract deep-tissue signals.

To extend and improve the efficacy of the EMG ICA system on the upper arm, a simple genetic algorithm was implemented to optimize the electrode placement and reduce the number of electrodes necessary. This was able to successfully reduce

the number of electrodes for each subject to an average of 8 electrodes, achieving an average root mean squared error of 0.0211 and 0.0225 for the brachialis and bicep muscle respectively. This reduction allows the system to produce near "gold standard" separated signals but with a reduced data requirement of approximately 73% less than the 30 electrode system. This GA optimization would allow the system to tailor the electrode placement for each individual. This system could then be used as a calibration phase in the implementation of a robotic prostheses. The GA could guide the placement of the electrodes, which could then be built into the prosthetic attachment socket.

It was noted during these optimizations that certain individuals performed considerably worse than others, for instance subjects 8 and 12 in Table 6.2. The direct cause of this poor RMSE performance is unknown, however, it could be attributed to many factors such as high impedance skin, abnormal musculature, *etc.*

It is also possible that poor performance in some of the subjects could be attributed to large variations in output mixing matrix A of the ICA [72], as there is no performance measure imposed on the separation matrix, and this can lead to a poor optimization in the GA.

From the optimized electrode placements from the 20 test subjects it was theorized that one may be able to extract certain trends and possibly produce a generalized solution to electrode placement that would be applicable to multiple users. To do this a histogram based method was used to determine which electrode regions were in general most important to the ICA algorithm. From this a couple of different variations of a general solution were generated and tested on the data from the 20 subjects.

It was found that the general solution did not produce very convincing results. These results seem to indicate that the variation from user-to-user is far to great to infer a one-size-fits-all solution. In all cases, it is more beneficial to use the computationally intensive GA solutions as they yield more accurate solutions with a fraction of the electrodes.

One of the more disappointing results during the experimentation was that of the isometric contraction tests performed using the static pull test rig. This test returned inconclusive results as it seems that the brachialis and bicep were co-contracting during the movement protocol, causing the ICA to not be able to separate the signals appropriately because the assumption of source independence was violated. It is assumed that this co-contraction is due to a high %MVC level, however, more testing would need to be performed to confirm this.

8 Recommendations and Future Work

In this research, a full system for EMG signal acquisition was presented, which was used to explore, and validate previous work done in the detection of deep-tissue EMG using noninvasive techniques. This research is part of a continuing body of work to produce robotic prostheses and orthotics to improve daily life of physically impaired patients. To this end the hardware system presented here is not ready to be used in commercial prostheses or orthotics.

The system itself is too heavy and cumbersome. In order for it to be used in these assistive technologies the frontend system would need to be drastically miniaturized and optimized for low power consumption, so it could be contained within the prosthetic and run off battery power. In order to reduce this system size one would need to look into designing a specific ASIC for signal acquisition.

Additionally it would be useful to design a MCU system from scratch, as this system used an off-the-shelf solution which was far larger and perhaps an over specification necessary for this project. The final system would ultimately need to process the FastICA on board the MCU, it would be interesting to implement this system using a FPGA with large memory capacity or use several smaller FPGAs in a cluster to quickly calculate the independent components. FPGAs would be an ideal architecture as it is possible to implement the FastICA algorithm in parallel.

It may also be interesting to look at minimum batch sizes for EMG separation in ICA algorithms as in this implementation, the entire recording was processed in one batch. It would be great to implement a windowed ICA algorithm, which operates on smaller "window" size batches and produces intermediate separating matrices. This would allow the system to run much faster and it may be a possibility to have a system which constantly updates the separating matrix as more useful data are available.

Another extension to the implementation of the FastICA algorithm is to run it multiple times and then use a Signal-to-Interference Ration (SIR) measure to rate the separation ability of the separation matrices. Then the final separating matrix is just the highest rated separation matrix out of all the runs performed. An implementation of this system has been discussed by Naik and Kumar [72] with very promising results. The benefit of this system is that it reduces the variations in ICA output matrix, allowing for much more repeatable results.

Another improvement would be look into different variations of the ICA algorithm. A study also performed by Naik, Kumar and Weghorn explores the use of several different blind source separation techniques for use in EMG separation [75]. They found that the temporal decorrelation separation method (TDSEP) performed the best, outperforming FastICA. They propose that systems like TDSEP perform better as they are based on Second-Order statistics as apposed to FastICA which is based on Higher-Order statistics (HOS). They theorize that HOS systems may need more sample points in the data batches to perform well. TDSEP has the added benefit of computational simplicity and efficiency.

It would also be beneficial to explore an extension of the GA. Many GA implementations exist, which help alleviate the general GA problem of population stagnation. One such solution is the Island Model GA. Stagnation can also be countered using clever selection and breeding procedures. Exploration in either of these directions could potentially assist the GA guided ICA in finding the global or near-global solutions for electrode placement.

In this and previous research, the FastICA was confirmed to be effective at extracting the deep-tissue EMG signals during the designed movement protocol, however, this same system was not tested on different movement protocols. A further study would be necessary to confirm applicability over all movements. However, the author is of the belief that it would work with the same efficacy.

A very simple muscle group was selected for this research so that we could confidently isolate the muscle movements during the dynamic movements. It would however be interesting to implement this system on a more complex muscle group such as the forearm or the lower leg muscle groups, where the muscles are more numerous and more densely packed.

One further study that would need to be performed is that of the retesting of the isometric contractions test. It would be necessary to retest the movement protocol at a significantly lower contraction strength level. It would also be worth having a physician present during the testing to confirm that the muscle are in fact co-contracting.

Lastly, in order for this system to one day be used in daily life of patients the system would need to be simple to use and not require pastes or gels for the application of the electrodes. It would be necessary to develop dry electrodes to embed in the armband or prosthetic socket for the system.

Bibliography

[1] L.R. John. Non-invasive Deep Muscle Electromyography.

[2] S.P. Moroaswi and L.R. John. *Preliminary study of sEMG and ICA for extraction of deep-tissue muscle activity of Brachialis (unpublished results).* University of Cape Town, 2010.

[3] S. Stoekigt, N.V. Divekar, and L.R. John. *Design of isometric pull test mechanical rig. Technical Note.* University of Cape Town, 2010.

[4] G. Robertson, G. Caldwell, and et al. *Research Methods in Biomechanics.* Human Kinetics, 2nd edition, 2013.

[5] C. Cipriani, F. Zaccone, S. Micera, and M.C. Carrozza. "On the Shared Control of an EMG-Controlled Prosthetic Hand: Analysis of User Prosthesis Interaction". *IEEE Transactions on Robotics*, 24(1):170–184, February 2008.

[6] R.A.R.C. Gopura, D.S.V. Bandara, J.M.P. Gunasekara, and T.S.S. Jayawardane. Chapter 12: Recent Trends in EMG-Based Control Methods for Assistive Robots. In *Recent Trends in EMG-Based Control Methods for Assistive Robots*, pages 237–268. InTech, University of Moratuwa, Sri Lanka.

[7] L. Hargrove. *"A comparison of Surface and Intramuscular Myoelectric Signal Classification."*. PhD thesis, University of New Brunswick, 2003.

[8] R. Bogey, K. Cerny, and O. Mohammed. "Repeatability of wire and surface electrodes in gait". *American journal of physical medicine & rehabilitation*, 82(5):338–344, 2003.

[9] The SENIAM project (Surface ElectroMyoGraphy for the Non-Invasive Assessment of Muscles).

[10] A. Hyvarinen. "A Family of fixed-point algorithms for Independent Component Analysis.". In *IEEE International Conference on Acoustics, Speech, and Signal Processing, 1997. ICASSP-97.*, volume 5, pages 3917 – 3920, Munich, April 1997. IEEE.

[11] P. Konrad. *The ABC of EMG-A Practical Introduction to Kinesiological Electromyography.* Noraxon INC. USA., April 2005.

[12] T. Pan and P. Fan. Mechatronic Experiments Course Design : Prosthesis Project. *IEEE Transactions on Education*, 47(3):348–355, 2004.

[13] C. De Luca. *DelSys Inc: Surface Electromyography: Detection and Recording.* 2002.

[14] M.Z. Jamal. Chapter 18: Signal Acquisition Using Surface EMG and Circuit Design Considerations for Robotic Prosthesis. In *Computational Intelligence in Electromyography Analysis - A Perspective on Current Applications and Future Challenges*, pages 427–448. InTech, 2012.

[15] B. Gerdle, S. Karlsson, S. Day, and M. Djupsjobacka. Acquisition, Processing and Analysis of the Surface Electromyogram. In *Modern Techniques in Neuroscience Research*, pages 705–755. Springer Berlin Heidelberg, 1999.

[16] G.S. Rash. *Electromyography Fundamentals*. 1999.

[17] Table of muscles of the human body: Upper limb, June 2013. Page Version ID: 557896936.

[18] J.C. Boileau Grant. *Grant's Atlas of Anatomy*. The Willianms & Wilkins Co., Baltimore, 6th edition, 1972.

[19] R.L. Drake, A.W. Vogl, and A.W.M. Mitchell. Gray's Anatomy for Students, Chapter 7: Upper Limb. In *Gray's Anatomy for Students*, page 1136. Churchill Livingstone, 2nd edition, February 2009.

[20] H. Gray. *Gray's Anatomy: Anatomy of the Human Body*. Lea & Febiger, Philadelphia, 20th edition, 1918.

[21] F. Martini, W.C. Ober, K. Welch, and R.T. Hutchings. *Fundamentals of Anatomy & Physiology*. Prentice Hall College Div, 5th edition, January 2001.

[22] A. Tax, J. Denier van der Gon, and C. Erkelens. "Differences in coordination of elbow flexor muscles in force tasks and in movement tasks". *Experimental Brain Research*, (81):567–572, February 1990.

[23] Medical Departments U.S. Army and Navy. *Manual of Surgical Anatomy*. The Division of General Surgery, Washington, DC, U.S.A., 1918.

[24] G.R. Naik and D. Kumar. "Estimation of independent and dependent components of non-invasive EMG using fast ICA : validation in recognising complex gestures". *Computer Methods in Biomechanics and Biomedical Engineering, Talor and Francis*, 14(12):1105 – 1111, 2011.

[25] N. S. Stoykov, M. M. Lowery, and T. A. Kuiken. A Finite-Element Analysis of the Effect of Muscle Insulation and Shielding on the Surface EMG Signal. *IEEE transactions on biomedical engineering*, 52(1):117–121, 2005.

[26] F. Sattar and C. Charayaphan. Low-cost design and implementation of an ICA-based blind source separation algorithm. In *15th Annual IEEE International*, volume 15, pages 15–19. IEEE, 2002.

[27] C. J. James and C. W. Hesse. "Independent component analysis for biomedical signals.". *Physiological measurement*, 26(1), 2005.

[28] A. Hyvarinen. "Fast and Robust Fixed-Point Algorithms for Independent Component Analysis". *IEEE Transactions on Neural Networks*, 10(3):626–634, May 1999.

[29] A. Hyvarinen and E. Oja. "Independent Component Analysis: Algorithms and Applications". *Neural Networks*, 4(13):411–430, 2000.

[30] E. Bingham and A. Hyvarinen. "A fast Fixed-point Algorithm for Independent Component Analysis of Complex Valued Signals". *International Journal of Neural Systems*, 10(1):1–8, February 2000.

[31] M. Affenzeller, S. Winkler, and A. Beham. *Genetic Algorithms and Genetic Programming: Modern Concepts and Practical Applications*. 1 edition, April 2009.

[32] R.L. Haupt and S.E. Haupt. *Practical Genetic Algorithms*. John Wiley & Sons, Inc., Hoboken, New Jersey., 2nd edition, 2004.

[33] N. M. Razali and J. Geraghty. Genetic Algorithm Performance with Different Selection Strategies in Solving TSP. In *Proceedings of the World Congress on Engineering*, volume II, pages 1134 – 1139, London U.K., July 2011.

[34] T. Blickle and L. Thiele. "A Comparison of Selection Schemes used in Genetic Algorithms". page 67. Swiss Federal Institute of Technology ETH, December 1995.

[35] H. Martin, S. Chevallier, and E. Monacelli. Fast calibration of hand movement-based interface for arm exoskeleton control. In *European Symposium on Artificial Neural Networks (ESANN)*, Bruges, Belgium, 2012.

[36] G. De Lee, W. Wang, and et al. Arm Exoskeleton Rehabilitation Robot with Assistive Systems for Patient after Stroke. In *12th International Conference on Control, Automation and Systems*, pages 1943–1948, Jeju Island, Korea, October 2012.

[37] Y. Ren, H. Park, and L. Zhang. "Developing a whole-arm exoskeleton robot with hand opening and closing mechanism for upper limb stroke rehabilitation". In *IEEE International Conference on Rehabilitation Robotics*, volume 11, pages 761–765, Kyoto,Japan, June 2009. IEEE.

[38] K. Strausser and H. Kazerooni. "The Development and Testing of a Human Machine Interface for a Mobile Medical Exoskeleton". In *IEEE International Conference on Intelligent Robots and Systems*, pages 4911–4916, San Francisco, USA, September 2011. IEEE.

[39] A. Wege and A. Zimmermann. Electromyography Sensor Based Control for a Hand Exoskeleton. In *IEEE International Conference on Robotics and Biomimetics*, Sanya, China, December 2007.

[40] M. Mulas, M. Folgheraiter, and G. Gini. An EMG-controlled Exoskeleton for Hand Rehabilitation. In *Rehabilitation Robotics*, volume 9th, Chicago, July 2005. IEEE.

[41] T. Lenzi, S.M.M. De Rossi, N. Vitiello, and M. Chiara Carrozza. "Intention-Based EMG Control for Powered Exoskeletons". *IEEE Transactions on Biomedical Engineering*, 59(8):2180–2190, August 2012.

[42] Z. Khokhar and Z. Xiao. "Surface EMG pattern recognition for real-time control of a wrist exoskeleton". *BioMedical Engineering Online*, 2010.

[43] C. Jutten and J. Herault. "Blind separation of sources, part 1: an adaptive algorithm based on neuromimetic architecture". *Signal Processing*, 24(1):1–10, 1991.

[44] H.Huang and et al. "An anthropomorphic controlled hand prosthesis system". *Journal of Zhejiang University-Science C*, 13(10):769–780, 2012.

[45] P. Shenoy, K. Miller, B. Crawford, and R. Rao. "Online Electromyographic Control of a Robotic Prosthesis". *IEEE Transactions on Biomedical Engineering*, 55(3):1128–1135, March 2008.

[46] A. Alkan and M. Gunay. "Identification of EMG signals using discriminant analysis and SVM classifier". *Elsevier: Expert Systems with Applications*, 39:44–47, 2012.

[47] A. Balbinot, A. Schuck Junior, and G. Winkler Favieiro. Decoding Arm Movements by Myoelectric Signal and Artificial Neural Networks. *Scientific Research: Intelligent Control and Automation*, 4:87–93, 2013.

[48] A.Singh. Prosthetic Hand Control. *International Journal of Computational Engineering Research*, 2(7):311–339, November 2012.

[49] C. Atkeson, A. Moore, and S. Schaal. "Locally Weighted Learning". *Artificial Intelligence Review*, 11:11–73, 1997.

[50] Publisher Taylor. Computer Methods in Biomechanics and Biomedical Engineering Estimation of independent and dependent components of non-invasive EMG using fast ICA : validation in recognising complex gestures. *Biomechanics*, (931414160), 2011.

[51] G.R. Naik and D. Kumar. *Chapter 6: Blind Source Separation Based Classification Scheme for Myoelectric Prosthesis Hand*. InTech, 2011.

[52] Y. Guangying. "Study of Myoelectric Prostheses Hand based on Independent Component Analysis and Fuzzy Controller". In *International Conference on Electronic Measurement and Instruments*, volume 8th, pages 174–178, Xian, China, August 2007. EMI Journal.

[53] *i-limb ultra revolution: Touch Bionics*.

[54] *Motion Control, Inc. ProControl Prosthesis Myoelectric Controller*.

[55] *Thalmic Labs: www.thalmic.com*. July 2013.

[56] G. Stein. Why Isn't The MYO Armband Open Source?: http://www.fastcolabs.com/3013885/why-isnt-the-myo-armband-open-source, July 2013.

[57] H. Motulsky. *Intuitive Biostatistics*. Oxford University Press, USA, 1st edition, 1995.

[58] A.M. McNaught and L.R. John. *Modifying the OpenEEG Board for EMG Acquisition. Technical Report.* Division of Biomedical Engineering, University of Cape Town, 2009.

[59] *The ModularEEG Design.*

[60] Instrumentation Amplifier - Dual Supply - INA128 - TI.com.

[61] *Operational Amplifier (Op Amp) - Precision Amplifier - TLC2274 - TI.com.*

[62] AD5206 datasheet and product info | 6-Channel, 256-Position Digital Potentiometer | Digital Potentiometers | Analog Devices.

[63] *NI sbRIO-9612/9612XT - Embedded Devices with Analog Input and DIO, 2M Gate FPGA - National Instruments.*

[64] *TMV 0505S Traco \textbar DC/DC converter,5Vin,5Vout 0.2A,1W \textbar 666-4026P \textbar Welcome to RS Online.*

[65] Fairchild Semiconductor. Adjustable/2.5 V, 2% Tolerance Shunt Regulator.

[66] Texas Instruments Incorporated. The "Rail Splitter" Precision Virtual Ground., 1998.

[67] H. Lee, K. Kim, and S.R. Oh. "Development of a wearable and dry sEMG electrode system for decoding of human hand configurations". In *International Conference on Intelligent Robots and Systems*, pages 746–750, Portugal, October 2012. IEEE.

[68] V. Zarzoso and P. Comon. How Fast is FastICA? *Submitted to EUSIPCO*, September 2006.

[69] J. Karhunen. *FastICA Matlab Package.*

[70] J. Karhunen, E. Oja, L. Wang, R. Vigario, and J. Joutsensalo. "A Class of Neural Networks for Independent Component Analysis". *IEEE TRANSACTIONS ON NEURAL NETWORKS*, 8(3):486–504, May 1997.

[71] A.J. Chipperfield and P.J. Fleming. The MATLAB Genetic Algorithm Toolbox. In *IEE Colloquium on*, pages 10/1–10/4. IET, January 1995.

[72] G.R. Naik and D. Kumar. Identification of Hand and Finger Movements Using Multi Run ICA of Surface Electromyogram. *Journal of Medical Systems*, (36):841–851, July 2010.

[73] M.P. Fay and M.A. Proschan. "Wilcoxon-Mann-Whitney or t-test? On assumptions for hypothesis tests and multiple interpretations of decision rules". *Statistics surveys*, 4:1, 2010.

[74] Z Table.

[75] G.R. Naik, D. Kumar, and H. Weghorn. "Performance comparison of ICA algorithms for Isometric Hand gesture identification using Surface". In *International Conference of Computer Engineering*, pages 613–618, 2007.

Appendix A

Additional Subject Waveforms

Here a representative set of output waveforms from Test 1, Test 2 and the static isometric test are shown. For brevity the author has only selected to show a representative subset of all the subjects here. Namely subjects 2, 5, 8, 15 and 17.

Each of the signals shown in Test 1 and Test 2 are the bicep signal at the top and brachialis below. The signals are also overlayed with their gold standard equivalents, to give an idea of how much error is present in the signal. The gold standard is the red signal and the blue signal is the signal produced after the optimization.

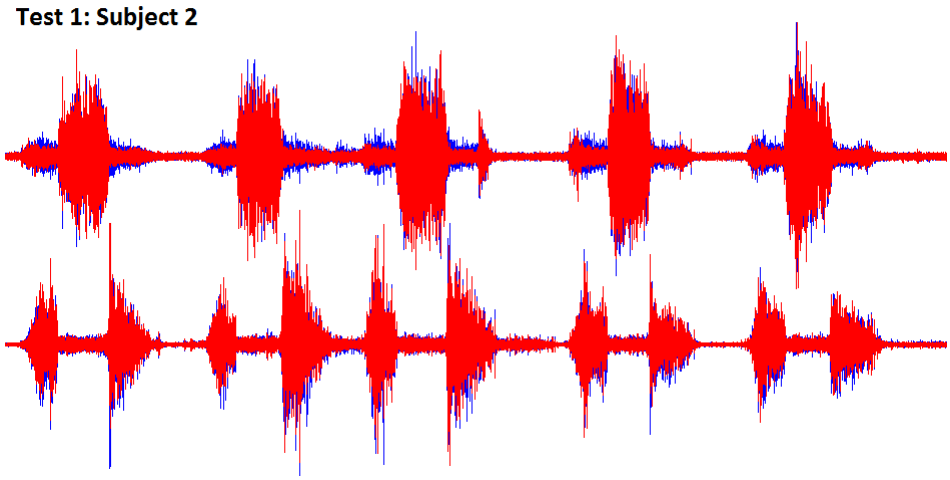

Figure A.1: Bicep and brachialis signals of subject 2 during Test 1.

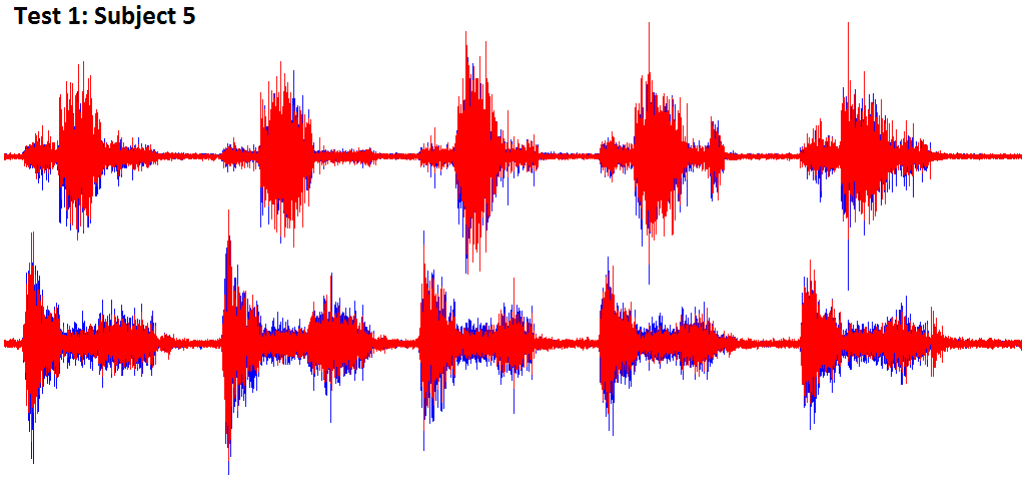

Figure A.2: Bicep and brachialis signals of subject 5 during Test 1.

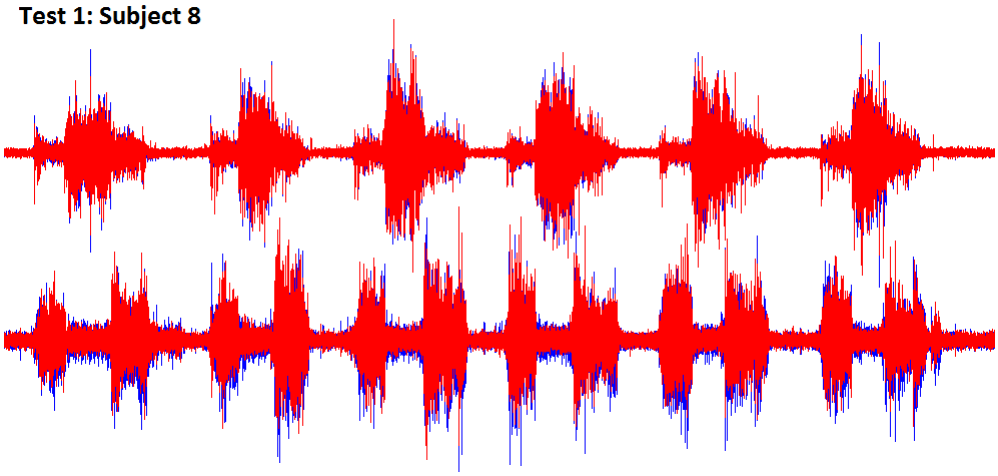

Figure A.3: Bicep and brachialis signals of subject 8 during Test 1.

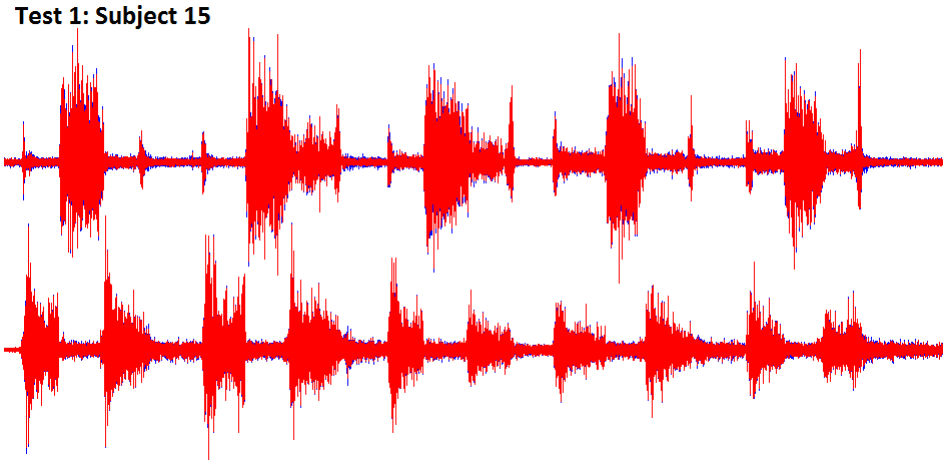

Figure A.4: Bicep and brachialis signals of subject 15 during Test 1.

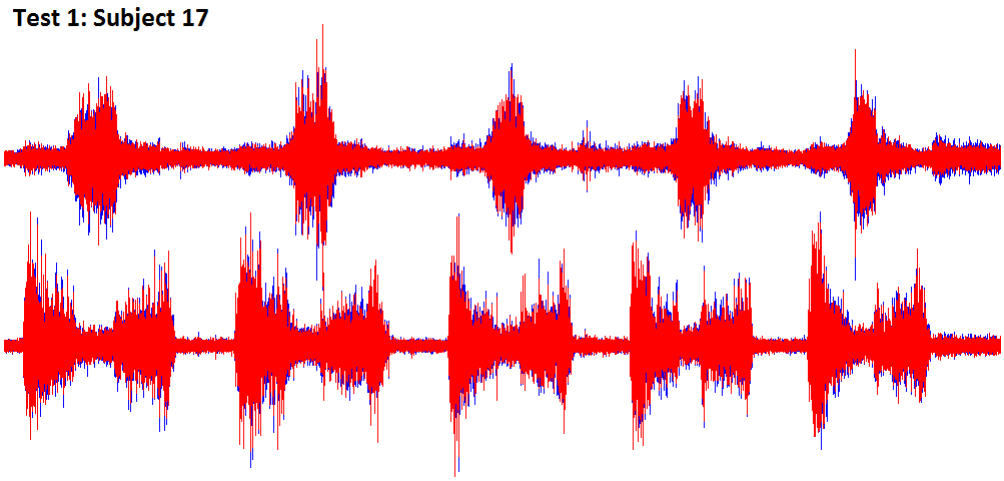

Figure A.5: Bicep and brachialis signals of subject 17 during Test 1.

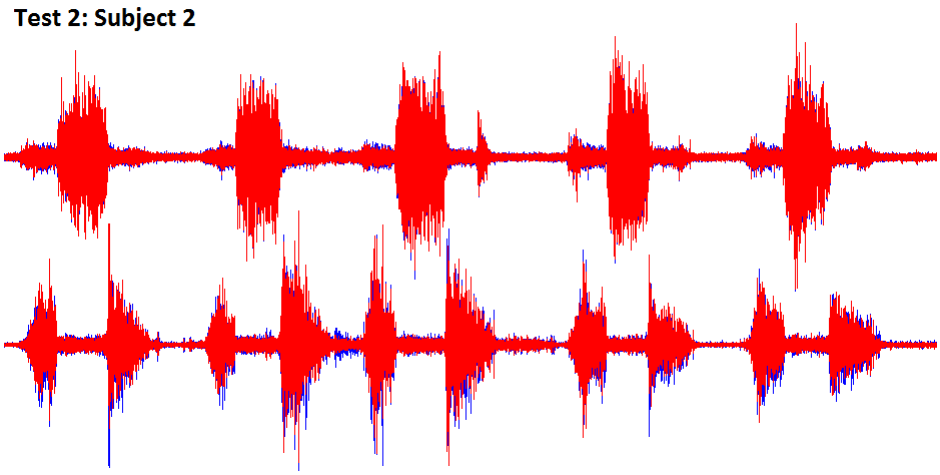

Figure A.6: Bicep and brachialis signals of subject 2 during Test 2.

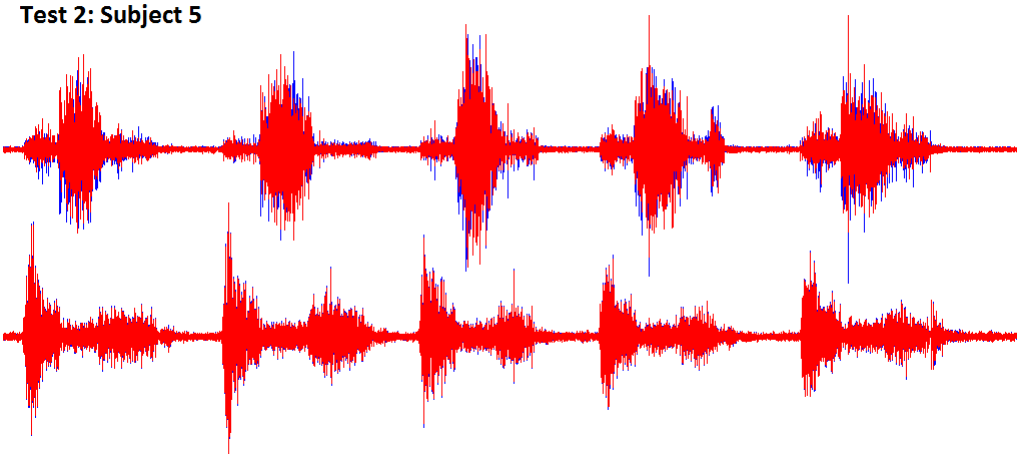

Figure A.7: Bicep and brachialis signals of subject 5 during Test 2.

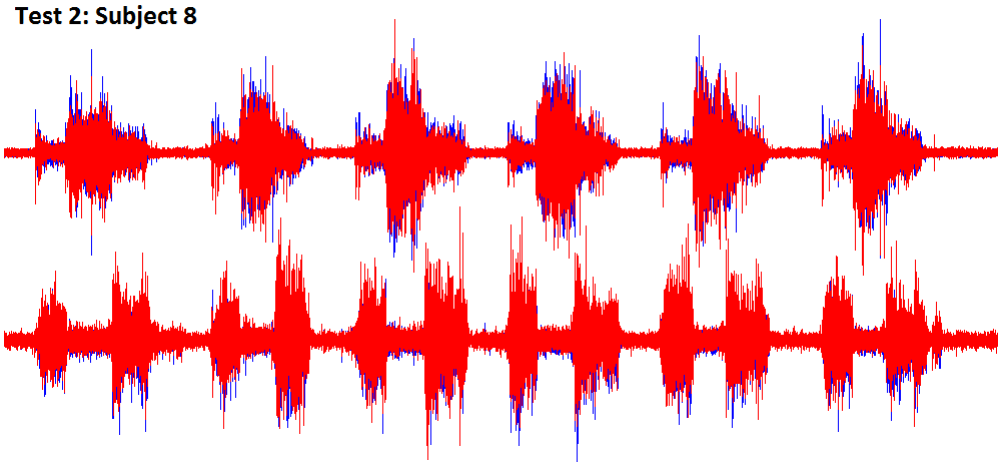

Figure A.8: Bicep and brachialis signals of subject 8 during Test 2.

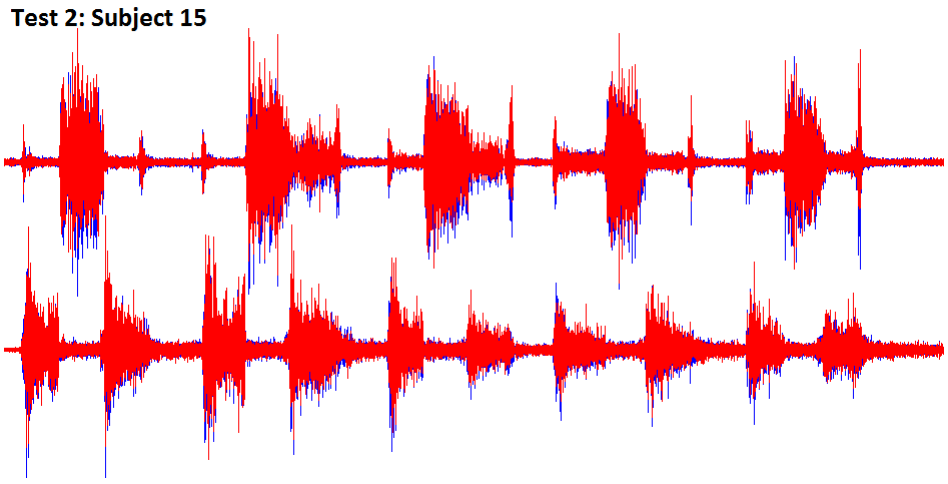

Figure A.9: Bicep and brachialis signals of subject 15 during Test 2.

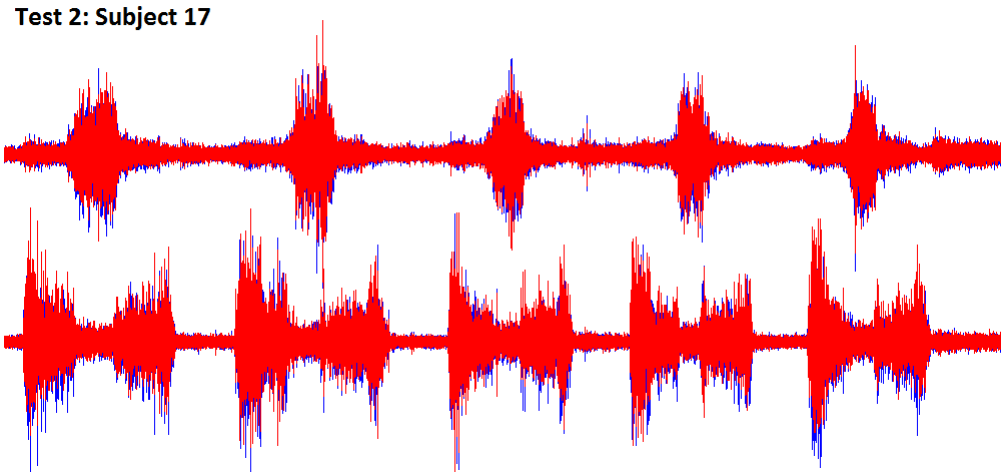

Figure A.10: Bicep and brachialis signals of subject 17 during Test 2.

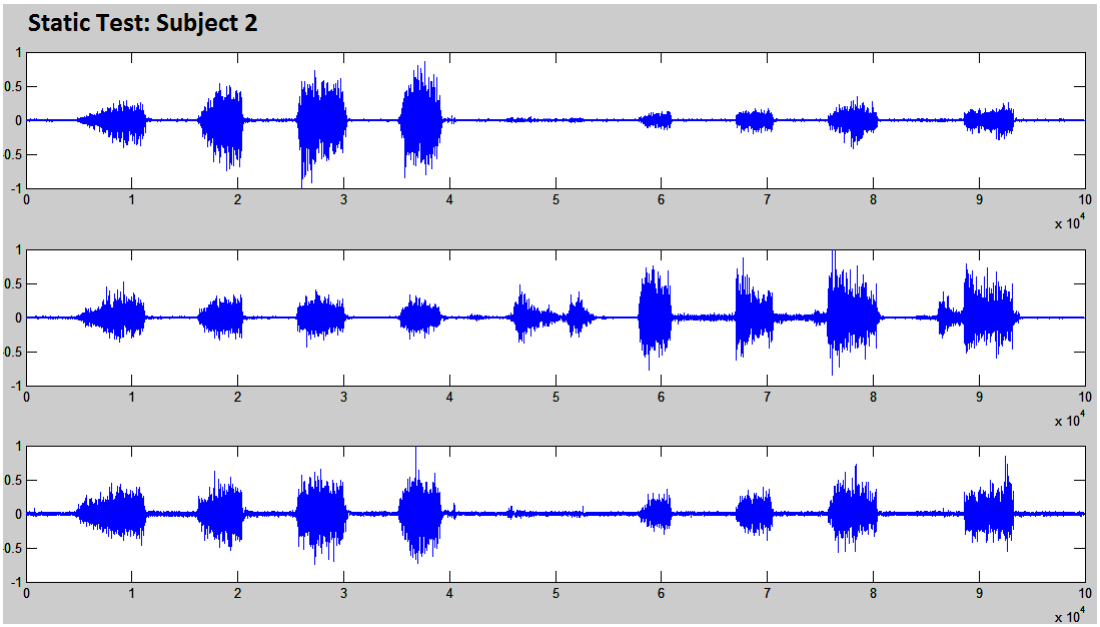

Figure A.11: 3 ICs output during isometric contraction test on subject 2.

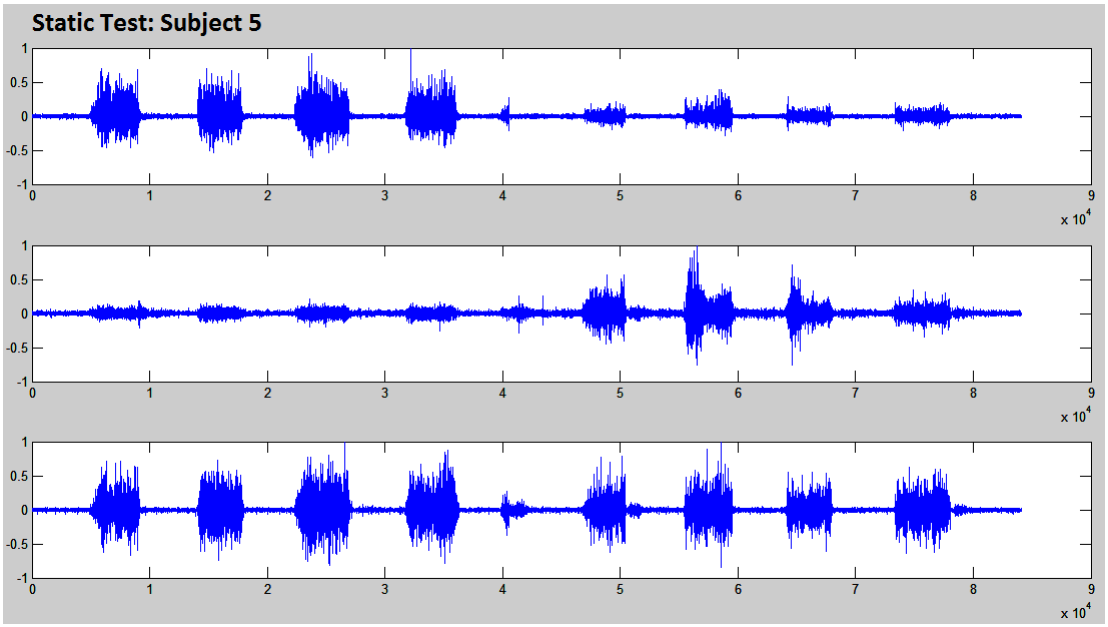

Figure A.12: 3 ICs output during isometric contraction test on subject 5.

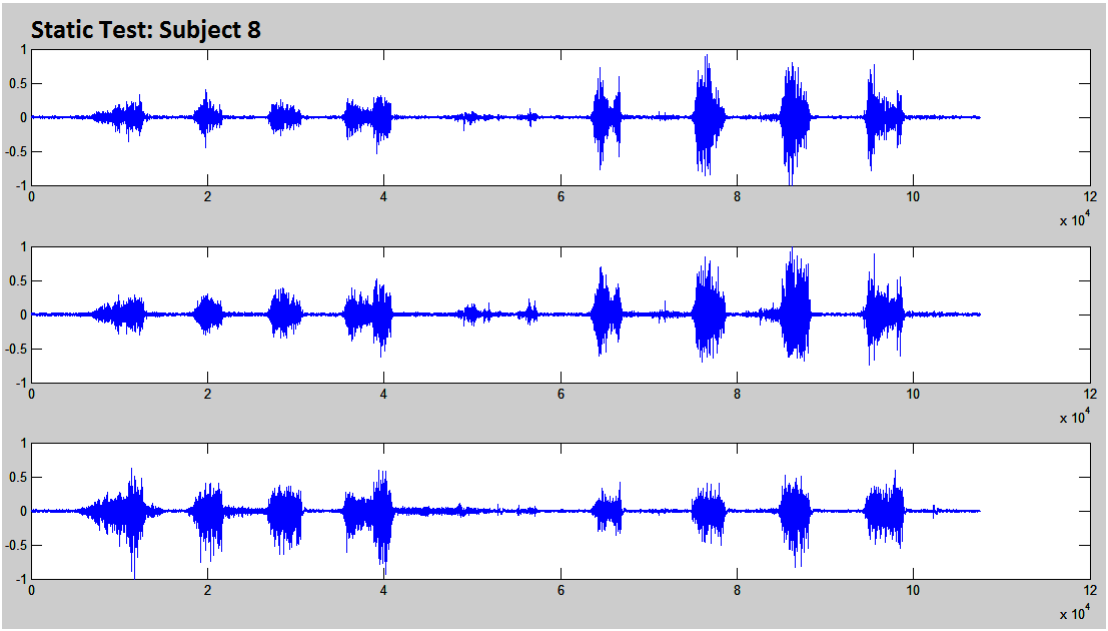

Figure A.13: 3 ICs output during isometric contraction test on subject 8.

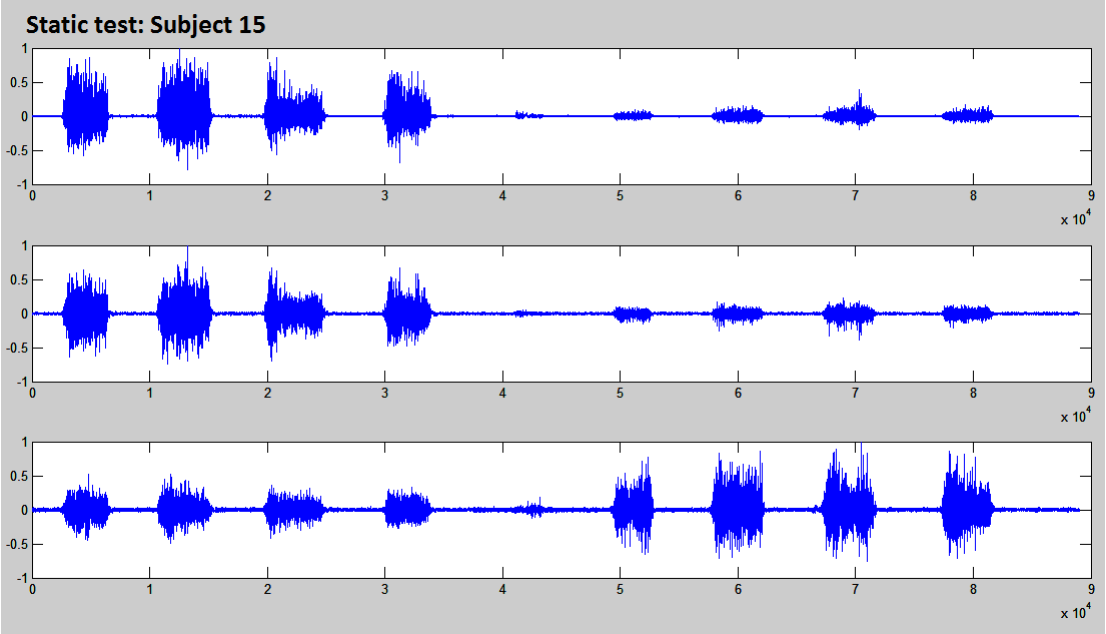

Figure A.14: 3 ICs output during isometric contraction test on subject 15.

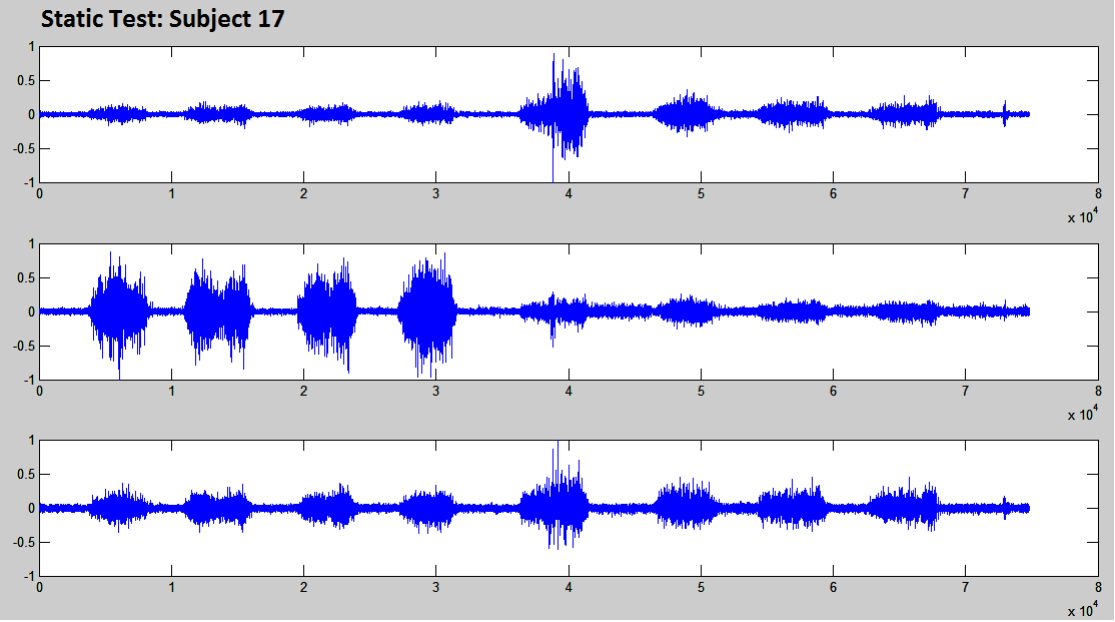

Figure A.15: 3 ICs output during isometric contraction test on subject 17.

Additional Data

#Subject	Electrode Positions for each individual after RMSE fitness function Test (TEST 2)																													Electrodes
1	1	0	0	0	0	0	1	0	0	1	1	1	0	0	0	1	0	0	0	0	0	0	0	0	1	0	1	1	1	0	10
2	0	0	0	0	0	0	0	0	1	0	0	1	0	1	0	0	1	0	0	0	0	0	0	0	1	1	0	1	0	0	1	8
3	0	0	1	1	0	0	0	0	1	0	1	0	0	0	0	0	1	0	0	0	0	0	0	0	0	0	0	0	1	1	0	7
4	0	0	0	0	0	0	0	0	0	1	1	0	0	0	0	0	0	0	0	1	1	0	0	0	0	0	0	1	1	0	0	6
5	1	0	1	0	0	1	0	0	0	0	0	0	0	0	0	0	0	0	0	0	1	0	0	1	1	1	0	0	1	0	0	8
6	1	1	1	1	0	0	0	0	0	1	0	1	0	0	0	0	0	0	0	0	1	1	0	0	0	0	1	1	1	0	0	11
7	0	0	0	0	0	0	0	0	1	0	1	1	1	1	1	0	1	1	0	1	0	0	0	0	0	0	0	1	1	1	12
8	0	0	0	0	0	1	0	0	0	0	1	1	0	0	0	0	1	0	0	0	0	0	0	0	0	1	0	1	0	1	7
9	1	0	0	0	1	0	0	0	0	1	1	0	0	0	1	0	0	0	0	0	1	0	0	0	1	0	1	0	0	0	8
10	0	0	0	0	0	0	0	0	0	0	0	0	0	0	0	0	0	0	1	1	0	0	1	1	0	0	1	0	0	1	6
11	0	0	0	0	1	0	0	0	0	0	1	0	0	0	0	0	0	0	0	0	1	0	0	0	0	0	0	0	1	1	5
12	0	0	1	0	0	1	0	0	0	0	0	0	0	0	0	0	0	0	0	0	0	0	0	1	1	1	0	0	1	1	7
13	0	0	1	0	1	1	0	1	1	1	0	1	0	0	0	0	0	0	0	1	0	1	1	1	0	0	0	0	0	1	12
14	0	1	0	0	1	1	0	1	1	0	0	0	0	1	0	0	0	0	1	0	0	1	0	0	1	0	0	0	1	0	10
15	0	0	0	0	0	0	0	1	0	0	1	1	0	1	0	1	0	1	1	0	1	0	1	0	0	1	0	1	0	1	12
16	0	1	0	0	1	1	0	0	0	1	0	0	0	0	0	1	0	1	0	0	0	0	0	0	1	0	1	1	0	1	10
17	1	1	1	1	0	0	1	1	0	1	0	1	0	0	0	1	1	0	0	1	1	0	0	0	1	1	0	0	1	1	0	16
18	0	0	0	0	1	0	0	0	0	0	0	0	0	1	0	1	0	1	1	0	0	0	0	1	1	0	0	0	0	0	7
19	0	1	1	0	1	0	1	0	0	0	0	0	0	0	0	0	0	0	0	0	1	0	0	1	1	0	1	0	0	0	8
20	1	1	1	1	1	0	0	1	0	1	1	1	0	0	0	0	0	0	0	0	1	0	0	0	0	0	0	0	0	1	11
total	6	6	8	4	8	6	3	5	5	8	9	9	1	5	2	5	5	4	5	7	7	2	4	8	10	4	8	10	7	10	9.05

Figure A.16: Electrode Positions Test2: Active electrode positions for all 20 subjects after optimization by Genetic Algorithm with RMSE based fitness function (Test2). The green blocks represent electrode position numbers that are active/used in the solution for that particular subject after the GA optimization. The last row of this table is the total number of electrodes per electrode position. This row was used to create the histograms which were used to select active electrode positions for the generalized solution.

Test2 Data					
#Subject	Brachialis	Bicep	Tricep	Total	# of Electrodes
1	0.006842108568041	0.011429447743514	0.01938216878004	0.037653725091595	10
2	0.008436454897035	0.02080459859846	0.027970809727707	0.057211863223202	8
3	0.015898946329282	0.018200997470358	0.034816324714443	0.068916268514083	7
4	0.027828269833913	0.012305176409468	0.026977465007998	0.067110911251379	6
5	0.005584395126112	0.014683537670646	0.02001569530963	0.040283628106388	8
6	0.010280640115647	0.026153916090258	0.028225354343425	0.06465991054933	11
7	0.015645783778433	0.007056777940204	0.015267067467116	0.037969629185753	12
8	0.039410444085733	0.06521377119435	0.022588074573145	0.127212289853228	7
9	0.016745015861893	0.006372696867526	0.025387115231896	0.048504827961315	8
10	0.01510364765918	0.025070082909362	0.025033742773498	0.06520747334204	6
11	0.010462925500599	0.021697595062009	0.010462925500599	0.042623446063207	5
12	0.021300022409381	0.022707467911174	0.023256545198707	0.067264035519262	7
13	0.08405368239956	0.018610130298475	0.007887188971449	0.110551001669484	12
14	0.011485640119314	0.01625952700276	0.023315183824738	0.051060350946812	10
15	0.05507006848843	0.009054721632495	0.009181593336841	0.073306383457766	12
16	0.012020869651375	0.023972462713928	0.045167153503245	0.081160485868548	10
17	0.015273314184039	0.013959957448419	0.008983301962502	0.03821657359496	16
18	0.007352254495544	0.032650159748288	0.019150546541766	0.059152960785598	7
19	0.024406676745829	0.021969601102544	0.027155965853687	0.07353224370206	8
20	0.025843011206781	0.0098491930563	0.009212562730348	0.044904766993429	11
average	0.021452208572806	0.019901090943527	0.021471839267639	0.062825138783972	9.05
STD	0.019019096380651	0.012754464700508	0.009567691705136	0.023565343842061	2.72367785404801

Table A.1: RMSE results for each muscle of all 20 subjects for Test 2.

Standard 30 Electrode Configuration Data					
#Subject	Brachialis	Bicep	Tricep	Total	# of Electrodes
1	0.001472471300657	0.000644079958825	0.002018085072858	0.00413463633234	28
2	0.000389257222276	0.001388718805753	0.032205992202138	0.033983968230167	28
3	0.005286760338943	0.000380257523098	0.04654835682133	0.052215374683371	28
4	0.042003494227961	0.000498912064632	0.047036639690617	0.08953904598321	28
5	0.008327619435377	0.001063791640883	0.055282743514457	0.064674154590717	22
6	0.028194241571202	0.006224839320414	0.002724561117213	0.037143642008829	26
7	0.077916307947816	0.000742071403624	0.002388981953859	0.081047361305299	24
8	0.077413980204005	0.066621857551416	0.050100809876159	0.19413664763158	20
9	0.001455740651553	0.000492967032632	0.044184133151071	0.046132840835256	18
10	0.000775304334298	0.001173513741644	0.023941817509507	0.025890635585449	25
11	0.000397097500225	0.000480673167169	0.080688788511805	0.081566559179199	25
12	0.002680436534946	0.000578143727905	0.00495969397609	0.008218274238941	25
13	0.081003495556121	0.00133530739731	0.000254384895468	0.082593187848899	24
14	0.006152897238697	0.001650270273763	0.040705726977554	0.048508894490014	8
15	0.055238618302364	0.082339511857165	0.000142987667627	0.137721117827156	17
16	0.002012464549423	0.003974915569926	0.052862864914752	0.058850245034101	26
17	0.109997726135897	0.002643851436912	0.000770428889548	0.113412006462357	28
18	0.001432256614789	0.074454908601114	0.001511961504456	0.077399126720359	12
19	0.000091937216191	0.07216404786467	0.000626919879696	0.072882904960557	24
20	0.010421735365615	0.002660943806216	0.00451827843502	0.068950032839358	29
average	0.025633192112418	0.016075679137254	0.024673707828061	0.068950032839358	23.25
STD	0.035136205960827	0.029806950256238	0.025505415833418	0.043947939097356	5.66498943186639

Table A.2: RMSE results for each muscle of all 20 subjects for 30 Electrode Configuration.

Standard 12 Electrode Configuration with Equal Spacing				
#Subject	Brachialis	Bicep	Tricep	Total
1	0.00870205882298	0.026237806710394	0.04589243794111	0.080832303474484
2	0.00401157807592	0.052749000392756	0.032505310972462	0.089265889441138
3	0.079515202588513	0.010901388766662	0.045735184210556	0.136151775565731
4	0.017241703388523	0.017858878234364	0.041192107296021	0.076292688918908
5	0.023389425782305	0.037490676656345	0.055954693531336	0.116834795969986
6	0.021743219160937	0.028506578904922	0.079360222870107	0.129610020935966
7	0.048636370479108	0.033669715540484	0.086098947759412	0.168405033779004
8	0.081460196682252	0.066330575116768	0.072064985101056	0.219855756900076
9	0.022736459613038	0.072656333454042	0.040730192782287	0.136122985849367
10	0.012151127621312	0.055478993685311	0.023248713431152	0.090878834737775
11	0.004259056226506	0.044298490523609	0.063723479467423	0.112281026217538
12	0.032319007836738	0.030611160653211	0.059694493661758	0.122624662151707
13	0.079971745772569	0.010909599425504	0.019364451780622	0.110245796978695
14	0.018915621163292	0.054193364851437	0.038667970377802	0.111776956392531
15	0.055623936904628	0.047427058676861	0.028761516640914	0.131812512222403
16	0.008503009701447	0.067447268482525	0.05291500688528	0.128865285069252
17	0.10813753847634	0.0694991524337	0.02863060299384	0.20626729390388
18	0.008288298227113	0.073891745245399	0.060637348668949	0.142817392141461
19	0.019087858370165	0.074337306765648	0.025612162239696	0.119037327375509
20	0.028623524962529	0.0646503236535	0.012194192584835	0.105468041200864
average	0.034165846992811	0.046957270908672	0.045649201059831	0.126772318961314
STD	0.03076197899402	0.021357861981497	0.020431971069614	0.036906244841126

Table A.3: RMSE results for each muscle of all 20 subjects for the standard configuration which was used in the preliminary study performed by Moroaswi and John [2].

	Threshold 1 (0.2 %)				Threshold 2 (1%)			
#	Brach	Bicep	Tricep	Count	Brach	Bicep	Tricep	Count
1	0.003380542235	0.005539238557	0.008113863779	30	0.03480723871	0.02776867698	0.0213916417	30
2	0.009390445244	0.007818790756	0.021465159	30	0.03126597915	0.06613033313	0.02144217953	30
3	0.01607963309	0.002001517778	0.03122270012	30	0.05087030142	0.03356763475	0.03166625884	30
4	0.004200323281	0.003406540403	0.03140088329	30	0.02671532431	0.01230350572	0.03114552433	30
5	0.004999080704	0.01261522704	0.03681805158	30	0.03606652826	0.01539476077	0.03727585079	30
6	0.01831165243	0.009543470566	0.004861848651	30	0.01972849894	0.02552567204	0.01406963681	30
7	0.0422766446	0.009080848985	0.002257198303	29	0.03058210816	0.02887648744	0.02660954965	29
8	0.01852335855	0.0452726887	0.03341970362	29	0.05074157233	0.05407345271	0.04303475236	29
9	0.003443686467	0.04798732636	0.007706593683	30	0.03145504549	0.05240591306	0.02790357715	30
10	0.004081972413	0.01171302975	0.01604335249	30	0.02224484202	0.0244348207	0.01600084797	30
11	0.001288272136	0.008032473593	0.05342471938	30	0.0319627059	0.05462307409	0.05417931312	30
12	0.019888309	0.00419562091	0.01254633679	30	0.04677841669	0.01262084565	0.01650391365	30
13	0.05380415895	0.009020409442	0.002159886331	30	0.04495876091	0.06424790327	0.02104604197	30
14	0.006111645084	0.01907021864	0.02664670903	30	0.03665561763	0.03936737257	0.02538585583	30
15	0.03654738432	0.05588474745	0.01257266574	30	0.03589900179	0.06252848194	0.01029801151	30
16	0.007446735556	0.006207927247	0.0352108597	30	0.02077328365	0.0114906633	0.03528825552	30
17	0.05157162575	0.01007161495	0.002154028003	30	0.05542634012	0.03580943593	0.01168110224	30
18	0.004094311529	0.05058831182	0.007093936712	30	0.00947229274	0.04673592242	0.009162838114	30
19	0.008701131557	0.04818673693	0.003892155373	30	0.04523283426	0.04959002549	0.03733159471	30
20	0.006744723788	0.01587637668	0.01874375463	30	0.01306050257	0.01881532959	0.02583535258	30
AVG	0.01604428183	0.01910565583	0.01838772031	29.9	0.03373485975	0.03681551558	0.02586260492	29.9
STD	0.01664630665	0.01857081465	0.01466986688	0.3077935056	0.01274741708	0.01842020122	0.01174913383	0.3077935056

Table A.4: Part 1: RMS error averages for zeroing electrodes in ICA weighting matrix.

	Threshold 3 (5 %)				Threshold 4 (10%)			
#	Brach	Bicep	Tricep	Count	Brach	Bicep	Tricep	Count
1	0.0339660466	0.04999884347	0.03227386892	30	0.03483074805	0.05196403295	0.03824386267	24
2	0.02443615948	0.06723138638	0.04979355463	29	0.03461191046	0.07454813949	0.03443754402	24
3	0.04120559607	0.05601452353	0.04268703484	30	0.05157342337	0.04512168215	0.03706021973	28.66666667
4	0.05331869017	0.03781378797	0.03423012454	30	0.061918753	0.0638284243	0.03326478083	27
5	0.04379618072	0.0572126209	0.03972309383	28	0.04444314033	0.05539268502	0.04925907915	22
6	0.04395799584	0.04797261564	0.03479563633	30	0.05233435246	0.04362254968	0.03321127099	21.66666667
7	0.04961019398	0.06133557285	0.05413176171	25	0.04437068889	0.06133557285	0.04669152706	24
8	0.07255385499	0.06452355468	0.06077863795	25.66666667	0.07966485053	0.05441357846	0.0627255996	19.33333333
9	0.04193142235	0.04392726319	0.03257971428	27.33333333	0.04130169682	0.04347411831	0.03424773579	12.33333333
10	0.02877238507	0.05968349499	0.0174268564	29	0.02982898417	0.05615036782	0.01953550652	20.66666667
11	0.04864226038	0.07589952908	0.05402680052	30	0.04872953647	0.07218580204	0.05410625488	26
12	0.04954209445	0.03891982527	0.02549042638	29.33333333	0.05780337934	0.03630718408	0.04357052581	21.66666667
13	0.05102396206	0.06375566437	0.01922866017	30	0.04507823764	0.07157254537	0.03220802919	18
14	0.04307268544	0.03785674669	0.05490803851	16.66666667	0.04517510111	0.05362149902	0.05469588953	8.333333333
15	0.03668956007	0.06265821138	0.02187607354	25	0.03723994791	0.06298768822	0.04620398615	8.666666667
16	0.0532779193	0.06711203648	0.04396486535	28.66666667	0.04953924004	0.06671453747	0.0505886974	22.66666667
17	0.06306754362	0.07536464984	0.03617818683	30	0.0706300591	0.06647715087	0.0433942879	27
18	0.008022693961	0.06097719095	0.04648380238	16.33333333	0.01034995005	0.06164403675	0.04266632453	7
19	0.04734193217	0.04252734206	0.03482540679	29.66666667	0.05052427295	0.06185315966	0.03171125338	24.66666667
20	0.06147688519	0.05753349667	0.03731182691	30	0.06883009271	0.0739096816	0.0400775449	27.66666667
AVG	0.04478530309	0.05641591782	0.03863571854	27.48333333	0.04793891827	0.05885622181	0.041394996	20.76666667
STD	0.01426306915	0.01179712591	0.0123073442	4.117392862	0.01553033689	0.01094599113	0.01005356655	6.648308055

Table A.5: Part 2: RMS error averages for zeroing electrodes in ICA weighting matrix.

	Threshold 5 (5 %)				Genetic Algorithm 1			
#	Brach	Bicep	Tricep	Count	Brach	Bicep	Tricep	Count
1	0.03443618871	0.05898306336	0.0378858883	20.66666667	0.009820765686	0.02130031607	0.02355609444	7
2	0.03926367874	0.07470858722	0.02759512459	17	0.005478521454	0.02878333568	0.02670595271	6
3	0.0447635464	0.04512168215	0.03493055253	25.66666667	0.01966446427	0.01765979954	0.03346943241	5
4	0.06784284103	0.07477544849	0.0430479849	23.66666667	0.02550423491	0.01251773148	0.03277525637	6
5	0.04688014123	0.0522974626	0.04370216378	11.66666667	0.02383053406	0.01987772986	0.02411800258	6
6	0.04684607834	0.05375336187	0.02680533861	18	0.01900200534	0.02842789885	0.02185608748	9
7	0.05096921917	0.06425452846	0.04669152706	17.33333333	0.03145515929	0.01539803911	0.01672873602	8
8	0.08212799987	0.05958997468	0.05853570178	15	0.04765389724	0.03360388251	0.05635974797	9
9	0.04338845576	0.04483355294	0.0319880661	7.333333333	0.01689217903	0.008309034687	0.02174679879	8
10	0.02681569406	0.06800340303	0.01654456268	15	0.01604810768	0.03069987431	0.02464545828	6
11	0.05011295215	0.07637871644	0.05231900169	20	0.008291564824	0.02145587373	0.008291564824	6
12	0.06462672483	0.0364571468	0.04250076152	18.66666667	0.03746133983	0.02703152836	0.02507580938	5
13	0.04736835891	0.06630480365	0.02340048967	9	0.0196282475	0.02000457705	0.007185168148	11
14	0.04366063785	0.05362149902	0.05312529977	5	0.01866290591	0.02692051234	0.0208748353	7
15	0.03602458824	0.06461273915	0.04944171929	2.333333333	0.007574222992	0.01621127136	0.02017413953	8
16	0.04857277941	0.07193632301	0.06227405721	12.66666667	0.01420091043	0.02513720404	0.04190237985	9
17	0.06107390981	0.07831280004	0.07257637616	21.66666667	0.03804487408	0.01773056889	0.02287876567	10
18	0.0230559768	0.06134348514	0.04266632453	6	0.009441754829	0.03308569432	0.02060128855	6
19	0.04741489132	0.06501554066	0.0432084143	16.66666667	0.0270491278	0.02890948629	0.01784396123	7
20	0.06160346443	0.07160532166	0.0363768366	23	0.02641341964	0.01873534877	0.01103697974	10
AVG	0.04834240635	0.06209547202	0.04228080955	15.31666667	0.02110591184	0.02258998536	0.02389132296	7.45
STD	0.01401266341	0.01157049141	0.01369337126	6.648637903	0.01127923016	0.007004348577	0.01118829683	1.761428846

Table A.6: Part 3: RMS error averages for zeroing electrodes in ICA weighting matrix.

	Genetic Algorithm 2			
#	Brach	Bicep	Tricep	Count
1	0.006842108568	0.01142944774	0.01938216878	10
2	0.008436454897	0.0208045986	0.02797080973	8
3	0.01589894633	0.01820099747	0.03481632471	7
4	0.02782826983	0.01230517641	0.02697746501	6
5	0.005584395126	0.01468353767	0.02001569531	8
6	0.01028064012	0.02615391609	0.02822535434	11
7	0.01564578378	0.00705677794	0.01526706747	12
8	0.03941044409	0.06521377119	0.02258807457	7
9	0.01674501586	0.006372696868	0.02538711523	8
10	0.01510364766	0.02507008291	0.02503374277	6
11	0.0104629255	0.02169759506	0.0104629255	5
12	0.02130002241	0.02270746791	0.0232565452	7
13	0.0840536824	0.0186101303	0.007887188971	12
14	0.01148564012	0.016259527	0.02331518382	10
15	0.05507006849	0.009054721632	0.009181593337	12
16	0.01202086965	0.02397246271	0.0451671535	10
17	0.01527331418	0.01395995745	0.008983301963	16
18	0.007352254496	0.03265015975	0.01915054654	7
19	0.02440667675	0.0219696011	0.02715596585	8
20	0.02584301121	0.009849193056	0.00921256273	11
AVG	0.02145220857	0.01990109094	0.02147183927	9.05
STD	0.01901909638	0.0127544647	0.009567691705	2.723677854

Table A.7: Part 4: RMS error averages for zeroing electrodes in ICA weighting matrix.

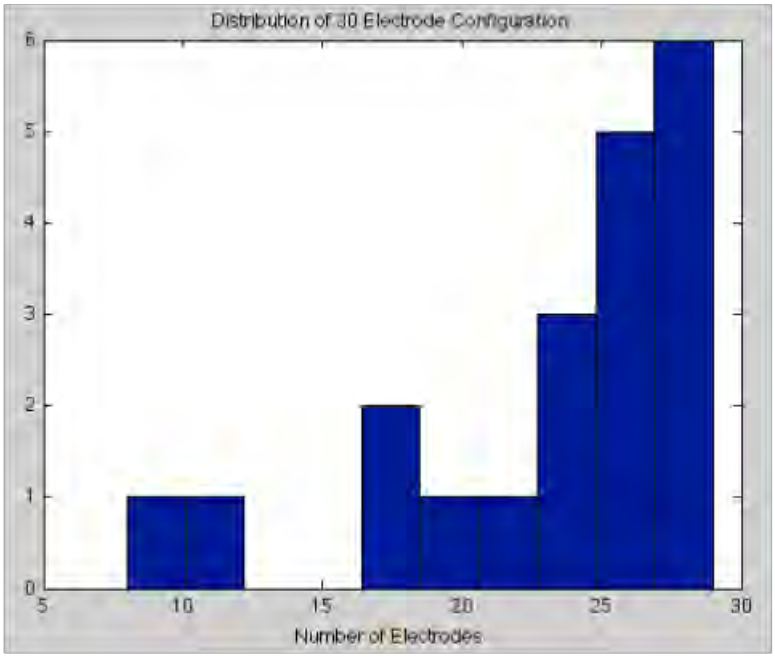

Figure A.17: Sample distribution of the standard 30 electrode configuration's active electrodes.

Appendix B

Twin Ring sEMG apparatus proposed by S.P. Moroaswi and L.R. John [2]

In Figure B.1 we can see a sketch of the proposed twin ring apparatus with 6 evenly spaced sEMG electrodes on each ring. It can also be seen that a reference electrode has been applied at the elbow region. This system was proposed by S.P. Moroaswi and L.R. John [2] and has a provisional patent pending, patent number: 20120184838 [1].

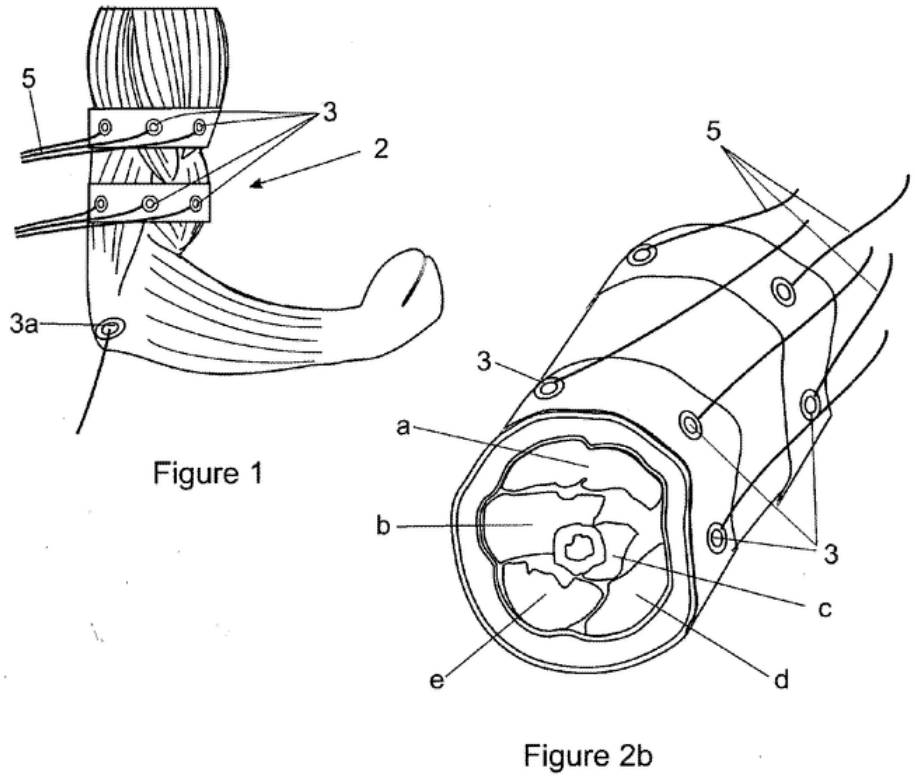

Figure B.1: Twin Ring EMG system proposed by L.John.

OpenEEG Analog Front-end Design

Presented here is the schematic design of the open source analog frontend used in the OpenEEG project [59].

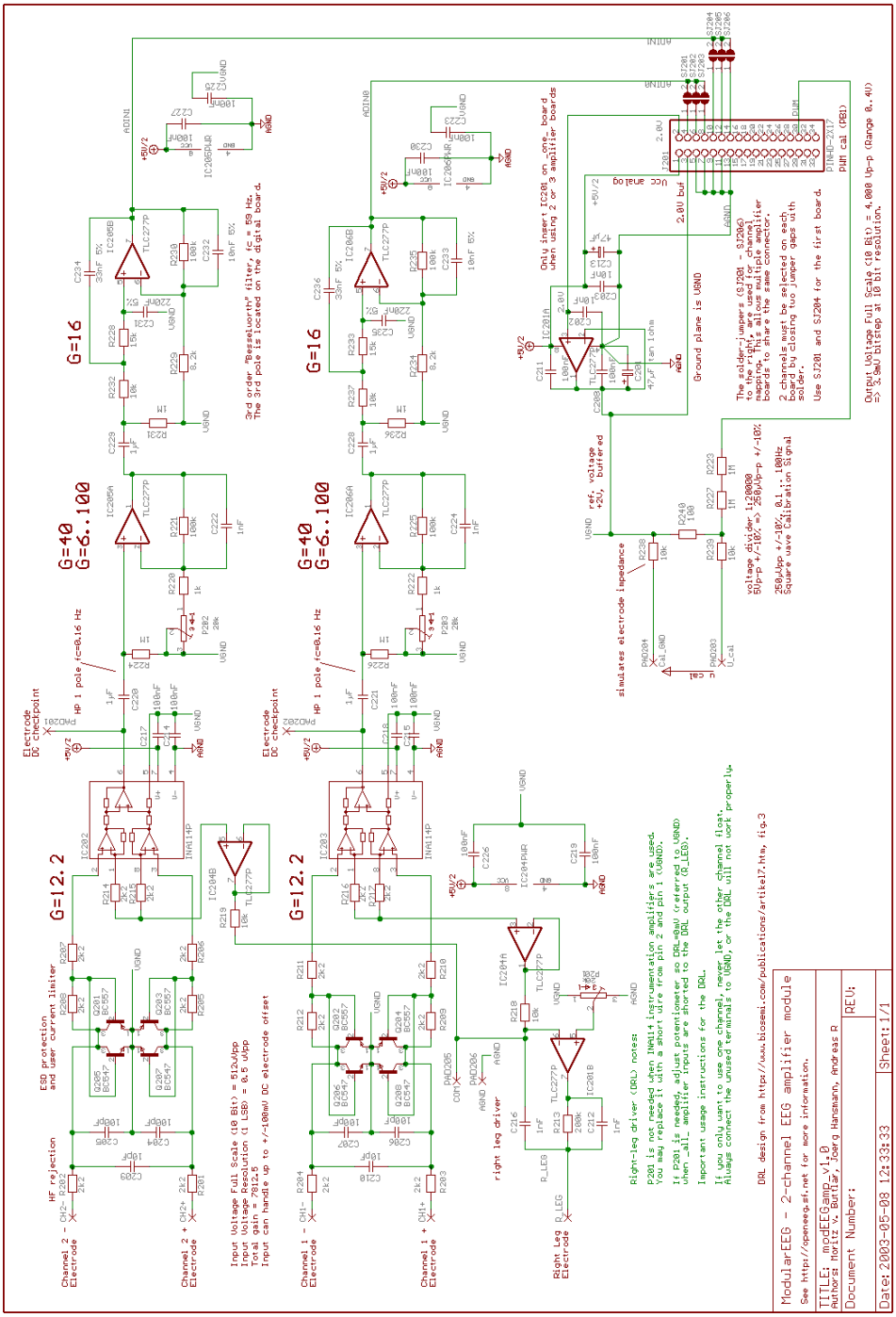

Figure B.2: OpenEEG Analog Frontend Design Schematic.

Final EMG Frontend Design

Final Electromyography analog front-end board. This design consists of 6 input channels, and is capable of being used in a monopolar or bi-polar electrode configurations. The design also allows for control of gain by a digital potentiometer board or with standard potentiometers.

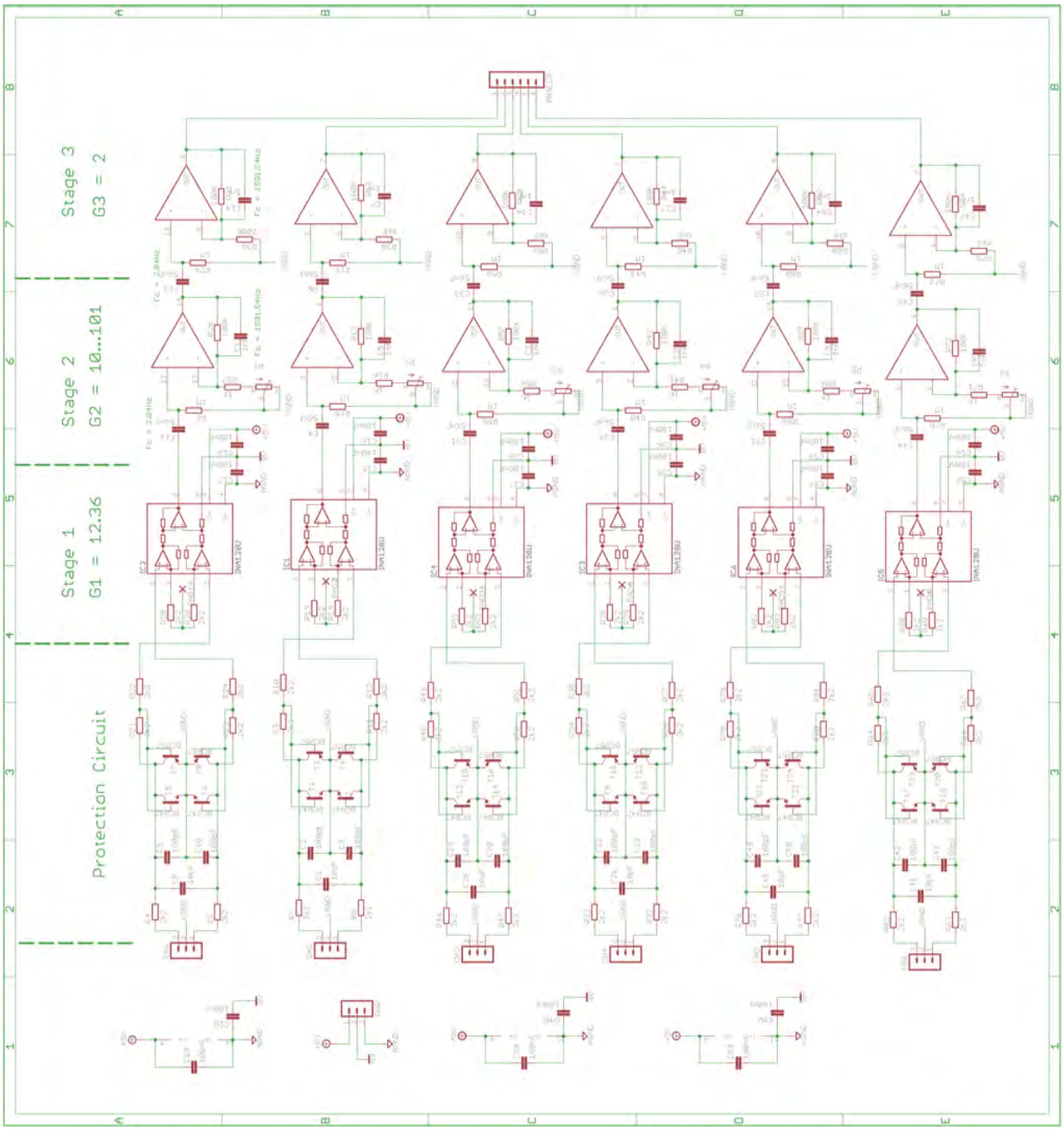

Figure B.3: Final schematic design for 6 channel EMG front-end.

Electrode Design

This electrode design along with the accompanying electrode press, used to fabricate the electrodes, were both designed by Jeremy Pitman, a Biomedical Engineering Masters student at the University of Cape Town.

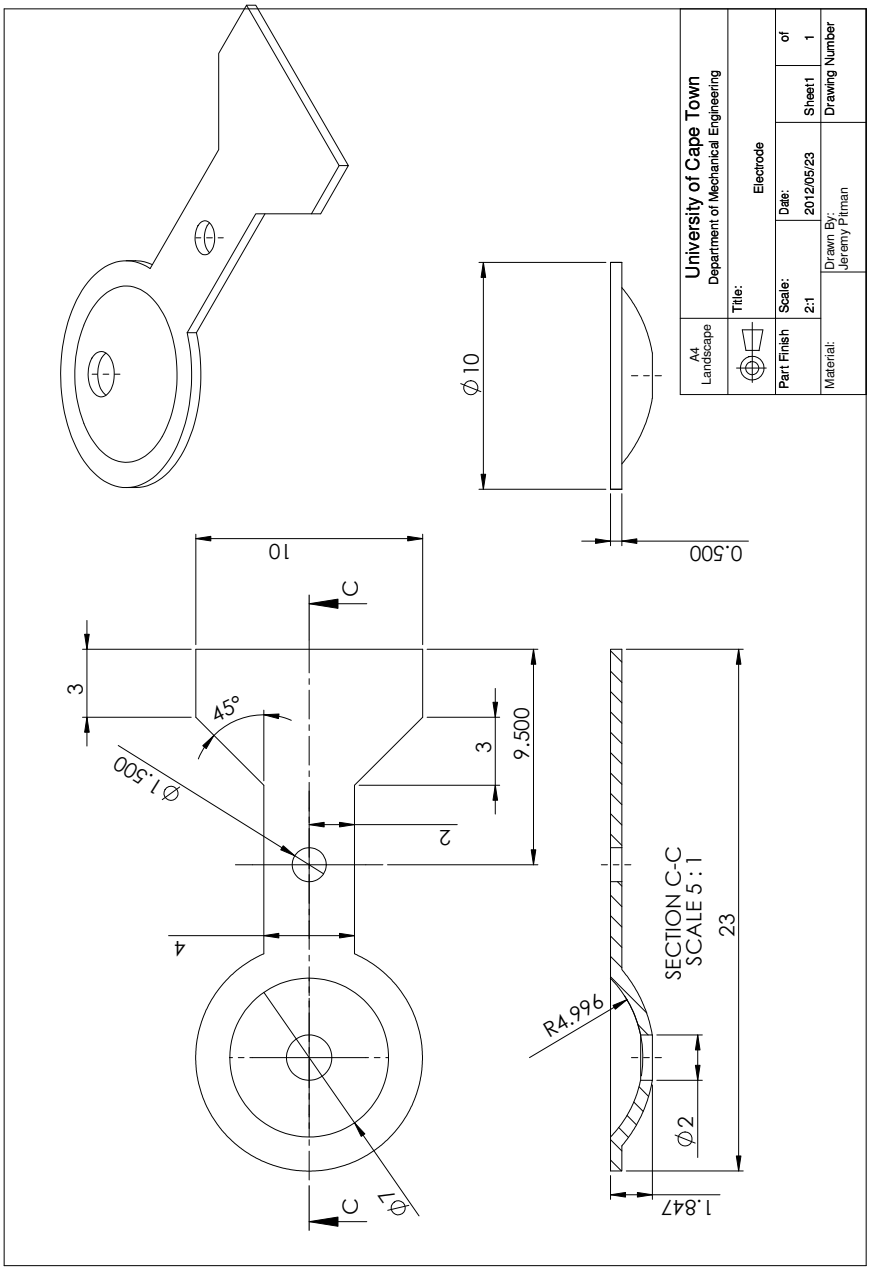

Figure B.4: Silver Electrode Design by Jeremy Pitman.

Additional Photos

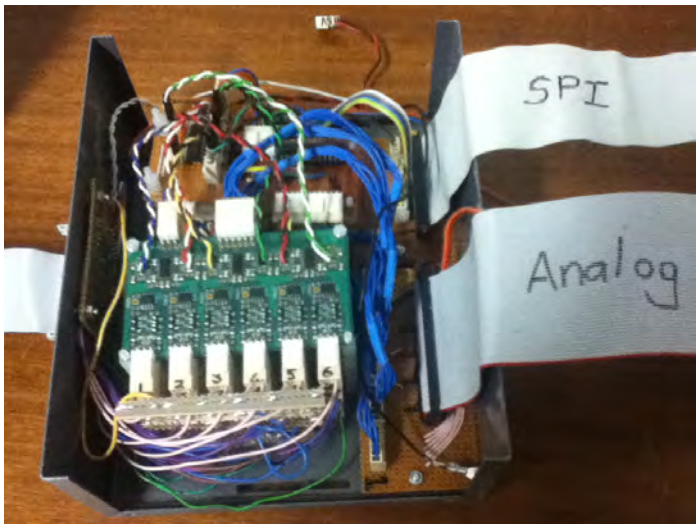

Figure B.5: Photo of the internal systems in the frontend. Here we can see a stack of analog frontend boards connected to digital poteniometer control boards.

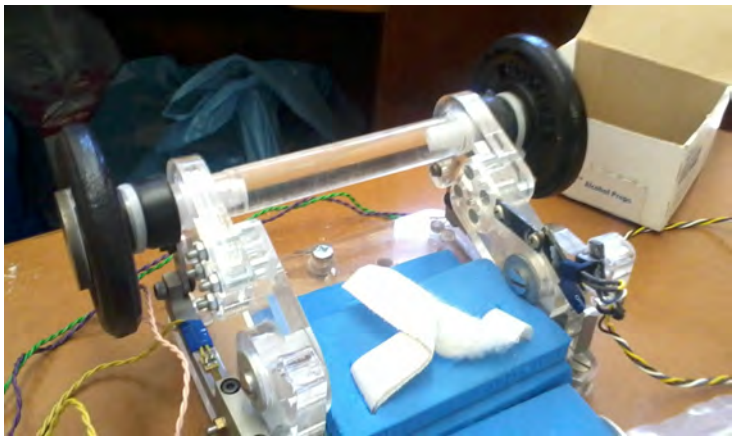

Figure B.6: Static pull test rig used in the isometric contraction movement protocol. The rig was developed by Stoekigt and Divekar [3] at the University of Cape Town, South Africa.

Appendix C

Genetic Algorithm Code

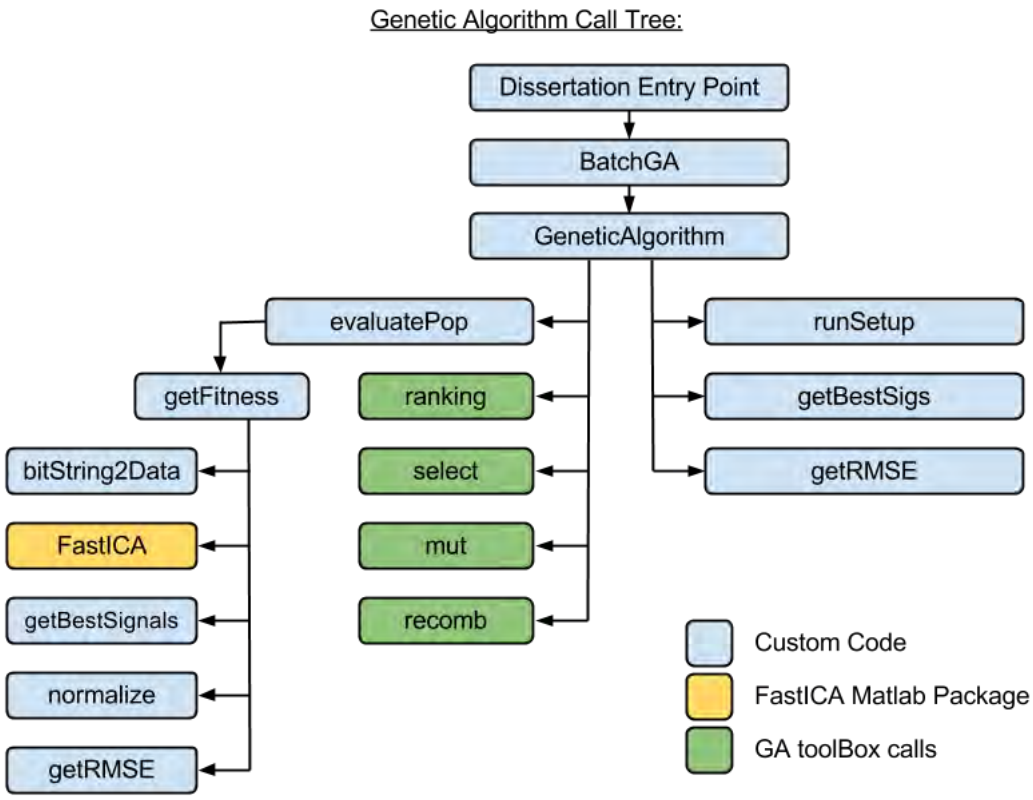

Figure C.1: System call tree for the GA which processed all 20 subjects for each test.

Dissertation Entry Point

This is the entry point for the entire analysis procedure, it calls the batch GA operation on a list of the subjects we would like to run the test on. It also defines the directory in which the results will finally be stored.

```
% dissertation_entryPoint:
str = computer;
list = {'subject1' 'subject2' ... 'subject20'}; %folders where
  data is.
%the batch function runs a SGA on each subject in the list:
batchGA (names,numberGenerations,numberIndiv);
[solutionsMatrix RMSEMatrix fitnessVector]= batchGA(list,24,40);
%select directory to save to dependent on which OS we are using
    if(strcmp(str,'PCWIN'))
        save('C:\Dissertation\Dynamic_test_results\','
          solutionsMatrix','RMSEMatrix', 'fitnessVector', 'list');
    end
    if(strcmp(str,'MACI64'))            save('/Users/admin/
      Desktop/results.mat','solutionsMatrix','RMSEMatrix','
      fitnessVector', 'list');
    end
    imagesc(solutionsMatrix);
```

batchGA

This section of code implements a function which iterates over all the subjects passed to it in the 'names' parameter and runs a GA on each of them with a predefined number of generations and population size.

```
function [solutionsMatrix RMSEMatrix fitnessVector]= batchGA(
  names,numberGenerations,numberIndiv)
%names: names of subjects in the batch that GA needs to run on.
%numberGenerations: number of generations that will run.
%numberIndiv: number of individuals in each population.
[cols rows] = size(names) ;
solutionsMatrix = zeros(rows,30);
RMSEMatrix = zeros(rows,3);
fitnessVector = zeros(rows,1);
str = computer ;
char(names(1)) ;
for i = 1:rows
    if(strcmp(str,'PCWIN'))
        filePath=strcat('C:\Dissertation\Dynamic_Test_Analysis\
          test1\',char(names(i)));
        disp(filePath);
    end
    if(strcmp(str,'MACI64'))
        filePath=strcat('/Users/admin/Desktop/Test_RMSE_fitness/'
          ,char(names(i)),'/');
        disp(filePath);
    end
    [solution fitness solutionRMSE]=geneticAlgorithm(filePath,
      numberGenerations,numberIndiv);
    solutionsMatrix(i,:)=solution;
    fitnessVector(i)=fitness;
```

```
    RMSEMatrix(i,:)= solutionRMSE;
end
```

geneticAlgorithm

This function implements the core structure of the SGA, it sets up the workspace and imports all the data for the subject which is being optimized by calling the runSetup.m function. It loops through each generation of the GA and keeps track of the best individual. It also allows for visualization of some of the key components, this was mainly used in the debugging of the GA, and has been commented out for the batch mode.

```
function [solution fitness solutionRMSE]=geneticAlgorithm(
  filePath,numberGenerations,numberIndiv)
%##################################################
%file specification
%filePath = ['C:\Dissertation\Analysis\' subject];
%##################################################
startTime = clock;
disp(sprintf('Start Time is: %d:%02d ',startTime(4),startTime(5))
  )
runSetup;
%##################################################
%GA parameters
NIND = numberIndiv;
MAXGEN = numberGenerations;
%Chrom = crtbp(NIND,30,2);
Chrom = floor(rand(NIND,30)*1.2);
%##################################################
%Reset counters
Best = NaN*ones(MAXGEN,1);
%best in current population
gen = 0;
%generational counter
%Evaluate initial population
disp('Evaluating initial population...')
[ObjV,finalSigs,RMSE] = evaluatePop(Chrom,data,goldStd,refSigs,
  filePath);
%Track best individual and display convergence
[val,bestInit]=min(ObjV);
disp('Best individual from initial population:')
disp(num2str(Chrom(bestInit,:)))
disp(sprintf('with fitness: %f \n',val))
Best(gen+1) = min(ObjV);
%figure(1)
%plot((Best),'ro');
xlabel('generation');
ylabel('Fitness');
%text(0.5,0.95,['Best = ', num2str(Best(gen+1))],'Units','
  normalized');
```

```
%drawnow;
%Generational loop
while gen < MAXGEN,
    %Assign fitness-value to entire population
    FitnV = ranking(ObjV);
    %Select individuals for breeding
    SelCh = select('sus', Chrom, FitnV,0.9);
    %Recombine selected individuals (crossover)
    SelCh = recombin('xovdp',SelCh,0.7);
    %Perform mutation on offspring
    %mutation probability of 5%
    SelCh = mut(SelCh,0.05);
    %Evaluate offspring, call objective function
    if(strcmp(computer,'PCWIN'))
        fileID = fopen([filePath '\outputFiles\logFile.txt'],'a+');
        fprintf(fileID,'Evaluating generation %d...\r\n',gen+1);
        fclose(fileID);
    else
        fileID = fopen([filePath '/outputFiles/logFile.txt'],'a+');
        fprintf(fileID,'Evaluating generation %d...\r\n',gen+1);
        fclose(fileID);
    end
    disp(sprintf('Evaluating generation %d ...',gen+1))
    [ObjVSel,finalSigs,RMSE] = evaluatePop(SelCh,data,goldStd,
      refSigs,filePath);
    %Reinsert offspring into current population
    [Chrom ObjV]=reins(Chrom,SelCh,1,1,ObjV,ObjVSel);
    [val index]= min(ObjV);
    BestIndiv = Chrom(index,:);
    disp(sprintf('Generation: %d',gen))
    disp('The Best Individual is: ')
    disp(num2str(BestIndiv))
    disp(sprintf('With a fitness of: %f\n',val))
    %Increment generational counter
    gen = gen+1;
    %Update display and record current best individual
    Best(gen+1) = min(ObjV);
    %figure(1)
    %plot((Best),'ro');
    xlabel('generation');
    ylabel('Fitness');
    %text(0.5,0.95,['Best = ', num2str(Best(gen+1))],'Units','
      normalized');
    %drawnow;
end
% End of GA
newData = bitString2Data(BestIndiv,data);
Sigs = fastica(newData,'g','tanh','approach','defl','verbose','
  off');
clear newData;
```

```
clear labviewIC;
[o,c,finalSigs] = getBestSignals(Sigs,refSigs);
clear Sigs;
%goldStd = normalize(goldStd);
finalSigs = normalize(finalSigs);
bicepRMSE = getError(finalSigs(1,:),goldStd(1,:));
brachRMSE = getError(finalSigs(2,:),goldStd(2,:));
tricepRMSE= getError(finalSigs(3,:),goldStd(3,:));
solutionRMSE = [bicepRMSE brachRMSE tricepRMSE];
solution = BestIndiv;    fitness = min(ObjV);
%figure(2);visualizeIndex(finalSigs,[1 2 3]);
%disp(sprintf('Best Individuals RMSE is: %f ',finalRMSE));
endTime = clock;
disp(sprintf('end Time is: %d:%02d',endTime(4),endTime(5)))
%figure(3)
%plotElectrodes(BestIndiv)
if(strcmp(computer,'PCWIN'))
    fileID = fopen([filePath '\outputFiles\logFile.txt'],'a+');
    fprintf(fileID,'end Time is: %d:%02d\r\n',endTime(4),endTime
      (5));
    fclose(fileID);
    saveTo = [filePath '\outputFiles\savedVariables.mat'];
else
    fileID = fopen([filePath '/outputFiles/logFile.txt'],'a+');
    fprintf(fileID,'end Time is: %d:%02d\r\n',endTime(4),endTime
      (5));
    fclose(fileID);
    saveTo = [filePath '/outputFiles/savedVariables.mat'];
end
save(saveTo,'BestIndiv', 'Chrom', 'Best', 'finalSigs', 'goldStd')
```

runSetup

The runSetup script sets up the workspace for the subject which is being optimized. It is responsible for importing all the data from the logged files and loading it into active memory for later manipulation by the GA.

```
disp('Reading Data from Files...')
if(strcmp(computer,'PCWIN'))
    try
        dataStruct = lvm_import([filePath '\rawData.txt'],false);
        %import data from logged experiment file
    catch err
        dataStruct = lvm_import([filePath '\rawData.lvm'],false);
        %import data from logged experiment file
    end
    %import data from reference signal file
    refStruct = lvm_import([filePath '\refSigs'],false);
    %import labview generated ICs with all 30 channels as a gold
      standard reference.
    labviewStruct = lvm_import([filePath '\goldStd'] ,false);
```

```
else
    try
        %import data from logged experiment file
        dataStruct = lvm_import([filePath '/rawData.txt'],false);
    catch err
        %import data from logged experiment file
        dataStruct = lvm_import([filePath '/rawData.lvm'],false);
    end
    %import data from reference signal file
    refStruct = lvm_import([filePath '/refSigs'],false);
    %import labview generated ICs with all 30 channels as a gold
      standard reference.
    labviewStruct = lvm_import([filePath '/goldStd'] ,false);

end
data = dataStruct.Segment1.data;
data(:,1)=[];
data = data';
%delete unneccesary stuff from mem.
clear dataStruct;
[rows cols] = size(data);
disp(sprintf('number of samples is: %d\n',cols))
refSigs = refStruct.Segment1.data;
refSigs(:,1)=[];
refSigs = refSigs';
clear refStruct;
labviewIC = labviewStruct.Segment1.data;
labviewIC(:,1)=[];
size(labviewIC)
labviewIC = labviewIC';
clear labviewStruct;
labviewIC = normalize(labviewIC);
%generate 3 gold standard signals to compare against.
[out,cor,goldStd]=getBestSignals(labviewIC,refSigs);
```

getBestSignals

This function takes in the reference signals which have been created by a person with knowledge of the movement protocol. This function then returns the 3 signal that are most correlated to the reference signals and these are taken as the gold standard signals used in comparison measures later.

```
function [out,correlation,goldStd]= getBestSignals(inputMatrix,
  refSigs)

%create empty index vector
out = zeros(1,3);
%create empty correlation vector
correlation = zeros(1,3);
%transpose the input matrix so dimensions are correct
```

```
inputMatrix = inputMatrix'
%transpose the refSigs matrix so dims are correct
refSigs =refSigs';
%get number of samples in inputMatrix
[samples,channels]=size(inputMatrix);
goldStd = zeros(3,samples);
%normalize the input data
normData = normalize(inputMatrix);
%find the first best signal
correlated1 = corr(refSigs(:,1),abs(normData));
[max1,index1]=max(correlated1);
out(1) = index1;
correlation(1)=max1;
goldStd(1,:)=inputMatrix(:,index1);
%find the second best signal
correlated2 = corr(refSigs(:,2),abs(normData));
[max2,index2]=max(correlated2);
out(2) = index2;
correlation(2)=max2;
goldStd(2,:)=inputMatrix(:,index2);
%find the third best signal
correlated3 = corr(refSigs(:,3),abs(normData));
[max3,index3]=max(correlated3);
out(3) = index3;
correlation(3)=max3;
goldStd(3,:)=inputMatrix(:,index3);
```

getRMSE

Returns a vector of RMS error values between the two sets of input signals.

```
function [RMSE] = getRMSE(sigs1,sigs2)
%returns the RMSE values between each signal in the two
%signal sets.i.e. sigs1(1) will be compared to sigs2(1).

e1 = abs(sigs1(1,:))-abs(sigs2(1,:));
RMSE(1) = sqrt(mean((e1).^2));
e2 = abs(sigs1(2,:))-abs(sigs2(2,:));
RMSE(2) = sqrt(mean((e2).^2));
e3 = abs(sigs1(3,:))-abs(sigs2(3,:));
RMSE(3) = sqrt(mean((e3).^2));
```

evaluatePop

This function is responsible for evaluating the fitness of each individual of the given population and returns a vector of fitness values corresponding to all the solutions in the population.

```
function [popFit,Best,RMSE] = evaluatePop(pop,data,goldStd,
  refSigs,filePath)
%evaluated each individual in the population and outputs a vector
%of the fitness values for each individual.
[Nind,cols]=size(pop);
popFit = zeros(1,Nind);
RMSE = zeros(1,Nind);
if(strcmp(computer,'PCWIN'))
    chromFileID=fopen([filePath '\outputFiles\chromosomes.txt'],'
      a+');
else
    chromFileID=fopen([filePath '/outputFiles/chromosomes.txt'],'
      a+');
end
%put each individual into fitness function.
for i = 1:Nind
    [popFit(i),Best,RMSE(i),channels]=getFitness(pop(i,:),data,
      goldStd,refSigs);
    %print channels and fitness to screen
    formatSpec='Ind %02d: %d channels,fitness of %f and RMSE:%f';
    disp(sprintf(formatSpec,i,channels,popFit(i),RMSE(i)));
    %##########################################
    if(strcmp(computer,'PCWIN'))
        fileID = fopen([filePath '\outputFiles\logFile.txt'],'a+'
          );
        fprintf(fileID,'Ind %02d: %02d channels, fit = %f, RMSE %
          f\r\n',i,channels,popFit(i),RMSE(i));
        fclose(fileID);
    else
        fileID=fopen([filePath '/outputFiles/logFile.txt'],'a+');
        fprintf(fileID,'Ind %02d: %02d channels, fit = %f, RMSE =
           %f\r\n',i,channels,popFit(i),RMSE(i));
        fclose(fileID);
    end
    bitString = dec2hex(pop(i,:))';
    fprintf(chromFileID,'%s, %f, %f, %d\r\n',   dec2hex(pop(i,:))
      ',log(bin2dec(bitString)),popFit(i),length(find(pop(i,:))));
    %##########################################
end
fclose(chromFileID);
popFit = popFit';
```

getFitness

Returns the fitness of a particular individual. If the number of active channels are less than 2, then it just returns a fixed fitness of 0.5.

```
function [fitness,best,RMSE,channels] = getFitness(bitString,data
  ,goldStd,refSigs)
%returns the fitness of a chromosome given the chromosome,
```

```
%the raw data and the gold standard

newData = bitString2Data(bitString,data);
[channels samples]=size(newData);
if(length(find(bitString))>2)
    if (channels < 15)
    [icaSig,A,W]=fastica(newData,'g','tanh','numOfIC',channels,'
      approach','defl','verbose','off');
    else
        [icaSig,A,W]=fastica(newData,'g','tanh','numOfIC',15,'
          approach','defl','verbose','off');
    end
    [o,c,best] = getBestSignals(icaSig,refSigs);
    goldStd = normalize(goldStd);
    best = normalize(best);
    simAbs = corr(abs(goldStd'),abs(best'));
    simRMSE = getRMSE(best,goldStd);
    RMSE = sum(simRMSE);
    %Correlation fitness function for TEST 1
    %fitness=1-((2*simAbs(1,1)+2*simAbs(2,2)+simAbs(3,3)+2.5*(1 -
       (length(find(bitString)))/30))/7.5);
    %RMSE fitness function for TEST 2
    fitness = simRMSE(1) + simRMSE(2)+ 0.8*simRMSE(3) + 0.15*(
      length(find(bitString))/30);
else
    fitness = 0.5;
    best = zeros(3,samples);
    RMSE = 0.5;
end
```

bitString2Data

Returns a matrix of data created from the raw data, but only consisting of the channels of data that are active. Active channels of data are indicated by a 1 in the input bit string.

```
function [dataOut]=bitString2Data(bitString,rawData)
%takes in bit string (genenotype) and selects only
%the channels in the data that have a bit = 1
%in the gene to add to the output data, this
%data can then be fed into the ica for
%evaluation of gene fitness.

%finds all the instances of 1 and returns their indices in a
  vector.
indices = find(bitString);
%creates a zeros matrix with correct dimensions
dataOut = zeros(length(indices),length(rawData));

for i = 1:length(indices)
    dataOut(i,:)=rawData(indices(i),:);
```

```
end
```

normalize

Returns a normalized data matrix, so that the data is constrained between [-1, 1].

```
function[outputMatrix]=normalize(inputMatrix)
%normalizes each signal in the inputMatrix,
%so that the signals are bounded between 1 and -1.
inputMatrix = inputMatrix';
[maxRows,maxCols]=size(inputMatrix);
outputMatrix = zeros(maxRows,maxCols);
for col=1:maxCols,
    chanNorm = 1/norm(inputMatrix(:,col),inf);
    outputMatrix(:,col) = inputMatrix(:,col)*chanNorm;
end
outputMatrix = outputMatrix';
```

Appendix D

Appendix D consists of all consent form used during the testing phase as well as the ethics approval from the Engineering and Built Environment Department of UCT.

The consent form used in testing is shown in the proceeding pages, providing details of the experimental procedure.

EMG Testing: Subject Consent Form

Electrodes: The electrodes used are small, pure silver caps with a diameter of 9mm. These are placed on the skin with an adhesive gel and measure the electrical signals from the muscles.

Electromyography (EMG): This is the measurement of the electrical biological signals emitted by the contracting mucles.

Informed Consent:

The thesis of this Masters Research project is to determine experimentally, the best electrode placement for EMG measurement and separation using an algorithm called Independent Component Analysis.

This will be carried out by recording EMG activity from the upper arm while you perform natural arm movements. The EMG signals are measured using surface electrodes placed full way around the upper arm. Surface EMG is a safe and non-invasive recording technique.

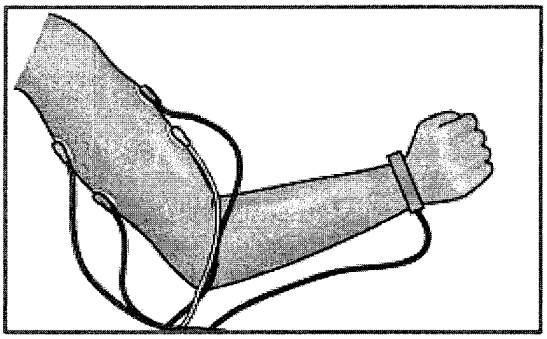

Figure 1: EMG electrodes applied to upper arm

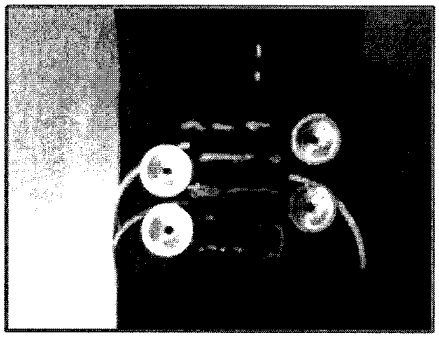

Figure 2: Section of EMG electrode Band

Testing Procedure:

All testing will be carried out at the UCT Faculty of Health Sciences, and has been pre-approved by the Electrical Engineering Ethics Commitee. To ensure good electrical conductivity, the skin of the upper arm will be lightly abraded and cleaned with medical alcohol to remove dead skin cells and dirt. At the very most this will cause slight discomfort. The electrode band will then be fitted and secured on your upper arm. The electrodes will be covered in an electrolyte gel, which causes no discomfort. The electrolyte gel is applied to the electrodes to help maintain contact and to provide better signal quality. The electrode gel can be easily washed off the skin after the experiement.

A series of instructions will be given to you prior to the start of the testing. You will have to perform 3 tests.

The first test is to determine your Maximum Voluntary Contraction. Here you will be asked to pull or push on a rigid bar for a few seconds and repeat this procedure 3 times.

The second test is the Isometric contraction test. In this test you will need to perform the following set of actions, resisting against the rigid bar.

1. Pronated resistance against bar for 3 seconds. (i.e. pushing down on the fixed bar.)
2. Rest for 4 seconds.
3. Repeat 3 times
4. Supinated resistance against bar for 3 seconds.(i.e. pull up on the fixed bar.)
5. Rest for 4 seconds.
6. Repeat 3 times.

The third test is a dynamic movement test; here you will be required to perform different arm movements while holding a dumbbell weight. The movements are as follows.

1. Hold weight at side with arm relaxed and hand supinated (i.e. palms facing forward.)
2. Pronated flexion. This requires pulling the weight up, palm facing down.
3. Supinate the forearm. This means you need to rotate your arm so your palms face up.
4. Pronate the forearm back to the position in instruction 2, palm facing down.
5. Now with the hand supinated extend the arm back down to your side into the relaxed position.
6. Repeat the whole procedure 3 times.

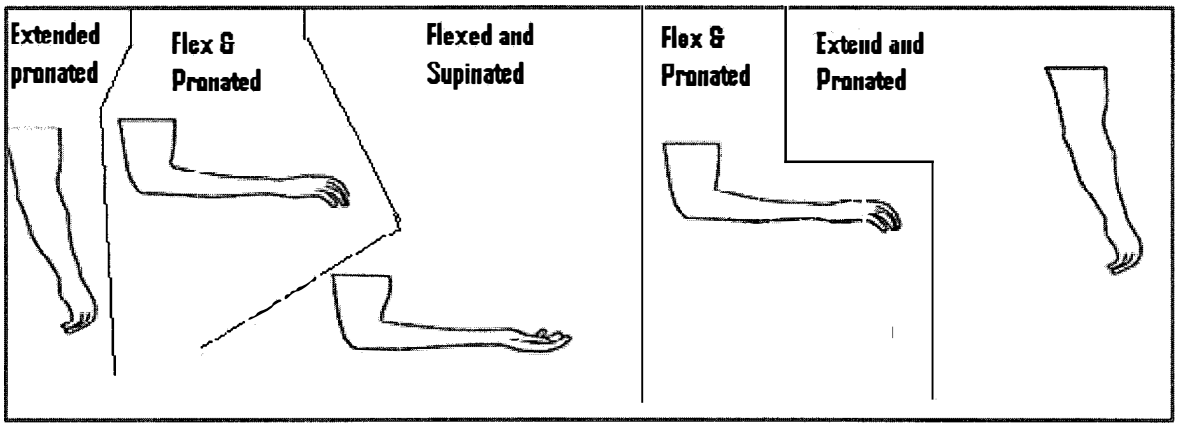

Testing should take approximately 1 hour. There will be no direct benefit to you personally, but the results of the research will be used to add to the understanding and application of non-invasive deep tissue EMG.

Possible risks associated with participation:

EMG measurement is a painless and harmless procedure. The recording equipment will be isolated from mains electrical supply; the system will be connected to a battery powered laptop during testing. Temporary, mild skin irritation may occur as a result of the of the electrolyte gel used on the electrodes. Only the right arm will be used for testing, thus there is no risk of cardiac arrest caused by the system.

In the unlikely event that you experience discomfort, the investigator should be alerted immediately. The University of Cape Town has a no-fault insurance policy should some unforeseen event occur during your participation in this study.

Statement of understanding and consent:

I confirm that I am 18 years of age or older and that the exact procedure, techniques and the possible complications of the above tests have been thoroughly explained to me. I am free to withdraw from the study at any time should I choose to do so. I understand that I may not go through with the testing procedure if I suffer from muscular disorders of any kind, and may ask questions at any time during the testing procedure. I know that the personal information required by the researchers and derived from the testing procedure will remain strictly confidential and will only be revealed as a number in classification analysis. I have carefully read this form and understand the nature, purpose and procedures of this study. I agree to participate in this research project conducted by the Electrical Engineering Department of UCT.

Name of volunteer / guardian (if necessary): Shaun Mulligan

Signature: _____

Name of Investigator: R. A. VERRINDER

Signature: _____

Date: 06/09/2012

Research Team:

Principal Investigator:	Ms R. Verrinder (Lecturer, UCT)
Principal Investigator:	Mr S. Mulligan (MSc Electrical Engineering UCT)
Principal Investigator:	Dr L. John (Senior Lecturer, UCT)

EBE Faculty: Assessment of Ethics in Research Projects

Any person planning to undertake research in the Faculty of Engineering and the Built Environment at the University of Cape Town is required to complete this form before collecting or analysing data. When completed it should be submitted to the supervisor (where applicable) and from there to the Head of Department. If any of the questions below have been answered YES, and the applicant is NOT a fourth year student, the Head should forward this form for approval by the Faculty EIR committee: submit to Ms Zulpha Geyer (**Zulpha.Geyer@uct.ac.za**; Chem Eng Building, Ph 021 650 4791). Students must include a copy of the completed form with the thesis when it is submitted for examination.

Name of Principal Researcher/Student: **Shaun Mulligan** Department: **Electrical Engineering**

If a Student: Degree: **MSc Electrical Engineering** Supervisor: **Robyn Verrinder**

If a Research Contract indicate source of funding/sponsorship: **NRF Scarce Skills Scholarship**

Research Project Title: **Independent Component Analysis Electrode placement and Optimization for use in Myoelectric Exoskeletons.**

Overview of ethics issues in your research project:

Question 1: Is there a possibility that your research could cause harm to a third party (i.e. a person not involved in your project)?	YES	NO
Question 2: Is your research making use of human subjects as sources of data? If your answer is YES, please complete Addendum 2.	YES	NO
Question 3: Does your research involve the participation of or provision of services to communities? If your answer is YES, please complete Addendum 3.	YES	NO
Question 4: If your research is sponsored, is there any potential for conflicts of interest? If your answer is YES, please complete Addendum 4.	YES	NO

If you have answered YES to any of the above questions, please append a copy of your research proposal, as well as any interview schedules or questionnaires (Addendum 1) and please complete further addenda as appropriate.

I hereby undertake to carry out my research in such a way that

- there is no apparent legal objection to the nature or the method of research; and
- the research will not compromise staff or students or the other responsibilities of the University;
- the stated objective will be achieved, and the findings will have a high degree of validity;
- limitations and alternative interpretations will be considered;
- the findings could be subject to peer review and publicly available; and
- I will comply with the conventions of copyright and avoid any practice that would constitute plagiarism.

Signed by:

	Full name and signature	Date
Principal Researcher/Student:	Shaun Mulligan	27 June 2012

This application is approved by:

Supervisor (if applicable):	Robyn Verrinder	27 June 2012
HOD (or delegated nominee): Final authority for all assessments with NO to all questions and for all undergraduate research.		
Chair : Faculty EIR Committee For applicants other than undergraduate students who have answered YES to any of the above questions.		

ADDENDUM 1:
Please append a copy of the research proposal here, as well as any interview schedules or questionnaires:

ADDENDUM 2: To be completed if you answered YES to Question 2:

It is assumed that you have read the UCT Code for Research involving Human Subjects (available at http://web.uct.ac.za/depts/educate/download/uctcodeforresearchinvolvinghumansubjects.pdf) in order to be able to answer the questions in this addendum.

2.1 Does the research discriminate against participation by individuals, or differentiate between participants, on the grounds of gender, race or ethnic group, age range, religion, income, handicap, illness or any similar classification?	YES	NO
2.2 Does the research require the participation of socially or physically vulnerable people (children, aged, disabled, etc) or legally restricted groups?	YES	NO
2.3 Will you not be able to secure the informed consent of all participants in the research? (In the case of children, will you not be able to obtain the consent of their guardians or parents?)	YES	NO
2.4 Will any confidential data be collected or will identifiable records of individuals be kept?	YES	NO
2.5 In reporting on this research is there any possibility that you will not be able to keep the identities of the individuals involved anonymous?	YES	NO
2.6 Are there any foreseeable risks of physical, psychological or social harm to participants that might occur in the course of the research?	YES	NO
2.7 Does the research include making payments or giving gifts to any participants?	YES	NO

If you have answered YES to any of these questions, please describe below how you plan to address these issues:

2.1 The study focuses only on healthy male individuals above the age of 18. The decision to exclude females from the study is based on evidence that ignoring the hormonal fluctuations in females when observing gender differences related to neuromuscular fatigue may lead to contradictory results.[1]. Age is also a differentiating factor, this is due to the face that the Mean Power Frequency MPF) of EMG signals is age-dependent [2]. It was decided to choose 18 year olds and above as it is thought that the MPF will no longer vary as muscle growth has slowed down in these individuals.

[1]. Salomoni S, Soares FA, de Oliveira Nascimento FA, et al. Gender differences in muscle fatigue of the biceps brachii and influences of female menstrual cycle in electromyography variables. Conf Proc IEEE Eng Med Biol Soc 2008;2598-2601.

[2]. Yuen SWH, Hwang JC, Poon PW: EMG power spectrum patterns of anterior temporal and masseter muscles in children and adults. J Dent Res 68: 800±804, 1989

2.6 There is a very remote possibility of electrical shock, but this has been greatly reduced by optically isolating the participants from the power supply unit. The entire system will be run from a laptop computer, unplugged from the power outlet and running from battery. So no direct connection between the participant and the mains electrical supply exists. Slight physical irritation may also occur as the participants skin needs to be cleaned with medical alcohol prior to the experiment.

ADDENDUM 3: To be completed if you answered YES to Question 3:

3.1 Is the community expected to make decisions for, during or based on the research?	YES	NO
3.2 At the end of the research will any economic or social process be terminated or left unsupported, or equipment or facilities used in the research be recovered from the participants or community?	YES	NO
3.3 Will any service be provided at a level below the generally accepted standards?	YES	NO

If you have answered YES to any of these questions, please describe below how you plan to address these issues:

ADDENDUM 4: To be completed if you answered YES to Question 4

4.1 Is there any existing or potential conflict of interest between a research sponsor, academic supervisor, other researchers or participants?	YES	NO
4.2 Will information that reveals the identity of participants be supplied to a research sponsor, other than with the permission of the individuals?	YES	NO
4.3 Does the proposed research potentially conflict with the research of any other individual or group within the University?	YES	NO

If you have answered YES to any of these questions, please describe below how you plan to address these issues: